EVALUATION OF LAND SURFACE TEMPERATURE WITHIN THE FRAMEWORK OF URBAN SPRAWL: A CASE STUDY IN İZMİR, SEFERİHİSAR

A Thesis Submitted to
the Graduate School of Engineering and Sciences of
İzmir Institute of Technology
in Partial Fulfilment of the Requirements for the Degree of

MASTER OF SCIENCE

in City Planning

by
Dilara Büşra KÖSEOĞLU

July 2024
İZMİR

We approve the thesis of **Dilara Büşra KÖSEOĞLU**

Examining Committee Members:

Asst. Prof. Dr. Zeynep ELBURZ
Department of City and Regional Planning, İzmir Institute of Technology

Assoc. Prof. Dr. Deniz GERÇEK KURT
Department of City and Regional Planning, İzmir Institute of Technology

Assoc. Prof. Dr. İlgi ATAY KAYA
Department of City and Planning, Dokuz Eylul University

10 July 2024

Asst. Prof. Dr. Zeynep ELBURZ
Supervisor, Department of City and Regional Planning, İzmir Institute of Technology

Prof. Dr. Hasan Engin DURAN
Head of the Department of City and Regional Planning

Prof. Dr. Mehtap EANES
Dean of the Graduate School of Engineering and Sciences

ACKNOWLEDGMENTS

I would like to express my pride in being a part of the İzmir Institute of Technology family during my master's studies. I extend my gratitude to all my professors, especially the esteemed Rector Prof. Dr. Yusuf BARAN, for opening new horizons and providing new perspectives on this journey.

Of course, the most significant gratitude goes to my esteemed advisor and professor, Asst. Prof. Dr. Zeynep ELBURZ, who shared her knowledge, experience, and valuable time with me patiently and selflessly from our first meeting to our last.

Additionally, I would like to thank the members of my thesis defense jury, Assoc. Prof. Dr. Deniz GERÇEK KURT and Assoc. Prof. Dr. İlgi ATAY KAYA, for their support and contributions.

I am deeply grateful to my angel, my beloved mother Esra DURMUŞ, who has always supported me and made me who I am. Her words of encouragement, "come on, my girl," have been the greatest motivation for completing this thesis. I also extend my thanks to my dear brother, Ahmet Güralp DURMUŞ, whose presence brings me joy and for whom I aspire to be a good role model. I love you so much, my small but precious family.

And endless thanks go to my beloved Doğan KÖSEOĞLU, my thesis companion, life partner, and the love of my life, for sharing all his knowledge and emotional support with me, and for countless reasons I cannot list here. I love you so much, my dear.

ABSTRACT

EVALUATION OF LAND SURFACE TEMPERATURE WITHIN THE FRAMEWORK OF URBAN SPRAWL: A CASE STUDY IN İZMİR, SEFERİHİSAR

The creation of spaces that meet the needs of an increasing population, developing economy, and rising levels of human well-being is leading to the intensification, expansion, and sprawl of urban areas. As a result of this sprawl, changes in land cover have caused various issues, making urban sprawl a global problem. The transformation of natural areas into urban spaces exacerbates the impacts of climate change. The effects of climate change, such as stormwater accumulation and Urban Heath Island (UHI) formation, are more pronounced in urban areas. This thesis focuses on the effects of land cover changes resulting from urban sprawl on Land Surface Temperature (LST).

To observe urban sprawl and determine its impact on LST, this study utilizes remote sensing data to analyse Seferihisar district for each year between 2017 and 2023. The dataset includes remote sensing data from Landsat 8 and SRTM obtained from the NASA. These data were used to create spectral indices (NDVI, NDBI, MNDWI, NDBaI), land cover classification, and LST maps through image processing, random forest algorithm, and supervised learning methods. Subsequently, a land cover prediction for Seferihisar district for the year 2030 was made using the 2017-2023 land cover change map.

The analysis findings indicate noticeable changes in land cover within the study area. These changes reveal that built-up areas and bare lands have an increasing effect on LST, while vegetated areas have a decreasing effect. A significant finding of the study is the reduction in LST values in areas where vegetation has improved and increased, and the rise in LST values in areas where built-up areas and bare lands have expanded. Based on these findings, potential risks for the year 2030 were evaluated.

Keywords: Urban Sprawl, Land Surface Temperature, Spectral Indices, Land Cover Prediction

ÖZET

ARAZİ YÜZEY SICAKLIĞININ KENTSEL YAYILMA ÇERÇEVESİNDE DEĞERLENDİRİLMESİ: İZMİR, SEFERİHİSAR ÖRNEĞİ

Kentleşme oranı geçmişten günümüze kadar artarak gelmesine karşın, kentsel alanlardaki gelişme sınırlı olması nedeniyle, artan nüfusun kentsel hizmet ve arazi ihtiyacının karşılanabilmesi için çeperlerde yeni yapılaşma alanlarının açılması yönünde baskı oluşmaya başlamış ve kentler yayılmaya başlamıştır. Bu yayılma sonucunda arazi örtüsünde meydana gelen değişiklikler çeşitli sorunlara neden olduğundan, kentsel yayılma küresel bir sorun haline gelmiştir. Doğal alanların, kentsel mekânlar oluşturmak üzere tahrip edilmesi iklim değişikliği etkilerinin de giderek artması anlamına gelmektedir. Kentsel alanlarda iklim değişikliği etkileri (yağmur suyu birikimi, kentsel ısı adası oluşumu vb.) daha fazla hissedilmektedir. Bu tez çalışmasında kentsel yayılma sonucunda meydana gelen arazi örtüsü değişimlerinin arazi yüzey sıcaklığı (AYS) üzerindeki etkilerine odaklanılmıştır.

Kentsel yayılmayı gözlemlemek ve arazi örtüsündeki değişimlerin AYS üzerindeki etkileri belirlemek amacıyla yapılan bu çalışmada, uzaktan algılama verileri kullanılarak Seferihisar ilçesinin 2017 ve 2023 yılları arasındaki her bir yıl için analizler yapılmıştır. Analizlerin veri seti; Landsat 8 uydusundan ve NASA'dan elde edilen SRTM uzaktan algılama verilerinden oluşmaktadır. Bu veriler görüntü işleme, rastgele orman algoritması ve denetimli öğrenme yöntemleri ile spektral endeksler (NDVI, NDBI, MNDWI, NDBaI), arazi örtüsü sınıflandırması ve AYS haritaları oluşturulmuştur. Ardından 2017-2023 arazi örtüsü değişim haritası kullanılarak, Seferihisar ilçesinin 2030 yılı arazi örtüsü tahmini yapılmıştır.

Analiz sonuçlarına göre çalışma alanında arazi örtüsünde gözle görünür biçimde değişiklik yaşanmıştır. Bu değişiklikler sonucunda yapılaşmış alanların ve çıplak arazilerin AYS üzerinde artırıcı bir etkisi olduğu, bitki örtüsü ile kaplı olan alanların ise azaltıcı etkisi olduğu anlaşılmıştır. Bitki örtüsünün yer yer iyileştiği ve arttığı alanlarda AYS değerlerinde azalma meydana gelmesi, yapılaşmış alanların ve çıplak arazilerin artış gösterdiği alanlarda ise AYS değerlerinin artış meydana gelmesi çalışmanın önemli bulgularındandır. Bu bulgular doğrultusunda çalışmada 2030 yılında karşılaşılabilecek riskler değerlendirilmiştir.

Anahtar Kelimeler: Kentsel Yayılma, Arazi Yüzey Sıcaklığı, Spektral Endeks, Arazi Örtüsü Tahmini

TABLE OF CONTENTS

LIST OF FIGURES

Figure **Page**

LIST OF TABLES

Table **Page**

LIST OF SYMBOLS AND ABBREVIATIONS

API: Application Programming Interface

CA: Cellular Automata

DEM: Digital Elevation Model

EEA: European Environment Agency

EFTA: European Free Trade Association

EPA: Environmental Protection Agency

EU: European Union

GDP: Gross Domestic Product

GEE: Google Earth Engine

IPCC: Intergovernmental Panel on Climate Change

LST: Land Surface Temperature

LULC: Land Use Land Cover

MAD: Minimum Average Distance

MND-GDM: Ministry of National Defense- General Directorate of Mapping

MNDWI: Modified Normalized Difference Water Index

MODIS: Moderate Resolution Imaging Spectroradiometer

NASA: National Aeronautics and Space Administration

NDBaI: Normalized Difference Bareness Index

NDBI: Normalized Difference Built-up Index

NDSI: Difference Soil Brightness Index

NDVI: Normalized Difference Vegetation Index

NIR: Near Infrared

OLI: Operational Land Imager

PV: Proportion of Vegetation

RF: Random Forest

SBSS: Statistical Package for the Social Sciences

SUHI: Surface Urban Heat Island

SWIR: Shortwave Infrared

TIR: Thermal Infrared

TIRS: Thermal Infrared Sensor

TURKSTAT: Turkish Statistical Institute

UBL: Urban Boundary layer

UCL: Urban Canopy Layer

UHI: Urban Heat Island

US: United States

USA: United States of America

USGS: United State Geological Survey

WHO: World Health Organization

WMO: World Meteorological Organization

ε: Emissivity

CHAPTER 1

INTRODUCTION

Along with the advancement of science and technology, developments in the field of health, prolongation of human life, decrease in infant mortality, etc. have led to a rapid increase in the world population. This increase has had a significant impact on urbanization practices and perceptions of urban space, particularly since the Industrial Revolution (Thorns 2002). Creating spaces to meet the needs of a growing population, a developing economy, and an increasing standard of living have caused urban areas to become denser, expanded, and sprawled (Sudhira, Ramachandra, and Jagadish 2004). Population growth, economic development, and individualization have led to urban sprawl, which is characterized by the expansion of city boundaries, an increase in impervious surfaces, and the destruction of natural areas (Nechyba and Walsh 2004). This is now a global issue. Increasing urban sprawl has significant economic, social, and environmental consequences (EEA 2016). Examining the results of urban sprawl causes a decrease in agricultural lands, forested areas, and open-green areas on the urban periphery, which in turn leads to the destruction of wildlife and water resources, among other consequences. Investments in infrastructure and superstructure, aimed at meeting the demands of the expanding city, also contribute to the direction of urban sprawl, resulting in the emergence of environmental hazards (EEA 2016; Bruegmann 2005). When examining the environmental impacts of the changing land cover, it can be observed that natural vegetation is gradually decreasing and impervious surfaces are increasing along with urban development (Brueckner 2000; Alberti and Marzluff 2004; Jaeger et al. 2010).

Rapid change and growth in urban land cover mean that climate change effect is also rapidly increasing (Neog 2023). Therefore, cities are in a position to both affect and be affected by climate change. Researching and examining these influencing and affected events is important in terms of contributing to the adaptation process to climate change and protecting cities, which are fragile due to their dynamic structure, from the risks they may be exposed to. At this point, the increase in Land Surface Temperature (LST) resulting from urban sprawl is among the important issues that need to be examined.

High-rise buildings that are close to each other, narrow streets, and dark colored materials with low albedo values, such as asphalt and concrete, absorb and retain more heat, causing urban areas to be hotter than the rural areas in their immediate surroundings (Neog 2023; Shetty, Umesh, and Shetty 2022; Çağlak, Özlü, and Toy 2019). Surface temperature differences resulting from the decrease in natural areas and the increase in impervious surfaces in urban areas reveal the concept of "Urban Heat Island (UHI)". Because the concentration of impervious surfaces causes the heat stored in urban areas to increase, when the LST in the urban area and its surroundings are examined, the temperature differences between them clearly reveal this situation.

To create urban planning studies that are more resilient and sustainable against the effects of climate change, it is necessary to know the extent and trend of changes in the land surface and to determine what effects this change has on LST. Professionals such as urban planners, architects, landscape architects, environmental engineers, government executives, and policymakers need to have this awareness and work with a multidisciplinary approach.

In this study, the relationship between urban sprawl and LST is examined, emphasizing the importance of the subject. At the same time, in order to provide the necessary preliminary information to build sustainable cities, an urban sprawl simulation for the coming years is created, and the UHI risk that may be encountered is evaluated. The findings will provide valuable information for urban planning and urbanization policies.

1.1 Problem Statement

Since the Industrial Revolution until today, cities have become centers of attraction and have grown due to economic and social activities, transportation and infrastructure facilities, etc. However, in the changing and transforming world conditions, the change and individualization of people's living habits, the improvement of transportation and infrastructure facilities, recent epidemics such as COVID-19, and natural disasters such as earthquakes and climate change have caused the population to be located on the periphery of the urban area and urban sprawl. Although it may be thought that this situation can be interpreted positively in that it will reduce the density in the urban area, as the urban sprawl to the periphery, it causes consequences such as the

destruction of natural areas such as forests, open-green areas, agricultural lands and wetlands, and the increase of impervious surfaces and environmental pollution. In connection with these results, sprawling cities become warmer than their peripheries. The increase in impervious surfaces and the use of heat-retaining materials cause the heat to remain on the city surface for a longer time, causing the UHI effect to be felt intensely. Thus, the quality of life decreases in urban areas and causes health problems such as heart diseases, respiratory problems and dehydration. From this perspective, the main problem of the study is that urban sprawl causes an increase in LST, and if urban sprawl is not controlled, this increase will have more pronounced and severe effects in the coming years.

1.2 Aim and Scope of the Research

The aim of this study is to observe urban sprawl using remote sensing data, determine the relationship between changes in land cover and LST, and predict land cover for the year 2030. This study is significant for guiding planning processes to be used in adaptation and mitigation efforts against UHI effects.

To achieve this goal, the study aims to analyze the temporal and spatial changes in land cover and land LST in the Seferihisar district of İzmir between the years 2017 and 2023. It also aims to analyze the relationship between land cover, spectral indices, and LST, predict the land cover of Seferihisar for the year 2030, and create a roadmap that will guide future planning efforts based on these predictions.

A pilot study was initially conducted to select the study area. In this pilot study, the LST map of İzmir province was produced. Subsequently, peripheral regions the city center with high LST values were focused on. The area narrowed down in the LST analysis was re-evaluated according to urban sprawl criteria such as low-density residential areas, population increase, and economic development. Based on these criteria, Seferihisar differ from other districts where has similar features. This differentiation is explained in detail under the title "Selection of the Case Study" in Chapter 5.

Accordingly, the study was conducted in the Seferihisar district of İzmir province, located in western Türkiye. Seferihisar is a region with a coastline along the Aegean Sea, high tourism potential, and a tranquil urban life. The region has drawn attention due to

rapid urbanization and rising land prices, particularly in recent years. This situation has led to an increase in the intensity of the urban heat island effect, which affects the region's climate, environmental conditions, and socio-economic development. The boundaries of the study area were obtained from the Ministry of National Defence General Directorate of Mapping (MND-GDM) for use in the analyses.

In this study, remote sensing data obtained from the OLI and TIRS sensors of the Landsat 8 satellite and the NASA SRTM were used to create Normalized Difference Vegetation Index (NDVI), Normalized Difference Built-up Index (NDBI), Modified Normalized Difference Water Index (MNDWI), and Normalized Difference Bareness Index (NDBaI) spectral indices through image processing methods. Temporal and spatial changes in land cover and LST were analyzed with these indices. A machine learning algorithm (supervised learning and random forest) was used for the classification and prediction of land cover. Correlation analysis was employed to determine the relationship between spectral indices, land cover classes, and LST. The Google Earth Engine (GEE) platform and the Statistical Package for the Social Sciences (SPSS) software were utilized for processing, analyzing, and visualizing the information obtained from the dataset. The methodological framework of the study is generally determined as 2017 and 2023, based on the 2030 projection year in the upper-scale plans. The primary reason for selecting a short time interval in the study is the desire of people to live in detached houses away from residential areas following natural disasters such as the COVID-19 pandemic and earthquakes in 2019. This situation has caused rapid changes in urban structures. 7-year time frame was chosen to examine short-term changes and to conduct the prediction analysis for the year 2030. The time period is limited to June, July and August of all years in order to eliminate seasonal differences and to make the data comparable and consistent.

In line with the purpose and scope of the study, the following research questions were determined in order to analyze the relationship between land cover and LST in Seferihisar district between 2017 and 2023 and to produce 2030 predictions in line with this relationship.

- How has the urban sprawl in Seferihisar district changed between 2017 and 2023?
- How did the temporal and spatial change of LST in Seferihisar district occur between 2017 and 2023?
- What is the relationship between spectral indices, land cover and LST?

- What are the land cover predictions for Seferihisar district in 2030?
- What types of risks are anticipated based on these predictions?
- What precautions can be taken against the risk of LST increase?

With the findings obtained from the answers to the research questions, this study will provide significant scientific contributions to the literature on the relationship between urban sprawl and LST through the use of remote sensing data and machine learning techniques. Additionally, the study will contribute to environmental sustainability by identifying the environmental impacts of urban sprawl and the measures that need to be taken to struggle climate change. The land cover predictions for 2030 will provide practical information to local governments and planners for the creation of sustainable urban development plans. Consequently, the study will offer policy recommendations that can be used by local governments and decision-makers to develop sustainable urban planning and climate change strategies, thereby providing applied contributions.

The study is unique in its examination of the concept of LST in the context of urban sprawl. Additionally, by predicting land cover and discussing developments in urban sprawl and LST based on these predictions, the study stands out and contributes innovation to the literature.

1.3 Structure of the Thesis

This thesis consists of 9 chapters to answer the research questions within the scope of the purpose of the study. The study begins with a literature review, focusing on topics that form the conceptual framework of the subject. Chapter 2; This is the "Urban Sprawl" section, which starts with clarifying the city and urbanization issues and then talks about what urban sprawl is, how and why it occurs, what its effects are, and the debates that create dilemmas in the literature. Chapter 3 focuses on the concepts of climate change, urban climate, UHI, and LST in the section titled "Urban and Climate." Chapter 4, titled "Remote Sensing" explains what remote sensing is, the characteristics of satellites used to obtain remote sensing data, and the tools used for processing and analyzing the acquired data. Chapter 5 is the "Data and Method" section, where the dataset used is described, and the methodology is explained. Chapter 6 is the "Case Study" section, where the reasons for selecting the study area and its characteristics are described.

Chapter 7 is the "Findings" section, where the findings obtained from the study's methodology are presented. Chapter 8 is the "Discussion and Conclusion" section, where the obtained results are evaluated, and recommendations are provided within the framework of sustainable urban planning and policies, and summarizes the findings of the study, presents the contributions and limitations of the research, and offers suggestions for future studies. The structure of the thesis, facilitating the easy tracking of the study's progress, is provided in Figure 1.1 as a flowchart.

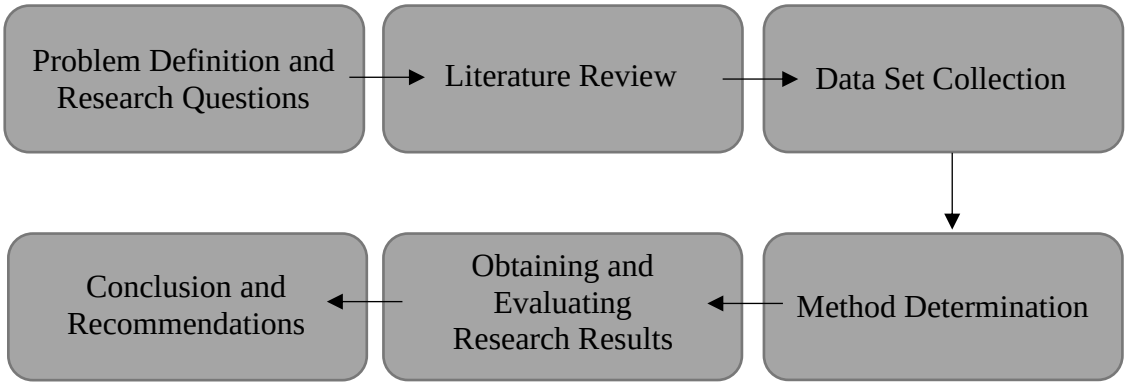

Figure 1.1 Research structure flowchart

CHAPTER 2

URBAN SPRAWL

The concept of a city has taken on different meanings throughout history and has been defined differently in each era. This indicates that a city is not only a spatial entity but also a socio-economic, political, and cultural phenomenon, meaning it is a living, dynamic entity (Marshall 2005; Wirth 1938). Looking at the historical development of cities, they emerged with the advancement of civilizations and were designed as centers of administration, commerce, and religion, independent of agriculture. By the medieval period, cities had become economically linked to agriculture (Pirenne 1946), surrounded by walls, and had turned into trade centers where craftsmanship developed (Thorns 2002). Following the Industrial Revolution, cities became stronger, their populations grew rapidly, and they evolved into structures with significant immigration due to increased economic activities (Sassen 1991). This rapid population growth significantly changed the function and structure of cities. Today, cities have become larger and more complex structures. With globalization, technological advancements, and modernization in transportation systems, cities have started to establish national and international connections, giving rise to the concept of "Modern Cities" (Thorns 2002; Castells 2010). With the emergence of modern cities, the importance of city boundaries has diminished, their structure has changed, and perceptions of them have shifted (Yaşar 2010). As a simple example, thanks to modern technology and amenities, the need for workplaces and residential areas to be close to each other has disappeared, altering the direction of urbanization from city centers to the outskirts in the form of suburbs and satellite cities.

In fact, all the technological, economic, social, and spatial developments experienced affect the urbanization process (Yaşar 2010). In this context, urbanization can be broadly defined as the movement of an increasing urban population and the number of cities in a country, depending on industrialization and economic development. Urbanization is a universal phenomenon experienced everywhere in the world (Sudhira, Ramachandra, and Jagadish 2004) and expresses economic, social, spatial, and societal changes (Wirth 1938). Looking at the urbanization processes of countries, the urban population in the United States of Amerika (USA) began to increase towards the end of the 1700s under the influence of the Industrial Revolution. After the Industrial

Revolution, the effects of World War II accelerated the process, leading to rapid population growth in urban areas. By the end of the 20th century, nearly 65% of the population had urbanized, and 35% lived in the suburbs (Nechyba and Walsh 2004). In Türkiye, the year 1950 marked a turning point in terms of the increase in the urban population (Garipağaoğlu 2010). As a result of rapid population growth, cities reached their saturation point, and the importance of places diminished with technological developments, reducing the attractiveness of city centers. This situation resulted in the sprawl of the urban periphery. Nechyba and Walsh (2004) state that the percentage of urban population in United States of America (USA) reversed after 1990, and the area occupied by city centers decreased from approximately 40% to 20% of all urbanized regions (Nechyba and Walsh 2004).

Since development in urban areas is limited, there has been increasing pressure to open new construction areas on the periphery to meet the urban services and land needs of the growing population (Chin 2002). As a result of urbanization, urban sprawl becomes inevitable. As cities expand, it becomes more challenging to meet the rising demand for land and distribute public services equally to these areas. We can divide urban sprawl into planned and unplanned growth. Planned sprawl is supported by large-scale plans, while unplanned urban sprawl occurs in areas without planning efforts, typically manifesting in slum areas. Whether the growth in urban areas is planned or unplanned, the tendency for urban sprawl cannot be prevented. Yaşar (2010) views urban sprawl as an unnatural and problematic process, referring to it as urban growth disorder (Yaşar 2010).

To understand why urban sprawl is seen as a disorder, it is essential first to define urban sprawl, evaluate its causes, and consider its consequences. Therefore, this study will explain the concept of urban sprawl. Although it will be evaluated from all perspectives, it will be beneficial to note that this study focuses on the physical dimension of urban sprawl.

Urban sprawl has become a globally debated phenomenon due to its significant pressure on infrastructure and the environment, especially towards the end of the 20th century. According to Jaeger et al. (2010), English and German literature first encountered the term "Zersiedelung" in the 1920s, which began to be widely used after World War II (Jaeger et al. 2010). Nechyba and Walsh (2004) state that in the USA, the term "sprawl" was first introduced by Early Draper, the US' first urban planner, in 1937. Discussion about sprawl and its relationship with transportation and income began towards the end of World War II (Nechyba and Walsh 2004).

Since the causes and consequences of sprawl will vary depending on the locations and conditions of regions, a definition with its own unique characteristics must be established (EEA 2016; Jaeger and Schwick 2014). However, despite being a subject of debate in the literature for many years, there is no consensus on a clear definition of urban sprawl. Indeed, with its common usage, urban sprawl is generally defined as a phenomenon where population density (Glaeser and Kahn 2004) disperses away from the city center (Brueckner 2000), creating low-density and scattered (Bruegmann 2005) residential and commercial areas.

Urban sprawl is defined by the European Environment Agency (EEA) as “the physical pattern of low-density expansion of large urban areas, under market conditions, mainly into the surrounding agricultural areas". The opposite of sprawl is compact and dense spatial development, as well as economical land use (EEA 2016).

According to Harvey and Clark (1965), urban sprawl is defined as the outward expansion of urban areas, particularly towards rural areas, which is often irregular and unplanned and typically involves low-density residential development (Harvey and Clark 1965).

Ewing (1997) characterizes urban sprawl by a series of features, which include the sprawling spread of urban areas across a wide area, development in a scattered manner, and a clear separation of urban functions such as residential, commercial, and industrial, often developing around highways (Ewing 1997). Additionally, Ewing (2008) emphasizes that urban areas naturally expand with population growth, and that this expansion tends to be haphazard and unplanned (Ewing 2008).

Brueckner (2000) considers urban sprawl as part of the urbanization process, defining it as the irregular expansion of development and land use from the city center to the periphery. According to this definition, urban sprawl typically involves an increase in low-density residential areas, infrastructure expansion, and the inclusion of agricultural or natural areas into the urbanization process (Brueckner 2000).

According to Jaeger et al. (2010), urban sprawl is characterized by poor accessibility, long and car-dependent travel, and unattractive developments. They also consider it to be a negative concept due to reasons such as being aesthetically unpleasing, leading to congestion, and increasing infrastructure costs (Jaeger et al. 2010). According to Chin (2002), sprawl is considered the opposite of compact city ideals and is seen as a "matter of degree" extending from compactness to sprawl. There is no absolute form to it, making it an open-ended term with no rigid boundaries (Chin 2002).

Urban sprawl, fundamentally, refers to the process of the outward expansion of urban functions such as residential areas, commercial establishments, and industrial facilities from the city center due to population growth and large-scale migration movements (Sudhira, Ramachandra, and Jagadish 2004), representing a dimension of urbanization. Sprawl implies a decrease in urban density as the city footprint expands (Nechyba and Walsh 2004). In other words, low-density expansion is a key characteristic of sprawl. According to Jaeger et al. (2010), the degree of urban sprawl increases with the extent and dispersion of urban development areas in a landscape (Jaeger et al. 2010). The fundamental difference between sprawl and alternative development models lies in the weak accessibility of urban uses to each other (Ewing 2008).

Urban sprawl can refer to both the state of expansion at a particular point in time and the process of expansion over time. Studies referring to low density, examining the relationship between built-up areas and population growth, define urban sprawl as a state (Frenkel and Ashkenazi 2008). According to this definition, buildings are the source of sprawl. Road and railway networks are not being considered as part of it (EEA 2016). In this context, the concept of urban form becomes prominent (Frenkel and Ashkenazi 2008). From this perspective, abnormal conditions in urban form indicate the degree and characteristics of urban sprawl (Yaşar 2010). Studies examining urban sprawl changes and their socio-economic impacts over time define sprawl as a process. According to this perspective, sprawl represents not only physical expansion but also a broader phenomenon encompassing population growth, economic development, and infrastructure improvement (Brueckner 2000; Galster et al. 2001).

2.1 Urban Sprawl Forms

Urban sprawl can take on various forms. Chin (2002) distinguishes urban sprawl forms as contiguous suburban growth, ribbon, scattered, and leapfrog development. These forms can occur in different regions, including mono-centric, multi-centric, or linear areas (Chin 2002). Nechyba and Walsh (2004) further elaborate on these types: the first being edge cities where urban population and economic activities cluster in low-density residential areas; the second being planned communities located near elements like parks or lakes, often with their own downtown area; and the third being a form of sprawl where houses emerge individually in rural areas (Nechyba and Walsh 2004). According to

Sudhira, Ramachandra, and Jagadish (2004), sprawl typically occurs radially around the city center or linearly along highways, often situated on urban edges, fringes, or along highways (Sudhira, Ramachandra, and Jagadish 2004). Regardless of its form, sprawl is observed through population movements between rural and urban areas and the relationship between suburbs and the city center (Nechyba and Walsh 2004).

While urban sprawl is often associated with suburbanization, they do not necessarily mean the same thing. Suburbanization can occur where urban sprawl exists, but not all instances of urban sprawl involve suburbanization. Suburbanization is just one form of urban sprawl. In sprawl, not only residential areas but also other urban uses such as commercial, industrial, and public facility areas tend to spread out from the center (Yaşar 2010). According to Ewing (2008), regardless of its form, a common characteristic of all sprawl models is the lack of functional open space (Ewing 2008).

2.2 Affecting Factors to Urban Sprawl

In scientific research, many indicators affect to urban sprawl have been discovered. However, the relationship between these indicators and sprawl remains unclear (Jaeger et al. 2010). Urban sprawl is influenced by various factors due to the dynamic nature of urban areas. Classifying these factors economically, politically, socially, and physically will help understand the factors contributing to urban sprawl more clearly.

Economic developments are one of the main factors influencing urban sprawl. The demand for land arises from the need to sustain and develop economic activities (Nechyba and Walsh 2004). The expansion of trade routes, industrial and commercial areas, the search for cheap land (Jaeger et al. 2010), and the urban area's response to these needs lead to urban sprawl. Parallel to economic development, the improvement of living standards (Glaeser and Kahn 2004) is a social factor influencing urban sprawl. People's desire for individualization, isolation from society, and the preference for living in detached houses with gardens (EEA 2016), or choosing locations away from the city center for second homes, trigger urban sprawl (Nechyba and Walsh 2004).

From a political perspective, implemented policies tend to encourage urban sprawl. Factors such as land use policies, support for transportation infrastructure through public means, the dynamics of the housing market (Galster et al. 2001), and tax policies

influence urban sprawl (Brueckner 2000). Additionally, urban planning studies often fail to keep pace with the speed of urban sprawl, resulting in uncontrolled growth through policies. Consequently, this leads to the formation of low-density, landscape-deprived environments, where natural areas, especially agricultural lands, are destroyed (Bhatta 2010).

2.3 Effects of Urban Sprawl

The reason why urban sprawl has become a global problem is the deterioration in and around the urban area, with decreasing density as the city's footprint increases, and one deterioration triggers another, creating even greater problems. To comprehend the significance of this issue, it would be beneficial to examine the challenges associated with urban sprawl.

Foremost among these, and particularly relevant to this study, is the rapid urbanization and environmental degradation of open spaces (Brueckner 2000). The fragmentation of natural habitats (Galster et al. 2001), diminishing quality (Alberti and Marzluff 2004; EEA 2016; Jaeger et al. 2010), and the consumption of open spaces (Jaeger et al. 2010; Nechyba and Walsh 2004), productive agricultural lands (Jaeger et al. 2010; EEA 2016), and leading to increased depletion of natural resources (Bruegmann 2005), result in degradation of ecosystem dynamics and ecological balance (Alberti and Marzluff 2004; Jaeger et al. 2010; EEA 2016). This situation results in changes in ecological conditions related to urbanization, such as loss of biodiversity, air, water, environmental pollution, and climate change (Alberti and Marzluff 2004). As a result of environmental degradation, increased impervious surfaces cause urban areas to heat up more, affecting the quality of life. Sudhira, Ramachandra, and Jagadish (2004) assert that urban sprawl is rapidly causing damage to natural resources, particularly in developing countries (Sudhira, Ramachandra, and Jagadish 2004). Studies examining the impact of changes in land cover due to urban sprawl on LST have proven that urban sprawl by damaging natural vegetation leads to an increase in temperature values. Sun, Wu, and Tan (2012) conducted a study using remote sensing to quantitatively examine the relationship between Land Use/ Land Cover LULC and LST. They employed NDVI, NDBI, MNDWI, and NDBaI spectral indices, along with DEM data. Their findings indicated that LST increases in urbanized areas and regions with a high concentration of bare land, while it

decreases in areas with dense vegetation. They also identified a negative relationship between MNDWI and LST, noting that clean water has a cooling effect on LST, whereas polluted water tends to increase LST. According to them, the indices they used are effective spatial parameters for measuring the impact of land cover on LST (Ersoy Tonyaloğlu et al. 2019; Sun, Wu, and Tan 2012) .

In their study Guo et al. (2020), utilized various spatial parameters, including Building Density, Sky View Factor, NDVI, NDBI, NDSI (Normalized Difference Soil Brightness Index), DEM, and several other metrics to evaluate and measure the impacts of LST change models in terms of spatial form, land cover, and landscape metrics. They concluded that while spatial forms have a weak relationship with LST, remote sensing indices and landscape metrics exhibit a strong relationship with LST (Guo et al. 2020).

Buo et al. (2021), in their study on urban expansion areas and UHI prediction, found that as the rate of urban expansion increases, natural vegetation decreases in newly constructed areas. This study emphasizes that changes in land cover during urban expansion affect the magnitude and intensity of SUHI, especially in large bare lands and areas with sparse vegetation (Buo et al. 2021).

In their study examining the seasonal impacts of temporal changes in LULC on climate variables, Shetty et al., (2022) emphasized the significant effects of urbanization on built-up and forested areas. They highlighted that the physical characteristics of urban areas are a dominant factor influencing LST changes. Additionally, they noted an increase in LST values in agricultural areas over time (Shetty, Umesh, and Shetty 2022).

Şentürk and Çubukçu (2022) investigated the distribution of relatively cooler areas in urban settings and the factors influencing their cooling capacity by using LST, NDVI, NDBI, and land cover data. Their study found a strong positive correlation between LST and NDBI and a moderate negative correlation between LST and NDVI, which was less pronounced than expected. Despite examining the relationship between water surfaces and LST, they observed a weak negative correlation. They noted that the limited water surface data within the study area prevented its use as a significant measure in their analysis (Şentürk and Çubukçu 2022).

Neog (2023) conducted a study to determine the extent of LULC changes and urban sprawl patterns and measure their impact on LST. The study found a strong positive correlation between built-up areas and LST, whereas vegetation exhibited a strong negative correlation with LST (Neog 2023).

Üstün Topal (2023) utilized NDVI, NDBI, MNDWI, and SAVI spectral indices to investigate the impact of LULC changes on LST. According to their study, NDBI values showed an increasing trend over the years, while the other indices exhibited a decreasing trend. The findings of Üstün Topal (2023) indicate higher temperatures in built-up areas and bare land, whereas lower temperatures were observed in areas covered by vegetation (Üstün Topal 2023).

Another identified problem is the difficulties and cost increases in the provision of infrastructure and public services. Expanding new settlements requires significant costs for the extension of roads, water, sewage, and other public services (EEA 2016). As cities expand, the need for transportation infrastructure increases, leading to increased dependence on automobiles (Bruegmann 2005). This results in increased transportation costs, inefficient traffic congestion, vehicle and noise pollution (Nechyba and Walsh 2004), and increased energy consumption (Bruegmann 2005). Nechyba and Walsh (2004) have highlighted the relationship between traffic congestion and urban sprawl within the framework of mobility and accessibility concepts. The authors note that traffic congestion in the USA (Brueckner 2000) has significantly increased commuting costs (Ewing 1997) and that the taxation policy, making urban transportation more expensive than suburban transportation, has contributed to sprawl (Nechyba and Walsh 2004). In their study, Ewing, Pendall, and Chen (2003) examined travel and transportation issues in the USA within the framework of urban sprawl and concluded that compact areas perform better in terms of commuting time and per capita traffic delays (Ewing, Pendall, and Chen 2003).

Along with the expansion of cities, the haphazard distribution of new settlement areas, decreased density in urban areas, and urban decay (Nechyba and Walsh 2004) are another problem. The dispersion of the urban population to the suburbs leads to the dispersal of retail trade (Bruegmann 2005) and the separation of residential areas from workplaces (Nechyba and Walsh 2004), causing the city center to lose its vibrancy (Bruegmann 2005) and begin to decay. Haphazard and aesthetically unappealing housing developments (Nechyba and Walsh 2004) in the natural environment led to the formation of distorted and aesthetically unpleasing urban textures (Bruegmann 2005).

Another negative consequence is the deterioration of the social structure and increased inequality in the sprawling city's low-density areas. According to Nechyba and Walsh (2004), individuals perceive open spaces in the suburbs as more important than urban open spaces (Nechyba and Walsh 2004). The trend towards individualism in

societies (Ewing 1997) and the desire to live in remote settlement patterns undermine the sense of belonging and weaken, or even eliminate, the sense of community (Nechyba and Walsh 2004; Bruegmann 2005). Additionally, the unequal provision of public services in suburban areas compared to urban areas leads to discrimination in housing areas (Brueckner 2000) and increases in poverty (Nechyba and Walsh 2004). It deepens economic imbalances between classes (Yaşar 2010).

Against all these challenges, there are very few tools available to significantly reduce urban sprawl (Jaeger et al. 2010). To control urban sprawl, it is necessary to thoroughly understand the dynamics of sprawl and undertake initiatives to develop policy strategies that contribute to sustainability (Sudhira, Ramachandra, and Jagadish 2004). According to Ewing (1997), density-focused urban planning and the preservation of green spaces are essential to curbing urban sprawl, and affordable housing projects should be supported (Ewing 1997). Glaeser and Kahn (2004) reiterate the recommendation for dense urban centers and emphasize the necessity of promoting environmental conservation policies (Glaeser and Kahn 2004). Brueckner (2000) discusses various policy proposals to reduce or control urban sprawl, including land-use regulations, transportation investments, tax policies, and sustainable urban planning strategies. However, he emphasizes that each policy option has its own advantages and disadvantages (Brueckner 2000).

2.4 Urban Sprawl Experiences of Countries

The United States and Western European nations have had significantly different urban sprawl experiences. This difference underscores the complexity of defining and explaining urban sprawl in the literature. Towards the late 1800s and into the 1900s, both North America and Europe underwent rapid urbanization due to the industrial revolution and economic developments (Chettry 2023). Despite experiencing similar periods of economic growth, the ways in which urban sprawl is evaluated differ between the two continents. In American cities, factors such as individual car usage, significant public investments in transportation infrastructure, limited investments in the city center, heterogeneous populations, and household characteristics have fostered a desire for expansion into larger areas (Nechyba and Walsh 2004). In contrast, Western European cities have seen significant public investments in public transportation, ensuring the

sustainability of resources in city centers, developing a homogeneous population structure, and not requiring housing mobility for household welfare, which has fostered a desire for living in a more compact area (Nechyba and Walsh 2004). Ewing (1997) suggest that urban sprawl policies in the United Kingdom, when compared to sprawl processes in the United States, are more effective. According to him, the UK's stricter planning laws and environmental protection measures allow for more sustainable management of urban sprawl (Ewing 1997).

The EEA conducted a study between 2006 and 2009 to assess the degree of urban sprawl and changes in urban sprawl in 32 European Union (EU) and European Free Trade Association (EFTA) countries. According to the study, the rate of urban sprawl varied greatly across different regions of Europe. While urban sprawl progressed more regularly and planned in Western Europe, it was more irregular and uncontrolled in Eastern and Southern Europe. In Eastern European countries, it was observed that urban sprawl was faster and more irregular due to the effects of the economic transition process (EEA 2016).

In developing countries, urban sprawl is still observed as scattered and low-density expansion (Jaeger et al. 2010). The structure of urbanization in these countries differs from that of developed countries due to the late onset of industrialization and technological advancements (Karaman 2003). The main reason for this difference is that the economy is based on agriculture. Societies that model industrialized communities but whose urbanization process does not rely on industrialization exhibit features with characteristics of both pre-industrial and industrial cities (Sjoberg 1955). Sjoberg (1955) refers to cities that carry features of both pre-industrial and industrial cities as "transitional cities" (Sjoberg 1955). Cities in Türkiye also have this characteristic.

In Türkiye, urbanization increased as a result of a significant wave of migration from rural to urban areas following the economic developments of the 1950s (Keleş 1961). The establishment of industrial facilities in major cities such as Istanbul, Ankara, and Izmir led job-seeking migrants to these cities (Dincer et al. 2019; Öncel and Levend 2023). According to Öncel and Levend (2023), between 1965 and 2014, 33% of Türkiye's population growth was concentrated in the provinces of Istanbul, Ankara, and Izmir (Öncel and Levend 2023). In the early stages of rural-to-urban migration in Türkiye, some family members would migrate to the city while others stayed in their villages or towns. In later periods, entire families were observed to migrate to the city as a whole (Keleş 1961).

As the rapidly growing population's needs could not be met, suburb settlements were quickly and unplanned formed to address the migrants' housing needs (Karaman 2003). This situation steadily increased until the 1980s, leading to the unplanned expansion of cities (Öncel and Levend 2023). After a while, the redevelopment of these suburban settlements resulted in new developments in different parts of the city, consequently leading to urban sprawl. This sprawl occurred not only for residential purposes but also for locating industrial areas outside the city (Tekeli 2009). Since the 2000s, there has been a decrease in both population growth and the rate of urban sprawl (Öncel and Levend 2023).

On the other hand, various policies, such as highways, bridges, and public transportation projects, have contributed to the expansion of cities into surrounding areas (Öncel and Levend 2023; Dincer et al. 2019). At this point, it is evident that it is crucial for decision-makers to develop strategies to reduce the pressure of urban sprawl and expansion on natural areas (Öncel and Levend 2023). Today, efforts such as urban renewal projects, conservation-oriented urban plans, planned and sustainable urban development policies, etc., are being carried out to reduce and prevent the effects of urban sprawl.

2.5 Detecting Urban Sprawl

Urban sprawl can certainly be planned, but it requires thorough research on aspects such as the growth rate, form, and scale of the sprawl. Without necessary information, planned sprawl can lead to infrastructure deficiencies and numerous problems (Sudhira, Ramachandra, and Jagadish 2004). Thus, to prevent or control urban sprawl, it is crucial to identify sprawl trends, conduct necessary analyses, and make timely and accurate decisions based on these analyses. Despite being a subject of scientific research for a long time, the measurement of urban sprawl still lacks clarity, consistency, and reliability due to its various and conflicting interpretations (Jaeger et al. 2010). Bhatta (2010) emphasizes that analyzing urban growth and sprawl can play an important role in guiding policy-making and decision-making processes for sustainable urban development (Bhatta 2010).

Since urban sprawl is a dynamic phenomenon and the processes differ by region, various methods have been developed for its detection. Chettry (2023) categorizes methods for detecting urban sprawl into two groups: one-dimensional and multi-

dimensional approaches. One-dimensional methods provide simple measurements, indicating whether sprawl exists or not. Multi-dimensional approaches focus on composite indices involving multiple interrelated dimensions (Chettry 2023). These dimensions can include analyzing changes in land cover, assessing the causes and consequences of sprawl (Jaeger et al. 2010), defining sprawl patterns, and measuring landscape metrics (Sudhira, Ramachandra, and Jagadish 2004) like water bodies, transportation networks, impervious surfaces, and natural areas. Observing changes in built-up areas is one of the fundamental parameters used to detect sprawl (Sudhira, Ramachandra, and Jagadish 2004). Jaeger et al. (2010) developed 13 criteria to accurately define and assess urban sprawl, emphasizing aspects such as representativeness, comprehensiveness, scale sensitivity, validity, reliability, transparency, usability, data accessibility, cost-effectiveness, adaptability, dynamism, comparability, and sustainability (Jaeger et al. 2010). Other indicators related to urban sprawl include population density, household size, government effectiveness, road and rail density, and the number of cars per capita etc. (EEA 2016).

Table 2.1 Indicators used to measure urban sprawl

	Indicators	Source
Density	Population Density	(Bhatta, 2010; Frenkel & Ashkenazi, 2008; Glaeser & Kahn, 2004)
	Road and Rail Density	(EEA 2016)
	Built-up Area Density	(Bhatta, 2010; Frenkel & Ashkenazi, 2008; Galster et al., 2001)
	Density of Second Home	(Bhatta, 2010; Jaeger et al., 2010)
Transportation	Level of Accessibility	(Chettry 2023)
	Higher usage of private vehicles	(Ewing, 2008)
Urban Extent	Change Dynamics Land Consumptions	(EEA 2016)
	Land Use Mix	(Ewing et al., 2003; Frenkel & Ashkenazi, 2008; Galster et al., 2001; Xu, 2006)
	Urban Footprint	(Bhatta, 2010)
	Open Space Accessibility	(Ewing et al., 2003)
	Developable	(Bhatta, 2010)
	Landscape Metrics	(Sudhira, Ramachandra, and Jagadish 2004)
Compactness	Single point Compactness	(Bhatta, 2010)
	Centrality	(Galster et al. 2001)
	Proximity	(Galster et al. 2001; Jaeger et al. 2010)
	Minimum average distance (MAD) center	(Bhatta, 2010)
Socioeconomic Status	Level of Education	(Chettry 2023)
	Gross Domestic Product (GDP)	(Alberti and Marzluff 2004)
	Household Size	(EEA 2016)

Despite the complexity, remote sensing and Geographic Information Systems (GIS) are widely accepted for detecting and measuring urban sprawl (Galster et al. 2001). These methods monitor and map land cover changes using satellite imagery, aerial photographs, and laser scanning techniques (Bhatta 2010). Metrics like Shannon's entropy, the Landscape Shape Index, the Urban Sprawl Index, and Spectral Indices can be used to assess the spatial pattern and intensity of urban sprawl (Galster et al. 2001). These techniques allow for comprehensive and objective analysis of urban sprawl, making it possible to identify sprawl trends over time and space. They also enable the prediction of future land cover patterns, contributing to effective use of natural resources and equitable distribution of public services (Sudhira, Ramachandra, and Jagadish 2004). In urban sprawl prediction, techniques such as cellular automata (CA), Markov Chains, Land Use Change Models (CLUE and SLEUTH), Regression Models, and GIS-based simulations are commonly used (Koko et al. 2022). In addition to all these methods, land cover maps and predictions can also be produced using the random forest method with state-of-the-art machine learning algorithms. This method is a practical approach for different disciplines due to its ease of application, applicability with missing data, etc. (Ebrahimy et al. 2021).

In summary, understanding and addressing urban sprawl requires detailed and comprehensive analysis, utilizing advanced methods and technologies. Accurate measurement and modeling are essential for sustainable urban planning and the effective management of urban growth.

CHAPTER 3

CLIMATE CHANGE

Climate is one of the most important concepts for humans to sustain their lives. Almost all living conditions depend on and are affected by climate conditions. Climate is influenced by many natural formations, depending on the position of the Earth, the tilt of the Earth's axis, and its rotation (Ebi, Mearns, and Nyenzi 2003). Therefore, climate exhibits different characteristics in various parts of the world (WMO 2020). While climate naturally changes due to various factors, recent human activities have accelerated this change (Neelin 2011). Thus, the human factor has become a significant element in the climate change process. The acceleration of climate change due to human activities has become a global issue. One of the most significant human activities causing global climate change is urbanization (UNFCC 2006; WHO 2003; Toy and Eren 2023). With urbanization, the development of new land and resource management models has become necessary. Since these models start with the transformation of natural areas, particularly agricultural lands, they have created sensitive areas vulnerable to climate change (Johnson, Toly, and Schroeder 2015). Consequently, urban areas have become more vulnerable to climate change compared to rural areas on their periphery (Masson et al. 2020). When the temperature increase, which is one of the effects of climate change, is examined specifically, it has been observed that urban areas are getting warmer than their peripheries (Oke 1982; Roth and Chow 2012). This temperature difference between urban and rural areas has led to the concept of the "UHI" (Oke 1982). In this study, which examines the relationship between urban sprawl and LST, the concepts of climate change, urban climate, UHI, and LST are examined to form the conceptual framework of the study.

Climate is a concept that expresses the weather conditions and seasonal changes resulting from long-term observations in a specific region (Johnson, Toly, and Schroeder 2015). While creating climate data, the long-term averages and variabilities of various meteorological data, such as temperature, humidity, precipitation, and wind, are examined (IPCC 2023). According to Neelin (2011), the average state of the atmosphere, water, land surfaces, and the ecosystems that live there is usually referred to as the climate. Weather, as opposed to climate, is the condition of the ocean and atmosphere at

a specific point in time (Neelin 2011). According to Türkeş (2001), the definition of climate is characterized by the extreme formations and long-term statistics of weather events, atmospheric processes, and climate variability (Türkeş 2001). Climate, by its nature, tends to change. External factors affecting the climate accelerate the usual course of climate change. This change occurs due to the interaction of human impacts and natural processes.

The acceleration of climate change due to external factors beyond its usual course has become a global issue because it leads to a variety of environmental, economic, and social problems. According to the (IPCC 2019) report, the primary causes of climate change are numerous anthropogenic effects such as industrial production, increased fossil fuel usage, urbanization, and deforestation, all of which increase greenhouse gas emissions. Greenhouse gases such as carbon dioxide (CO2), methane (CH4), and nitrogen (N) create a greenhouse effect in the atmosphere, leading to global temperature increases and climate change (IPCC 2023). Urban areas are where these human activities are most concentrated. Therefore, it is necessary to discuss the increase in urbanization. As the global population becomes concentrated in urban areas, the activities undertaken to meet the growing infrastructure needs increase construction and the consumption of natural resources. The increase in impervious surfaces and the destruction of natural areas are directly related to local climate change. The concept of "Urban Climate" has emerged as a result of temperature changes caused by transformations in urban areas.

3.1 Urban Climate

As urban areas become more concentrated, the increase in developed areas, the destruction of natural structures by human hands, and rising human activities have caused cities to exhibit different climate characteristics compared to their peripheral areas. Consequently, the concept of "urban climate," which describes the microclimate of a city, has emerged from the examination of climatic differences and their causes between urban areas and their surroundings.

Studies on urban climate date back to the early 19th century (Howard 1820) (Streutker 2003). However, these studies gained significant attention in the scientific community nearly a century later when the effects of climate change in urban areas on human life began to be felt (Oke 2006). Initially, urban climate research was focused on

air pollution, but later various aspects were examined by many researchers (Oke 1991; Toy and Eren 2023). Urban climate encompasses not only the air temperature but also soil temperature and hydrological conditions in and around urban areas (Pickett et al. 2011).

Changes in land cover due to urbanization (Wang et al. 2018), alterations from agricultural and forestry activities, increases in anthropogenic heat sources for transportation, production, heating, and cooling, rising emissions of air pollutants (Erell, Pearlmutter, and Williamson 2012), and the materials used in construction affect the physical and biological properties of the land surface in cities. These factors also impact natural cycles and processes, resulting in urban areas possessing unique climate characteristics (Wang et al. 2018; Marsh 2010). Oke (2006) defined urban climate as a multifaceted term that includes the long-term effects of meteorological and atmospheric phenomena on the climates of urbanized regions (Oke 2006). The differing climate conditions in urban areas compared to their peripheries, resulting from these urban changes, are described as urban climate (Marsh 2010; EPA 2008). In their study, Çağlak, Özlü, and Toy (2019) identified the characteristics of urban climate and examined the differences that distinguish urban climate from rural climate. According to them, urban areas exhibit different climate characteristics compared to rural areas, depending on their size, activities, and geographical features (elevation, proximity to the sea, etc.) (Çağlak, Özlü, and Toy 2019). Generally, cities have higher temperatures and precipitation amounts, more fog and cloud formation, lower relative humidity and wind speed (Masson et al. 2020), and higher air pollution compared to their surrounding rural and semi-urban areas (Demircan and Toy 2018; Oke 1991). This is due to the low and heterogeneous vegetation levels, the development of high and closely spaced building forms (Yoo et al. 2019), and the use of materials during construction that alter albedo, thermal capacity, and heat conductivity (Pickett et al. 2011). Additionally, impervious surfaces increase solar radiation absorption, reduce sky visibility, and lead to the formation of urban canyons (Oke 1991; Çağlak, Özlü, and Toy 2019; Yoo et al. 2019).

All these factors cause significant changes in temperature, one of the key elements of urban climate, leading to differences in local climates and extreme climatic events due to climate change (Oke 1982). These extreme climatic events are referred to in the literature as the "UHI" phenomenon.

3.2 Urban Heat Island

Unplanned and rapid urbanization leads to changes in land cover and surface temperature (Nimish, Bharath, and Lalitha 2020). The UHI is the most prominent climatic indicator of urbanization. The concept of the UHI is one of the best-known forms of local anthropogenic climate change and is defined simply as the temperature within the city being higher than that of the surrounding rural areas at the same time (Oke 1982). This temperature difference is usually caused by changes in land cover in urban areas (Streutker 2003).

The climatic difference between urban and rural areas, termed the "UHI", was first described in 1820 for the city of London by Luke Howard and has since gained increasing importance (Streutker 2003). Oke (1995) defines the term "heat island" as urban areas that are especially warmer than nearby rural areas, particularly at night. In densely populated cities, the air temperature is observed to be 1 to 3 °C warmer than the surrounding areas, and the temperature difference between day and night can reach up to 12 °C (Oke 1995). The UHI plays a positive role in providing relatively mild weather during winter for city dwellers. However, it negatively impacts human health and comfort during summer, contributes to air pollution, and causes changes in wind, humidity, and precipitation patterns (Streutker 2003). The formation of the UHI is due to many factors, and their combination makes temperature differences in urban areas pronounced. The main causes of the UHI include population density, the increase in built-up areas, and the reduction of vegetation. These factors contribute to pollution, albedo effect, global climate change, human activities, and energy usage (Somuncu 2021). Commonly used construction materials in urban areas, such as asphalt, concrete, and brick, have high heat absorption and storage capacities. These materials absorb solar energy during the day and slowly release it throughout the night, causing urban areas to remain warmer than rural areas.

Oke (1982) states that UHI can be observed in different layers of the atmosphere, various surfaces, and even underground. Accordingly, UHI types are divided into Surface UHI and Atmospheric UHI (Figure 3.1). The surface UHI is further divided into Surface UHI (SHUI) and Sub-surface UHI (Oke 1982). These types of heat islands differ in their formation, the techniques used to define and measure them, their effects, and the methods available to mitigate their impacts (Branea et al. 2016; Elmarakby et al. 2020; Somuncu

2021). This differentiation arises from the examination of temperatures in different layers of the UHI. The study of atmospheric UHI is divided into the Urban Boundary Layer (UBL) and the Urban Canopy Layer (UCL) (Figure 3.2) (Arellano and Roca 2018; Voogt and Oke 2003).

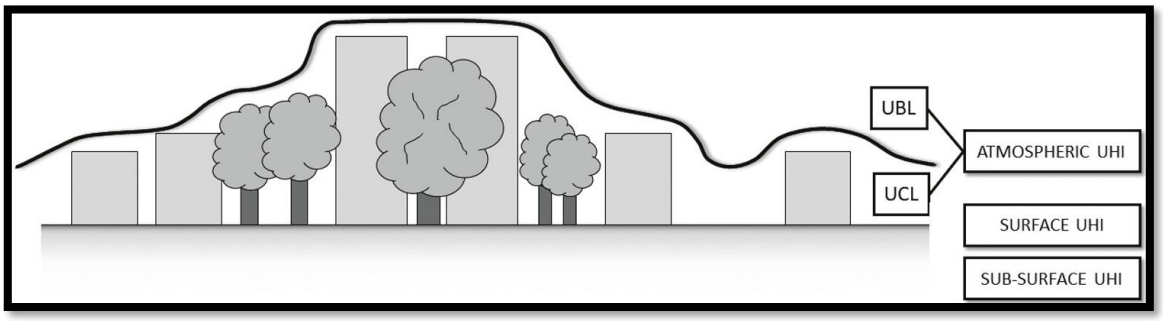

Figure 3.1 The type of urban heat islands diagram that are frequently observed (Source: (Feranec et al. 2019)

The urban boundary layer, the layer extending from the surface to the atmospheric boundary, is influenced by atmospheric factors. On the other hand, the urban canopy layer remains at the level of the ground and building roofs and is influenced by factors such as soil roughness, tree shading, land cover type, and height (Arellano and Roca 2018). While UCL is usually measured with sensors attached to fixed weather stations or vehicle crossbars, UBL is measured with more specialized instruments such as tall towers, radiosondes and aircraft (Zhou et al. 2019). UBL is also affected by the urban surface but is not generally measured with meteorological data of ground measurements (Schwarz et al. 2012). Due to the limited number of monitoring stations, these methods typically do not provide sufficient spatial details for measured UHIs, which are often necessary for urban land use/ land cover planning and climate change research (Anniballe, Bonafoni, and Pichierri 2014).

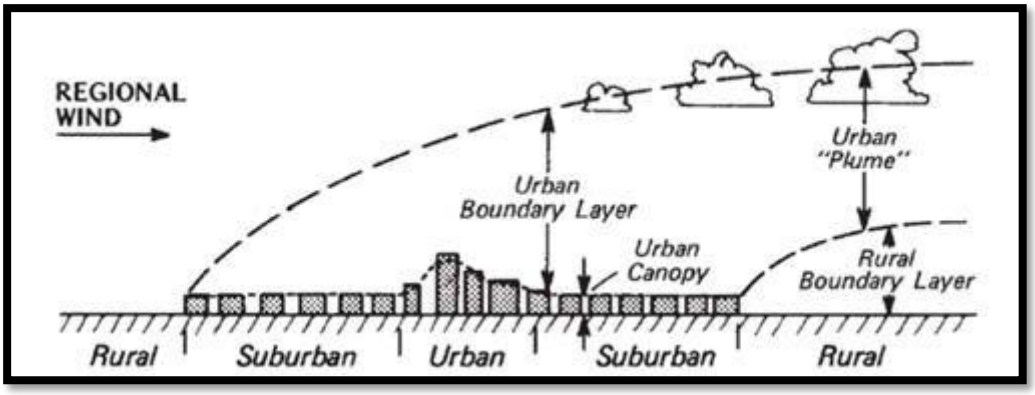

Figure 3.2 Urban boundary layers and urban canopy layer (Source: Arellano & Roca, 2018)

In contrast, SUHI represents the radiative temperature difference between urban and non-urban surfaces and is measured using LST data (Schwarz et al. 2012) obtained from satellite's thermal sensor with remote sensing (Voogt and Oke 2003). The SUHI varies depending on sunlight intensity, season, changes in land cover and weather conditions etc. (Yuan and Bauer 2007). It is often used when Atmospheric UHI cannot be measured or data is insufficient (Schwarz et al. 2012). SUHI is often preferred in studies because it allows for the examination of the urban thermal environment across various spatial scales (from local to global) and temporal scales (daily, monthly, and yearly) (Zhou et al. 2019). This enables the acquisition of consistent, verifiable, and repeatable observations of surface temperature (Anniballe, Bonafoni, and Pichierri 2014). In studies of UHI, the appropriate class of UHI research should be determined based on the data, methods used, and the scale of the area under investigation.

3.3 Land Surface Temperature

It represents the temperature of the Earth's surface. It is measured using satellite data or ground-based sensors and indicates the heat that the surface absorbs and re-emits from solar radiation (Weng 2009). LST is used to calculate diverse SUHI indicators, such as temperature differences for urban and agricultural area or make an effort to record the temperature's spatial pattern (Schwarz et al. 2012; Yoo et al. 2019). LST is a useful tool for controlling how heat is distributed in different land cover types. The configuration of land cover, impervious surfaces associated with urbanization, and vegetated permeable surfaces are among the most significant factors influencing LST (Arellano and Roca

2018). Additionally, various factors, such as incoming radiation, evaporation, and transitions between layers, affect LST (Guo et al. 2020).

LST represents the radiometric temperature of the surface and should not be confused with weather data. LST is always higher in urban areas and on bare surfaces, such as residential and industrial land use, while it is lower in vegetated areas, water bodies, parks, and other recreational land use areas (Yin et al. 2018).

With the advent of thermal imaging in remote sensing tools, the use of remote sensing methods in LST analysis has gained popularity (Okumuş 2022). The high quality, accuracy, and resolution of the obtained images, along with their applicability at different scales, make remote sensing methods advantageous in terms of time and cost, which is why they are frequently preferred (Voogt and Oke 2003). Therefore, LST is typically derived from thermal infrared data obtained from remote sensing satellites or aerial photographs (Zhou, Huang, and Cadenasso 2011). Thermal infrared band data obtained from satellites such as MODIS (Moderate Resolution Imaging Spectroradiometer), Landsat, AVHRR (Advanced Very High-Resolution Radiometer), and Sentinel-3 are commonly used for this purpose.

There are three different algorithms that can be used in LST calculation: the Mono-Window Algorithm, the Split-Window Algorithm, and the Single-Channel Algorithm (Wang, Lu, and Yao 2019). The Mono-window and Single-Channel algorithms perform calculations using a single thermal infrared band. The Mono-window thermal radiance calculation involves steps such as brightness temperature (BT) and surface emissivity and is commonly used in Landsat 8 satellite data (Wang, Lu, and Yao 2019). The Single-Channel algorithm performs radiance calculations with atmospheric correction and surface emissivity and is typically used in data from satellites with a single thermal band, such as Landsat 5 and Landsat 7 (Wang, Lu, and Yao 2019). The Split-Window algorithm, on the other hand, uses two different thermal infrared bands to reduce atmospheric effects. It is commonly used in satellite data, like MODIS (Zhou et al. 2019). This method corrects for atmospheric components by analyzing thermal radiation at different wavelengths, resulting in more accurate LST calculations (Wang, Lu, and Yao 2019). Converting raw data from satellite sensors into physical temperature values is an important step in calculating LST. The emissivity values of different surfaces and NDVI are important variables in LST calculation (Arellano and Roca 2018).

CHAPTER 4

REMOTE SENSING

With the placement of artificial satellites in space, a new era opened in the field of scientific research (Özbalmumcu and Erdoğan 2001) and remote sensing became a modern branch of science (Bhatta 2010). At the same time, remote sensing approaches have gained a popular place in scientific research in many disciplines for reasons such as ease of use, cost and time efficiency, and expandability of the data set (Jensen, Gatrell, and Mclean 2007). Similarly, it is an important place in urban planning research to examine the development and management of urban areas and their relationship with dynamic processes (Bhatta 2010). This study uses remote sensing to assess the current and future risks of climate change in urban areas by examining the relationship between land cover and surface temperature. Additionally, it is an example of the use of remote sensing in urban planning research. Remote sensing studies are an important tool for obtaining the necessary data to determine this relationship. For this reason, remote sensing and its features are explained in this section of the study.

Everything on Earth reflects, absorbs or transmits energy at various wavelengths. In other words, everything on earth has a unique spectral fingerprint. It is possible to process and analyze these fingerprints through technology. According to the definition published on the official website of the United States Geological Survey; the process of measuring the radiation reflected and spread around from a satellite or aircraft at a certain distance, in order to determine the physical properties of an area, by means of special cameras, is called "Remote Sensing" (USGS 2024b). In his book, Bhatta (2010) briefly defined remote sensing as a tool or technique that enables the electromagnetic energy of an object or geographical surface to be observed by sensors using electromagnetic spectrum bands such as infrared, microwave and ultraviolet, and to obtain valuable data using mathematical algorithms (Bhatta 2010).

Today, remote sensor systems can provide data from all kinds of energy emitted, reflected, and transmitted from the electromagnetic spectrum. This data is then used to transform information into products and make statistical decisions, either manually or through machine learning. Specifically, the areas of use of remote sensing images can be listed as demographic studies, archaeological investigations, energy studies using

hydrological models, city and regional planning, environmental monitoring, land use and land cover modeling, weather forecasting and agricultural production forecasting, and the detection and mapping of forest fires (Anyamba et al. 2015; USGS 2024a).

One of the features that make remote sensing important is, of course, the ability to obtain information about very large areas of the earth remotely, without any physical contact (Özbalmumcu and Erdoğan 2001) while examining the earth, and the technology that enables this. Satellites sent into Earth orbit and their sensors, data processing and analysis tools, software used during data detection and processing, and various features of all these are the factors that form the basic structure of remote sensing. These factors should be taken into account in order for the researcher to distinguish which information to use and to determine the most suitable data and method for the study area. Therefore, it would be appropriate to talk about the factors that are important for remote sensing in this study.

4.1 Satellites and Sensors

Since remote sensing is conducted via artificial satellites placed around the Earth's orbit, satellites are a fundamental factor in remote sensing. Satellites are positioned in orbits with different altitudes and inclinations and are equipped with sensors that collect data in electromagnetic waveforms from different layers of the Earth and the atmosphere. The purpose of use varies depending on the satellites' location and the sensors inside them. Satellites are divided into three classes: low, medium, and high orbits. The Landsat satellite used in this study is a satellite positioned in low orbit (EarthData 2024c).

Another important factor for remote sensing is the detection of an event or change in the environment, as well as the sensors that detect the data. Sensing is carried out through sensors, which are categorized into two types: passive and active. This distinction relates to the energy used during sensing. Passive sensors are those on satellites and aircraft that use the sun's natural energy source for illumination and measure the reflected energy. On the other hand, active sensors are those that generate their own energy source for illumination and measurement (Anyamba et al. 2015; EarthData 2024c).

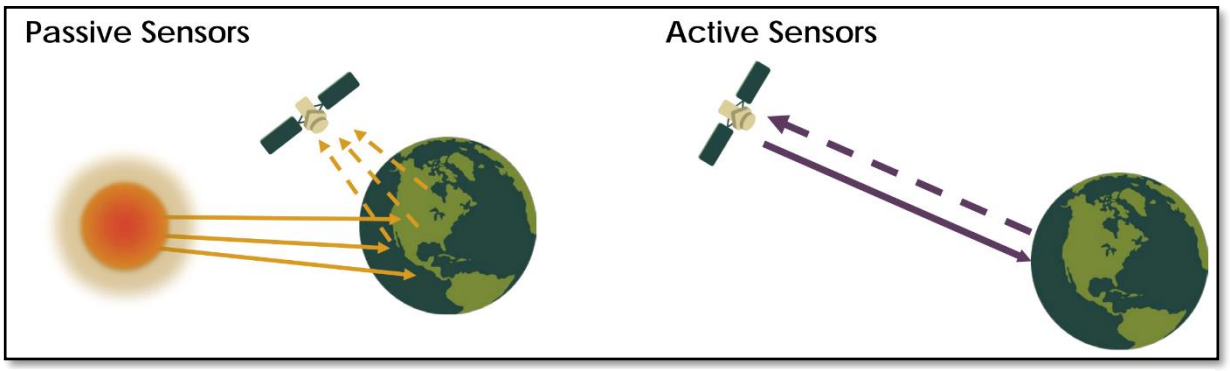

Figure 4.1 Diagram of passive and active sensors. (Source: NASA Applies Sciences Remote Sensing Training Program) (EarthData 2004)

According to information from the NASA's official website, active sensors include a variety of radio detection and ranging sensors, altimeters (devices used to measure altitude), and scatter meters (devices that measure the return of light or radar waves). Active sensors are generally able to penetrate the atmosphere because they operate in the microwave band of the electromagnetic spectrum. For this reason, its usage areas can generally be listed as detection of aerosols, examination of forest structure, rainfall and winds, examination of sea surface topography, etc. Passive sensors, on the other hand, include different types of radiometers (devices that measure the intensity of incoming light energy, convert light energy to heat energy, and convert heat energy to kinetic energy) and spectrometers (devices that measure the properties of the electromagnetic spectrum reflected from wide wavelengths, and analyze these, such as gamma rays and X-rays) (EarthData 2024b). Due to their operation within the visible, infrared, thermal infrared, and microwave parts of the electromagnetic spectrum, passive sensors are utilized for measuring physical properties such as sea or LST, cloud and aerosol characteristics, and vegetation properties. However, in regions with dense cloud cover, the observation ability is limited due to the inability of passive sensors to penetrate cloud cover (EarthData 2024c). This study focused on passive sensors such as MODIS, Sentinel, and Landsat.

4.2 Resolution

Another distinguishing feature of the sensors is resolution; that is, how the data from the sensors is used. Resolution varies based on factors such as the satellite's position and the sensor's design characteristics. There are four types of resolution: radiometric, temporal, spatial, and spectral (EarthData 2024c). Understanding these types of resolutions is crucial when selecting a specific sensor for the study area. Therefore, the characteristics of these types are explained below.

First, radiometric resolution refers to the number of bits that represent the recorded energy in each pixel. As radiometric resolution increases, so does the range of digital values used (such as contrast levels, gray levels, and so on), allowing for finer distinctions in energy differences (EarthData 2024c). MODIS, Landsat, and Sentinel have a 12-bit (NASA LANDSAT 2024; Copernicus 2024; NASA MODIS 2024) radiometric resolution.

Second, temporal resolution refers to the time interval required for satellites to complete their orbits and return to the same observation point. The shorter this interval, the better the data quality. Geostationary satellites, which synchronize with the Earth's rotation, offer good temporal resolution. In polar orbits, temporal resolution can range from 1 to 16 days (EarthData 2024c). MODIS has a temporal resolution of 1-2 days (NASA MODIS 2024), Sentinel 5 days (Copernicus 2024), and Landsat 16 days (NASA LANDSAT 2024).

Third, spatial resolution is defined as the area on Earth's surface represented by each pixel in a digital image. It indicates the smallest object a sensor can detect. Spatial resolution should be selected based on the study area's needs. While it is effective to work with a spatial resolution between 10 and 100 km on a global or national scale, it is more effective to work with a spatial resolution between 1 km and 10 m on a regional or neighborhood scale. Depending on the type of bands, MODIS offers a spatial resolution ranging from 1000 and 250 meters (NASA MODIS 2024), Sentinel from 60 and 10 meters (Copernicus 2024), and Landsat from 100 and 15 meters (NASA LANDSAT 2024).

Finally, spectral resolution refers to sensors' ability to distinguish fine wavelength intervals, which is directly proportional to the number and width of spectral bands they can record (Figure 4.2). Bands correspond to specific wavelengths in the electromagnetic spectrum, such as infrared, microwave, and visible light. The narrower the wavelength

range for a band, the better the spectral resolution. High spectral resolution means more bands and greater diversity (EarthData 2024c). MODIS has 36 bands covering near-infrared, shortwave infrared, thermal infrared, and microwave regions (NASA MODIS 2024); Sentinel has 13 bands (Copernicus 2024); and Landsat has 11 bands, with 9 for visible, near-infrared, and shortwave infrared (Operational Land Imager, OLI) and 2 for thermal infrared (Thermal Infrared Sensor, TIRS) (USGS 2024b). There is an inverse relationship between spatial and spectral resolution: a sensor with high spatial resolution tends to have low spectral resolution (EarthData 2024c).

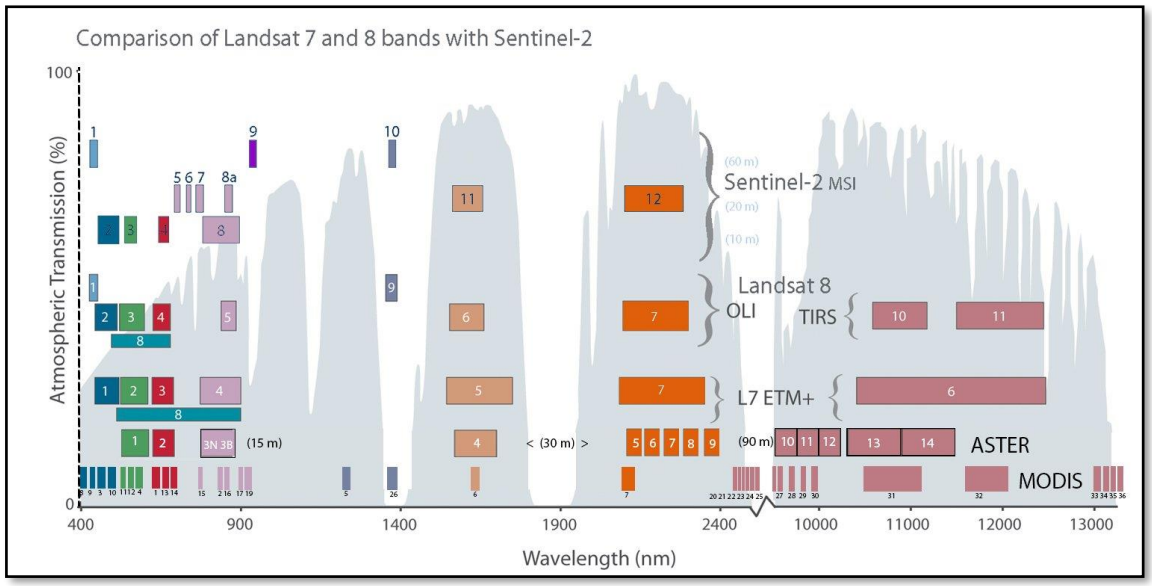

Figure 4.2 Comparison of satellites' bands

4.3 Digital Image Processing

Another important aspect of remote sensing research is data processing and access. The accessibility and ease of use of remote sensing data received from satellites is an element that should be taken into consideration. At this point, MODIS (from the NASA EarthData website), Sentinel (from the Copernicus Open Access Hub website), and Landsat (from the USGS EarthExplorer website) satellites are advantageous because they are accessible and free. At the same time, the raw data from the satellites is processed in a way that researchers can use. Data processing is done by NASA, Copernicus, and USGS respectively for the satellites mentioned above. NASA processes data in various ways, ranging from Level 0 to Level 4. Level 0 is the initial and unprocessed state of the

data coming from the devices. As the level increases, the data is converted into more user-friendly parameters and formats (Chandra, Christopherson, and Casey 2020; EarthData 2024a). It processes data received at MODIS Level 1A, Level 1B, Level 2, Sentinel Level 1C, Level 2A, and Landsat Level 1T, Level 2. The difference between Level 2 and Level 2A is that Level 2A includes additional geometric correction, which enhances geographic accuracy (EarthData 2024c). Consequently, using Level 2 data is more challenging than using Level 2A data, as the user must perform the geometric correction themselves when working with Level 2 data.

Table 4.1 Comparison of Satellites' Features (Source: (Claverie et al. 2018; Copernicus 2024; NASA LANDSAT 2024; NASA MODIS 2024)

FEATURE/SENSORS	MODIS	Sentinel-2	Landsat 8
Source	NASA EarthData website	Copernicus Open Access Hub website	USGS EarthExplorer website
Radiometric Resolution (bits)	12	12	12
Temporal Resolution (days)	1-2 (Terra/Aqua)	5	16
Spatial Resolution (meters)	250, 500, 1000	10, 20, 60	15, 30, 100
Spectral Resolution (Number of Bands)	36	13	11
Data Processing Levels	L0, L1, L2, L3, L4	L0, L1A, L1B, L1C, L2A	L1, L2, L3
Wavelengths (µm)	0.4- 14.4	0.443- 2.190	0.43- 12.51
Launch Date (Earliest Data Available)	1999	2015	2013
TIRS Bands	Band31, Band32	N/A	Band10, Band11

Since all desired features are not available in a single sensor, it is necessary to make an optimal choice that meets our needs. This selection should be made by comparing the features listed in Table 4.1 Comparison of Satellites' Features, and choosing according to the research objective. For example, if detailed information over a narrow area is required, data from the Landsat and Sentinel satellites, which have high spatial resolution, should be preferred. For weather-related research, data with high temporal resolution, such as that from MODIS, would be suitable. If the goal is to observe

changes in land or vegetation cover, data with high spectral and spatial resolution should be chosen. By carefully evaluating these factors, researchers can make informed decisions that align with their specific study requirements, ensuring the most relevant and useful data is utilized.

4.4 Satellite Image Analysis and Visualization Tools

In remote sensing studies, the tools used for data analysis are also of great importance. There are various tools available for utilizing satellite data. Some of the satellite imaging platforms include Google Earth Engine (GEE), Copernicus Open Access Hub, and USGS Earth Explorer. GEE provides free access to a wide range of satellite imagery, such as Landsat, Sentinel-2, and MODIS. The Copernicus Open Access Hub provides free access to satellite imagery from Copernicus satellites including Sentinel-1, Sentinel-2, and Sentinel-3. USGS Earth Explorer provides free access to various satellite images, including those from Landsat and Sentinel-2. These platforms offer an application programming interface (API) and web interface for downloading and processing images. Some of the software used for satellite image analysis includes Sentinel Application Platform (SNAP), ERDAS, R, ENVI, ArcGIS, and QGIS. These tools should be selected based on their functionality, ability to meet needs, ease of use, data accessibility, and capabilities in visualizing, comparing, and analyzing data. By considering these factors, researchers can choose the most appropriate tools to effectively analyze satellite imagery and derive meaningful insights from their remote sensing studies.

The Google Earth Engine (GEE) organizes spatial information, making it easier to process and analyze. This web-based platform allows for easy data combination from multiple sources and simplifies the calculation of regional statistics. Its accessible data sources, cloud-based system that negates the need for data storage, user-friendly interface, and other advantages have made it the chosen analysis tool for this study. In this section of the study, the features that are effective in using the GEE platform, the open-source data set, and its usage methods are mentioned. Google defines GEE primarily as a cloud-based geospatial analysis platform. It is designed for the scientific analysis and visualization of large spatial data sets (Gorelick et al. 2017; Shafizadeh-Moghadam et al. 2021; GEE 2024). It is also a web-based system, accessible for free to scientists and non-

profit organizations via https://earthengine.google.com/. It contains satellite images in large sets of geographic data and allows researchers to detect differences, trends, and changes on the Earth's surface and visualize their results on dynamic maps. The ability to process and analyze multi-petabyte satellite images without the need for downloading and storing them facilitates more efficient and quicker multi-dimensional analysis, making GEE a frequently preferred platform in remote sensing research (Gorelick et al. 2017; Shafizadeh-Moghadam et al. 2021).

GEE's working principle involves analyzing its stored historical and real-time data through various algorithms to meet user needs and visualizing these analyses on spatial representations for "real-world applications"(İneç 2023; GEE 2024). It offers ready-to-use tools and a simplified interface that do not require programming knowledge. The GEE data catalog comprises images from optical and non-optical wavelengths collected from imaging systems that capture environmental variables, climate and weather forecasts, land cover, topography, and socio-economic structures. The GEE data catalog is built with data from satellites such as MODIS (Moderate Resolution Imaging Spectroradiometer), Landsat, and Sentinel.

CHAPTER 5

DATA AND METHOD

Compared to their surrounding regions, urban areas are considered to be more affected by climate change impacts. Given this, examining LST increases, which are one of the most significant indicators of climate change effects, identifying their driving forces, and determining their relationship with urban areas are critical for contributing to the sustainability of planning efforts and future mitigation and adaptation activities. At this point, it is necessary to identify the sprawl tendencies of urban areas and evaluate the impact of this sprawl on LST.

In this section, materials such as spatial-temporal data sets, remote sensing images, software and platforms used, which are necessary for measuring urban sprawl and determining LST and then analyzing the relationship between them, are defined in accordance with the purpose of the study.

5.1 Dataset and Source

In this study, which aims to detect changes in land cover and LST and determine the relationship between them, spatial and temporal analyses are critical. This section explains the data set and analysis tools used for these analyses.

For the analysis of land cover prediction maps created based on the 2030 projection year in the top-scale plans of the study area, the period between 2017 and 2023 was examined. This time interval is the same for all spectral index, land cover change, and LST analyses. During the analysis stage, only data from the summer months (June 1–August 31) were focused on to ensure comparability, consistency of data, and a low number of cloudy days. Thus, inconsistencies due to seasonal changes are minimized.

The study's data set consists of Landsat 8 satellite images obtained from the United States Geological Survey (USGS) source, SRTM Digital Elevation data obtained from NASA, and provincial and district boundaries obtained from the Ministry of National Defense General Directorate of Mapping (MND-GDM) between 2017 and 2023, including the months of June, July, and August. The processing, analysis, and

visualization of the information obtained from the data set were carried out using the Google Earth Engine (GEE) platform and the Statistical Package for the Social Sciences (SPSS) software.

Table 5.1 Information about dataset used

	Data	Description	Data Type	Source
Landsat 8 OLI Bands	SR_B2, SR_B3, SR_B4, SR_B5, SR_B6, SR_B7	Bands required for spectral indices and land cover analysis	Image	USGS
Landsat 8 TIRS Bands	ST_B10	Bands required for land surface temperature analysis	Image	USGS
STRM Digital Elevation	Elevation	Data required for Land Cover Prediction Analysis	Image	NASA
Province and District Boundary	İzmir Provincial and Seferihisar District Boundary	To determine the study area	Spatial- Vector	MND-GDM

In the analysis of the study, spectral bands of the OLI (Operational Land Imager) and TIRS (Thermal Infrared Sensor) sensors of the Landsat 8 satellite, launched in 2013, were used. The characteristics of the bands used are summarized in Table 5.2.

Table 5.2 Features of Landsat 8 OLI/TIRS spectral bands

Band	Spectrum	Wavelength (μm)	Spatial Resolution (m)	Usage Purposes
SR_B2	Blue	0.45- 0.51	30	Bathymetric mapping, vegetation health, atmospheric monitoring
SR_B3	Green	0.53- 0.59	30	Vegetation health, water quality, greenness assessment
SR_B 4	Red	0.64- 0.67	30	Vegetation health, soil and plant differentiation
SR_B 5	Near Infrared (NIR)	0.85- 0.88	30	Vegetation health, water presence, biomass and forest monitoring
SR_B 6	Shortwave Infrared (SWIR) 1	1.57- 1.65	30	Vegetation moisture content, soil and mineral mapping
SR_B 7	Shortwave Infrared (SWIR) 2	2.11- 2.29	30	Vegetation moisture content, soil and mineral mapping
ST_B10	Thermal Infrared (TIR) 1	10.60- 11.19	100	Soil temperature, thermal analysis, surface energy balance

The indicators used for detecting land cover changes, predicting land cover for the year 2030, and analyzing LST based on data obtained from Landsat 8 satellite images are summarized in Table 5.3.

Table 5.3 Information about indicators used

Unit of Analysis	Type of Indicators	Indicators	Data Collection Techniques
Spectral Indices	Spectral Indicator	NDVI	GEE
		NDBI	
		MNDWI	
		NDBaI	
Land Cover Mapping	Spatial Indicators	Sample Points	
Urban Heat Island (UHI)	Thermal Indicator	LST	
		Emissivity	
	Spectral Indicator	Proportion of Vegetation (PV)	
Land Cover Prediction	Temporal Indicator	Land Cover Change	
	Topographic indicators	Digital Elevation Model (DEM)	

5.2 Method

This section of the study comprehensively explains the research method that determined the spatio-temporal parameters of spectral indices, land cover, and LST, and analyzed their correlation. Firstly, obtaining the inputs that form the basis for the research and the preparation stages before the process are mentioned. Secondly, the calculation of the spectral indices used in the research and what they are needed for in the research are

mentioned. Thirdly, the stages of the method used to determine the spatio-temporal variation of LST are explained. Fourth, the method used in land cover classification is explained. Fifth, the method used to determine the relationship between land cover, spectral indices, and LST is described. Finally, the stages of the 2030 land cover estimation method are explained by creating a transition matrix between the 2017 and 2023 land cover classifications. The research method is summarized in the workflow chart Figure 5.1.

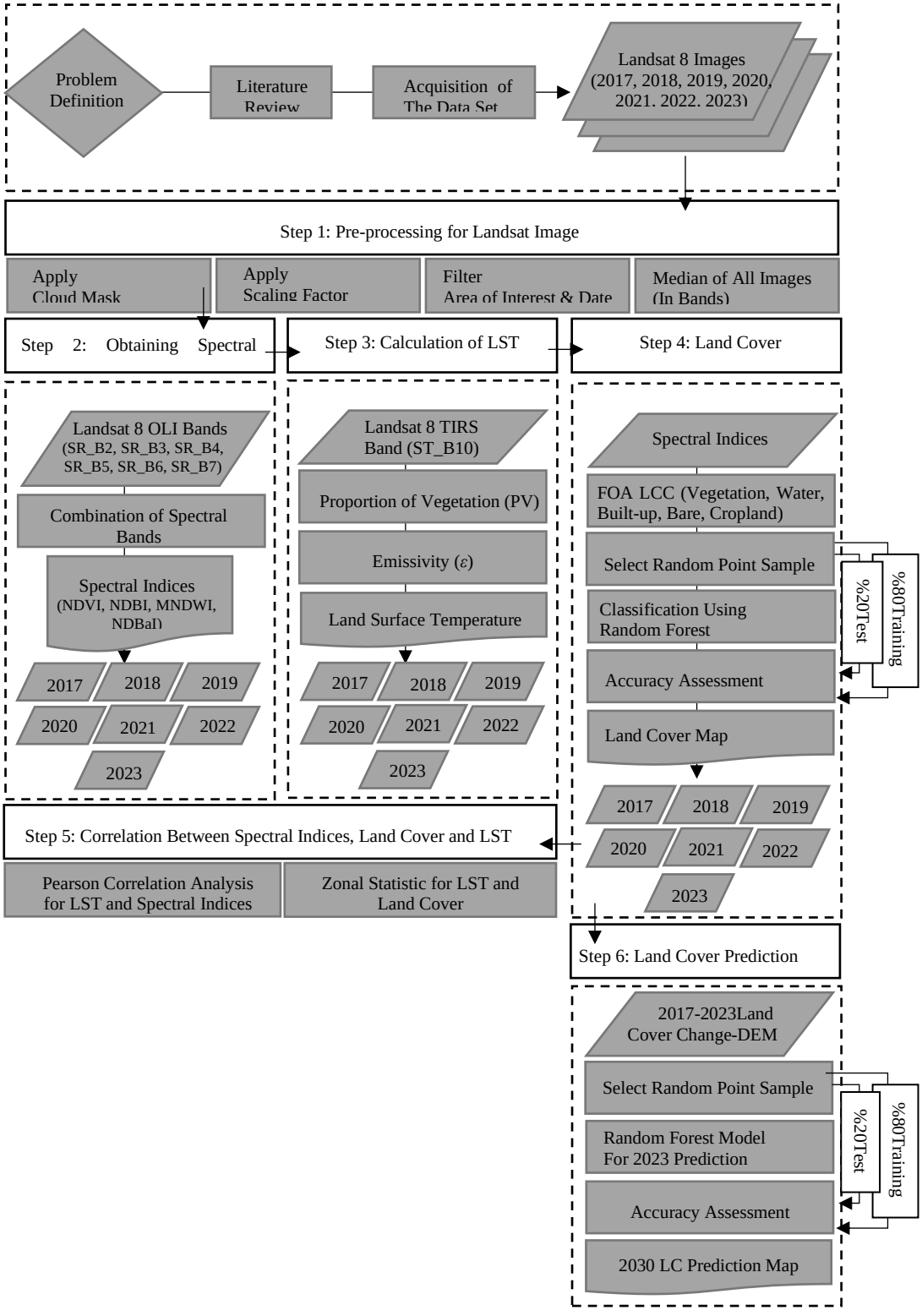

Figure 5.1 Research method flowchart

5.2.1 Preparation of the Remote Sensing Data

In this study, Google Earth Engine (GEE) software was used for processing, analyzing, and visualizing data to examine the relationship between land cover changes and LST. The first step in analyzing remote sensing data on Google Earth Engine or other platforms is importing the data. Before proceeding to other stages of analysis, it is crucial to define the visualization of the data and adjust parameters like brightness levels and color bands. This section explains the process of importing data and adjusting parameters, as outlined below.

Firstly, to perform geospatial analyses, filter the remote sensing data based on the study area's boundaries and specific dates. To ensure spatial standardization of data for all years, it is essential to determine the coordinates of the area of interest. Vector data on provincial and district boundaries obtained from the General Directorate of Mapping was used for this purpose. Data from summer months were chosen to minimize seasonal differences and the number of cloudy days, meaning date filtering was done for the months of June, July, and August for the years 2017 and 2023.

Second, to enhance the accuracy and reliability of the analysis, it is necessary to apply a scaling factor and cloud mask to the median image of the data. Remote sensing data provides raw data at certain scales. The level of processing of the data determines whether it is raw or not (USGS 2024b). Scaling factors are used to convert this raw data into meaningful and physically accurate values. Scaling factors are also used to ensure the comparability and consistency of the data obtained from different satellite images and sensors. This allows for consistent analysis between images taken at different times in the same region or between data from different sensors. For example, Landsat data is multiplied by a specific factor to convert to percentage reflectance values (i.e., Digital Number (DN) * scale factor + offset) (NASA LANDSAT 2024). As mentioned in Chapter 4, passive satellite sensors are unable to penetrate cloud cover, reducing observation capability in cloudy areas and decreasing analysis accuracy. Therefore, to minimize the error rate in the analysis, cloud and cloud shadow masks are used. Cloud masks identify cloudy regions in images and exclude these regions from the analysis.

5.2.2 Obtaining Spectral Indices

Spectral indices are ratios or formulas obtained from remote sensing data and calculated using combinations of specific spectral bands. These indices are used to identify and analyze different surface features or conditions. In this part of the study, to be used to detect the change in land cover and estimate LST, obtaining four spectral indices (NDVI, NDBI, MNDWI, and NDBal) and why they are used are explained.

Table 5.4 Equation of spectral indices

Indices	Equation	Reference
Normalized Different Vegetation Index	$NDVI = \frac{(\text{NIR} - \text{RED})}{(\text{NIR} + \text{RED})}$	Rosue et al., 1973
Normalized Different Built-up Index	$NDBI = \frac{(\text{SWIR1} - \text{NIR})}{(\text{SWIR1} + \text{NIR})}$	Zha et al., 2003
Modified Normalized Different Water Index	$MNDWI = \frac{(\text{GREEN} - \text{SWIR1})}{(\text{GREEN} + \text{SWIR1})}$	Xu, 2006
Normalized Different Bareness Index	$NDBaI = \frac{(\text{SWIR1} - \text{TIR1})}{(\text{SWIR1} + \text{TIR1})}$	Chen et al., 2006

5.2.2.1 Normalized Difference Vegetation Index (NDVI)

Normalized Difference Vegetation Index (NDVI) is an indicator used to measure the density and vigor of vegetation, making it useful for classifying land cover into green areas and agricultural fields as well as for estimating LST. NDVI is calculated using the red and near-infrared (NIR) bands. NDVI values range from -1 to 1, with higher values indicating greater density and vitality of vegetation (Deilami, Kamruzzaman, and Liu 2018; Jaiswal, Jhariya, and Singh 2023).

$$NDVI = \frac{(\mathrm{NIR} - \mathrm{RED})}{(\mathrm{NIR} + \mathrm{RED})}$$

(1)

Values close to -1: indicate areas with water, clouds, or snow.

Values near 0: correspond to bare soil or built-up areas with little to no vegetation.

Values between 0.2 and 0.5: indicate sparse vegetation.

Values above 0.5: signify dense and healthy vegetation.

By analyzing NDVI values, vegetation over time can be effectively monitored and classified; this is critical for understanding environmental changes and their effects on the ecosystem. Additionally, since dense vegetation is typically associated with lower surface temperatures due to shading and transpiration effects, NDVI can be used to estimate LST. This makes NDVI an important tool in remote sensing for environmental monitoring and urban planning.

5.2.2.2 Normalized Difference Built-up Index (NDBI)

Normalized Difference The built-up index (NDBI) is a spectral index derived from satellite imagery used to detect urban areas or built-up regions. It is an essential parameter for monitoring urban sprawl and change over time. NDBI is calculated using the shortwave infrared (SWIR1) and near-infrared (NIR) bands, and its values range from -1 to 1 (Jaiswal, Jhariya, and Singh 2023; ESRI 2024b).

$$NDBI = \frac{(\mathrm{SWIR1} - \mathrm{NIR})}{(\mathrm{SWIR1} + \mathrm{NIR})}$$

(2)

Values close to -1: indicate the presence of vegetation, water bodies, or bare soil, which are non-built-up areas.

Values around 0: Correspond to mixed areas where built-up areas and other land covers coexist.

Values above 0.5: signify densely built-up areas.

By analyzing NDBI values, urbanization patterns and the extent of residential areas can be effectively monitored and classified. This index helps track the expansion of urban areas and assess the impact of urbanization on the environment. Identifying and monitoring built-up areas using NDBI is very important for urban planning, infrastructure development, and environmental management.

5.2.2.3 Modified Normalized Difference Water Index (MNDWI)

MNDWI is used for detecting open water bodies, evaluating water presence, and analyzing changes in water areas. NDWI was calculated by McFeeters in 1996 using green and near infrared (NIR) bands to improve the water-related features of landscapes. However, it was modified by Xu (2006) because the NIR band perceives water areas as black and does not give completely accurate data. In its modified form, MNDWI is calculated using green and SWIR1 bands. MNDWI ranges from -1 to 1 (Xu 2006).

$$MNDWI = \frac{(\text{GREEN} - \text{SWIR1})}{(\text{GREEN} + \text{SWIR1})} \quad (3)$$

Values close to -1: indicate areas without water, such as bare soil or built-up areas.

Positive values (0 to 1): represent mixed areas with both the presence of water bodies, with higher values corresponding to more significant water content and other land cover.

Analyzing MNDWI values allows for effective monitoring and mapping of water bodies, monitoring changes over time, and assessing the impact of environmental changes on water resources. MNDWI is particularly useful in environmental monitoring as it helps distinguish water features from other land cover types and assess their extent and dynamics.

5.2.2.4 Normalized Difference Bareness Index (NDBaI)

Normalized Difference the Bare Land Index (NDBaI) is a spectral index used to detect bare soil areas. It helps identify bare soil and vegetation-free areas on the land

surface. NDBaI is useful for detecting fallow or unplanted fields in agricultural areas and monitoring deforested or tree-less areas in forested regions (Li and Chen 2014; Chen et al. 2006; Sun, Wu, and Tan 2012).

$$NDBaI = \frac{(\text{SWIR1} - \text{TIR1})}{(\text{SWIR1} + \text{TIR1})} \quad (4)$$

Negative values: Indicate the presence of vegetation or water bodies.

Values around 0: represent a mix of bare soil and other land cover types.

Positive values: Indicate bare soil areas, such as beaches, bare land, and areas under development.

By analyzing NDBaI values, changes in bare soil areas over time can be monitored, and the impact of land cover changes on soil exposure can be assessed. NDBaI is particularly useful in land classification and environmental monitoring as it helps distinguish bare soil from vegetation and water-covered areas and assess their extent and dynamics.

5.2.3 Calculation of the Land Surface Temperature (LST)

LST is a measurement expressing the temperature of the earth's surface. The LST is examined to determine the UHI effect. By examining LST, environmental and climatic data are integrated, allowing precise measurement of the thermal properties of different surface types and comprehensive analysis and modeling studies. LST is measured using land-surface emissivity and thermal infrared sensors. In this section, the necessary steps to obtain LST are explained.

Emissivity, which is the ability of materials to emit thermal radiation, is an important parameter at this point. In order to obtain the LST, it is first necessary to calculate the emissivity value. (Sobrino, Jiménez-Muñoz, and Paolini 2004) obtain emissivity by using the relative density ratio of vegetation. Using the obtained NDVI values, it is possible to measure the relative density of vegetation cover in the study area. This measurement is called the proportion of vegetation (PV). PV represents the ratio of

vegetation cover to the total land area. A high PV value indicates a high presence of vegetation in the region (Sobrino, Jiménez-Muñoz, and Paolini 2004).

$$Pv = \left(\frac{NDVI - NDVI_{min}}{NDVI_{max} - NDVI_{min}}\right)^2$$

(5)

Emissivity ranges from 0 to 1, with a value closer to 1 indicating a higher ability of the material to absorb and emit thermal radiation. Emissivity varies depending on the wavelength of the measured material. Therefore, to determine emissivity, the wavelength of the material must be within the range of the measured thermal band's wavelength. Knowing and calibrating the wavelengths of the bands and the thermal radiation emitted by the material is crucial for obtaining accurate temperature measurements.

$$\varepsilon = \varepsilon v * Pv + \varepsilon s * (1 - Pv) + d\varepsilon$$

(6)

where εv refers vegetation emissivity (average 0.96-0.99) and εs refers soil emissivity (average 0.95-0.98) (Demirkesen and Evrendilek 2017) and $d\varepsilon$ refers to the roughness of the surface of natural areas ($d\varepsilon=(1- \varepsilon s)(1- Pv)0.55\ \varepsilon v$), (Sobrino, Jiménez-Muñoz, and Paolini 2004). According to the explanation of Sobrino, Jiménez-Muñoz, and Paolini (2004) when the constants of soil and vegetation emissivity were placed in the formula, the final form of the formula was determined as;

$$\varepsilon = 0.004Pv + 0.986$$

(7)

where 0.004 is constant of average emissivity of soil and 0.986 constant of average emissivity of vegetation (Rasul 2023).

Another important parameter for calculating LST is the data obtained from the TIRS of the Landsat 8 satellite. Surface temperature is obtained using TIRS band 10. Since Band10 gives the temperature value in Kelvin, it is used in the LST calculation by

subtracting the value of 273.15. In line with all this information, the method of calculating LST maps is specified in equation (8).

$$LST = \frac{\mathrm{TB}}{1 + \left(\lambda * \left(\frac{\mathrm{TB}}{\rho}\right)\right) * \log(\varepsilon)} \quad (8)$$

where TB denotes 273.15 subtracted from the ST_B10 band of Landsat 8 OLI/TIRS Collection 2 atmospherically corrected surface reflectance images, λ is the central band wavelength of the emitted radiation (10.8 μm for Band10), ρ a is a constant value formed by Plank's formula (h) and Distortion (σ) constant and light speed values (c), that is, (ρ=h*c/σ=1.438x10-2 m K), (Dissanayake et al. 2019) ε represents the land-surface emission value estimated using equation (7).

5.2.4 Land Cover Classification

In the study, land cover between the years 2017 and 2023 was calculated using spectral bands. For each time interval, land cover classification was conducted using supervised learning methods and the random forest algorithm, leveraging the quantitative analysis and visual interpretation capabilities of the machine learning technique. This section systematically explains the steps of land cover classification.

First, supervised sample data were prepared for model training. Supervised sample data were determined using images created from a combination of red, green, and blue (RGB) bands, showing the earth's surface in natural colors for each year. 80% of this data was used as training samples to classify satellite images, while 20% was used as test samples to validate the classification results (Lee, Acharya, and Lee 2018). The reference data was selected to distinguish the features of land cover and to be spatially homogeneous. An average of 300 sample pixels was created for each year. For use in training data, five classes were determined according to the classification standard specified in the Food and Agriculture Organization (FAO)'s Land Cover Classification System (LCCS). These classes are water, bare land, cropland, vegetation, and built-up.

The characteristics of the classes are summarized in Table 5.5 Characteristics of land cover classes.

Table 5.5 Characteristics of land cover classes

Class	Spectral Characteristics	Physical Features	Visual Characteristics
Water	Low reflectance, very low in Green and SWIR bands	Rivers, lakes, seas, reservoirs, wetlands	Dark blue tones
Bare Land	High reflectance, especially in Red, NIR and SWIR bands	Bare soil, rocky areas, sandy regions, quarries, construction sites	Light brown tones
Cropland	Reflectance varies with crop growth cycles, generally Red, NIR	Cultivated fields, orchards, vineyards, greenhouses, fallow lands	Light green tones
Vegetation	High reflectance, especially in NIR bands	Forests, shrublands, grasslands, savannas, natural parks and protected areas	Green tones, dense vegetation appears dark green
Built-up	Medium to high reflectance, especially in NIR, SWIR1, SWIR 2 bands, distinct spectral signatures of concrete and asphalt	Buildings, roads, railways, industrial areas, urban centers, airports, ports, infrastructure	Gray, white, or light brown tones, regular street patterns and building structures

Secondly, land cover estimation was performed using the random forest algorithm, as it combines multiple decision trees to create a stronger model with higher generalization capability. In this study, the random forest model has 300 decision trees.

Finally, the accuracy and generalization ability of the resulting land cover model were checked using the test set data in GEE. Accuracy assessment is done automatically using the code cloud available on the GEE platform. For this purpose, a confusion matrix was produced, and based on this matrix, accuracy indices such as Overall Accuracy (OA), Producer Accuracy (PA), User Accuracy (UA), and the Kappa Coefficient were

calculated. Overall accuracy is computed as the ratio of all correct classifications to the total number of samples, which indicates how accurately the model classifies overall (Rasul 2023). Producer accuracy is the rate at which the model correctly classifies a specific class, evaluating the model's ability to recognize a particular class and comparing performance across classes. User accuracy is the ratio of correctly classified samples for a particular class to all samples predicted as that class, assessing the model's reliability and accuracy for a specific class (Rasul 2023). The Kappa Coefficient measures the model's classification accuracy compared to random classification, taking into account the possibility that the correct classifications occur by chance, thus going beyond OA (Bhandari, Saud, and Mahatara 2023; Rasul 2023). The calculation methods are summarized in Table 5.6. In academic studies and image processing methods, accuracy values are expected to be in the range of 85–90%, and a Kappa coefficient above 0.6 is generally considered acceptable performance (Bhandari, Saud, and Mahatara 2023).

Table 5.6 Evaluating the accuracy of the classification model (Source: (Bhandari, Saud, and Mahatara 2023; Rasul 2023)

Metric	Calculation Formula	Explanation
Overall Accuracy (OA)	$\mathrm{OA} = \frac{\text{Ratio of All Correctly Classified Samples}}{\text{Total Number of Samples}}$	Summarizes the overall performance of the model.
Producer Accuracy (PA)	$\mathrm{PA} = \frac{\text{Ratio Of Correctly Classified Samples of a Particular Class}}{\text{Total Actual Samples of That Class}}$	Indicates how well a class is identified by the model.
User Accuracy (UA)	$\mathrm{OA} = \frac{\text{Ratio Of Correctly Classified Samples of a Particular Class}}{\text{Total Samples Predicted as That Class}}$	Indicates the reliability of the model in predicting a specific class
Kappa Coefficient	$\mathrm{OA} = \frac{\text{Observed Accuracy} - \text{Expected Accuracy}}{1 - \text{Expected Accuracy}}$	Compares the classification accuracy of the model to random classification.

5.2.5 Identifying the Relationship between Spectral Indices, Land Cover and LST

In this section of the study, the analyses conducted to determine the relationship between spectral indices, land cover, and LST are explained. This section consists of two stages: the first stage involves a Pearson correlation analysis to examine the relationship between spectral indices and LST, and the second stage involves a Zonal statistics analysis to determine the relationship between changes in land cover and LST.

The correlation coefficient indicates whether the relationship between two variables is positive or negative and how strong that relationship is. Therefore, in this section of the study, the steps of the correlation analysis conducted to observe the effect of spatial parameters on LST are discussed.

To observe the effect of spectral indices on LST, a Pearson Correlation Analysis was conducted using the IBM-SPSS statistics program, based on data from the year 2023. The correlation coefficient indicates whether the relationship between two variables is positive or negative and how strong that relationship is. For this analysis, 3000 random points were assigned to maps prepared in Google Earth Engine using the "randomPoints" command, and the data at each point was collected in an Excel file. These points were evenly distributed across the entire study area. The data was then completely entered into SPSS. Using the "Bivariate" tool, the results included the Pearson correlation coefficient (r), the mean and standard deviation values of the variables, and the sample size (N) (Guo et al. 2020; Yin et al. 2018). The correlation coefficient (r) ranges from +1 to -1; +1 indicates a perfect positive relationship, -1 indicates a perfect negative relationship, and 0 indicates no relationship at all (Kent 2024).

r=0.00−0.19: Very weak relationship

r=0.20−0.39: Weak relationship

r=0.40−0.59: Moderate relationship

r=0.60−0.79: Strong relationship

r=0.80−1.00: Very strong relationship

To examine how changes in land cover affect LST, Zonal Statistics analysis was conducted, which is used to monitor the specific characteristics of geographic regions or areas and obtain summary statistics. This method is not frequently used on the Google Earth Engine platform. Therefore, the Zonal Statistics analysis was carried out by

transferring the land cover and LST raster data obtained from GEE to the ArcMap program (ESRI 2024a). Using the "Zonal Statistics Tool" in ArcMap, the LST values for land cover classes between the years 2007 and 2023 were obtained.

5.2.6 Prediction of Land Cover

Predicting land cover is an important analysis for conducting sustainable planning studies and accelerating the processes of developing adaptation and mitigation strategies against climate change. In this study, it was aimed to predict land cover based on the 2030 projection year in upper-scale plans. To perform the prediction analysis, the transition matrix of land cover classifications for the years 2017 and 2023 was created using the random forest method in GEE. Then, DEM data was added to the dataset. Initially, a 2023 land cover prediction was made to test the accuracy of the prediction. Subsequently, the land cover for the target year of 2030 was generated.

There are many different methods to predict and simulate changes in land cover. One of these methods is the random forest model (Sales et al. 2022). This method provides more accurate results compared to other methods because it is more resistant to outliers and noise. Random forest creates multiple decision trees by randomly selecting subsets of the original training dataset and then replacing them with new ones for ensemble tree training (Asif et al. 2023). In this study, a random forest model consisting of 150 trees was used to predict land cover.

CHAPTER 6

CASE STUDY

The research takes place in the geographical region known as the case study. A pilot LST study for 2023 was conducted to select the study area. The pilot study involves conducting LST analysis (Formula 8) across İzmir province using data obtained from the spectral bands of the OLI and TIRS sensors on the Landsat 8 satellite.

In addition to LST data, considering the most important criteria urban sprawl such as low density, population increase, and economic development, and observational elements, the districts of Urla, Güzelbahçe, Çeşme, Karaburun, and Seferihisar in the province of Izmir stand out in terms of sprawl. Therefore, the pilot study focused on these districts, which are similar in physical, economic, and social aspects.

According to the results of the pilot study conducted for 2023, among the districts of Urla, Güzelbahçe, Çeşme, Karaburun, and Seferihisar; Seferihisar (51 °C) district and a part of Çeşme (53°C) district had higher surface temperatures (Figure 6.1Figure 6.1 LST pilot study conducted across İzmir province). The lowest LST in the region are generally concentrated in Karaburun (18°C). The districts of Urla and Güzelbahçe do not reach very high LST, having occasionally low to medium LST. When examining LST map, the districts of Çeşme and Seferihisar, which have high LST values, stand out. However, in the district of Çeşme, areas with high LST values fall outside the urban settlement area, while in the district of Seferihisar, areas with the highest LST values are within the settlement area. As a result of this evaluation, it was deemed appropriate to focus on the district of Seferihisar for this study.

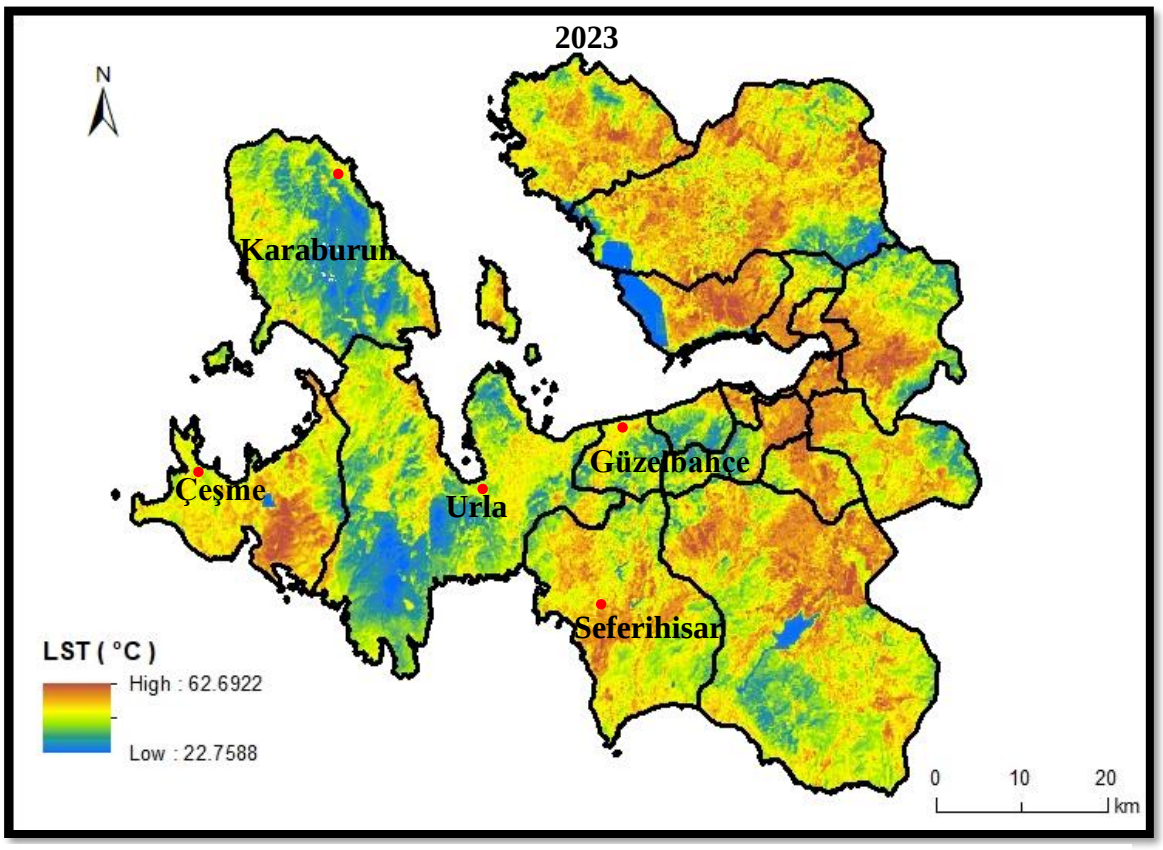

Figure 6.1 LST pilot study conducted across İzmir province in 2023

Seferihisar district in İzmir province was selected as the study area in line with the research objectives. Seferihisar is a region with a coastline along the Aegean Sea, characterized by high tourism potential and a tranquil urban lifestyle. In recent years, the area has drawn attention due to rapid urbanization, its preference as a secondary housing area, and rising land prices (Endeksa 2024). Its proximity to the city center and its non-rural nature make it highly exposed to urban sprawl (IZBB 2012). This situation contributes to the intensifying UHI effect, which impacts the local climate, environmental conditions, and socio-economic development.

One of the main reasons why Seferihisar was chosen as the study area is that it is under the pressure of urban sprawl and has a structure where urban areas, rural areas, and natural areas coexist, allowing the UHI effect to be observed. In particular, the problem of the fringe area between Güzelbahçe and Seferihisar being covered with partial construction for residential purposes is an issue that is also emphasized in the 1/25000 Scale İzmir Metropolitan Municipal Environmental Plan Explanation Report (this will be

referred to as the 1/25000 Scale Environmental Plan in the remainder of the study). This issue had a significant impact on the study area selection.

In this section of the study, the physical, social, and economic characteristics of Seferihisar district are examined, and the reasons for its selection as the study area are explained in detail.

6.1 Geographic Location

İzmir, Türkiye's third-largest city in terms of population, is located in the Aegean Region in the west of Türkiye, between 37° 45' and 39° 15' north latitudes and 26° 15' and 28° 20' east longitudes. The length of the city in the north-south direction of the province is approximately 200 km, and its width in the east-west direction is 180 km. Its surface area is 12,012 km^2 (Izmir Governorship 2024a).

Seferihisar is a district of İzmir province and is located between 26°45'00" and 27°01'30" eastern longitudes and 38°17'00" and 38°02'00" northern latitudes. It is surrounded by Urla in the north, Güzelbahçe and Karabağlar in the northeast, Menderes in the east, and the Aegean Sea in the south and west. Its surface area is 375 km^2 (GDM 2024). The location of the work area is an important criterion in choosing the work area. Because it is on the coast of the Aegean Sea and close to the city center of İzmir, the city is becoming a center of attraction and receives intense immigration (IZBB 2012). Therefore, there tends to be urban sprawl.

In Seferihisar district, with the Metropolitan Municipality Law No. 5216, accepted on July 10, 2004, the towns that previously had 2 towns (Doğanbey-Payamlı and Ürkmez) and 9 villages were closed, and the villages lost their legal entities and became neighborhoods.

Seferihisar District, one of the 30 districts of İzmir, consists of 21 neighborhoods. These are: Atatürk, Bengiler, Beyler, Camikebir, Çamtepe, Çolakibrahimbey, Cumhuriyet, Düzce, Gödence, Gölcük, Hıdırlık, İhsaniye, Kavakdere, Orhanlı, Payamlı, Sığacık, Tepecik, Turabiye, Turgut, and Ulamış (Figure 6.2). The works carried out in Seferihisar are carried out under the responsibility of İzmir Metropolitan Municipality and Seferihisar District Municipality.

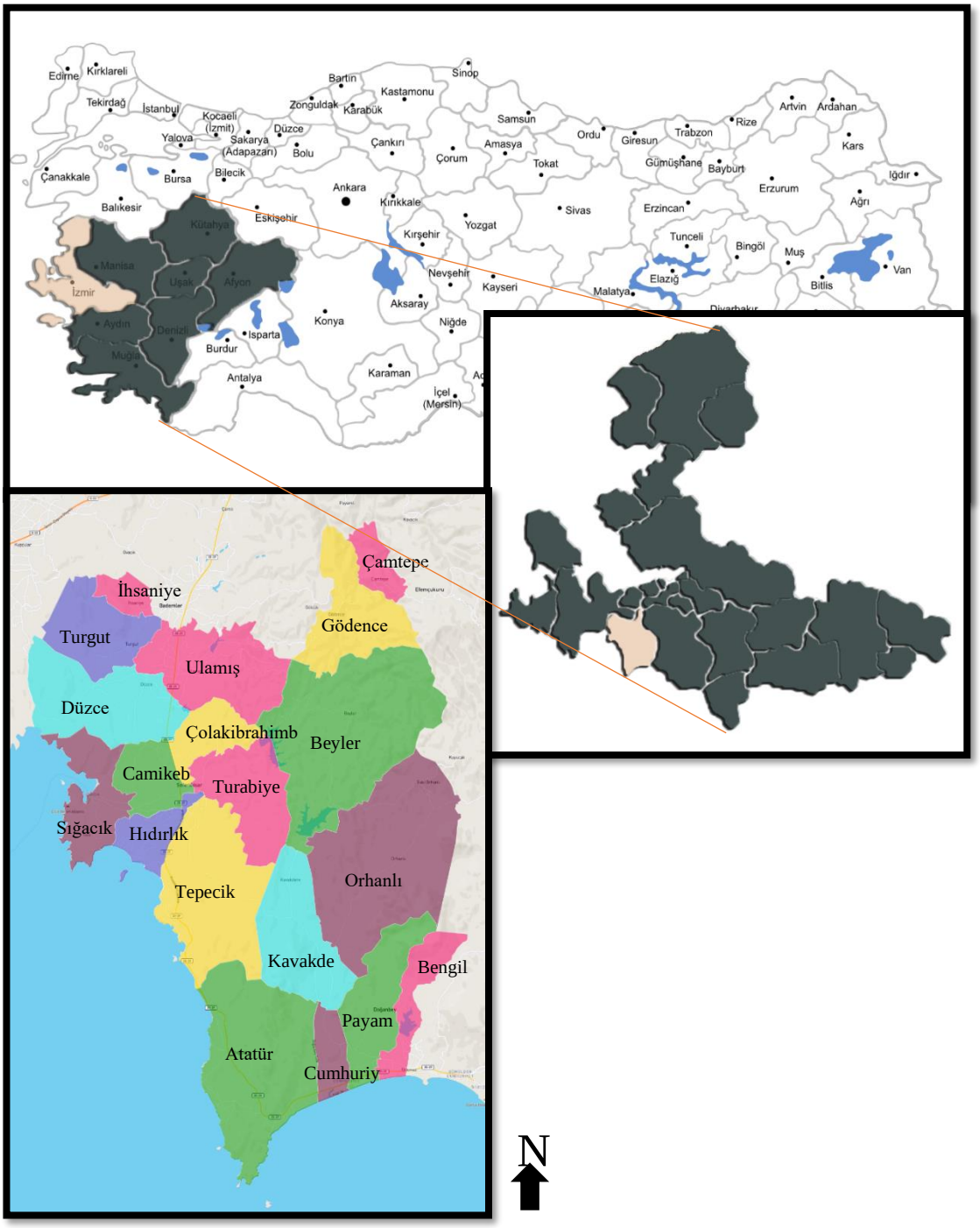

Figure 6.2 Case study location within country, region, province border and it's administrative division (Source: (AtlasBig 2024))

6.2 Seferihisar and Its Planning History

The study area is located within the borders of İzmir province, located in the west of Türkiye, and in the 1/100,000 scale Environmental Plan on sheets numbered L17, L18 (Figure 6.3), 1/25,000 scale Environmental Plan on sheets numbered 17-B-3, L17-B-4, L17-C-1, L17-C2, L17-C3, L17-C-4, L18-D-1, L18-D-4 (Figure 6.4), in an area of approximately 366 km2.

When examining the upper-scale Environmental Plans of the study area, it is observed that the area is predominantly proposed for tourism and residential functions. In the coastal areas, construction is generally for tourism purposes, while in and around the district center, development is observed for residential purposes. The majority of the construction in the region occurs around the roadway extending from the district center to the city center. The proposed development of residential areas is predominantly focused on the Seferihisar district center. The nature of the constructions in the coastal areas is generally for tourism purposes. The built-up area in the 1/25000 Scale Environmental Plan has more than doubled to current area in parallel with the projected 2030 population. When examining the population of the 1/25,000 scale plan's year of creation and the projected population for 2030, the population of Urla is determined to increase from 51,880 to 159,788, and the population of Seferihisar from 30,890 to 142,275. Projection population for Güzelbahçe, Çeşme, and Karaburun districts has not been specified (IZBB 2012).

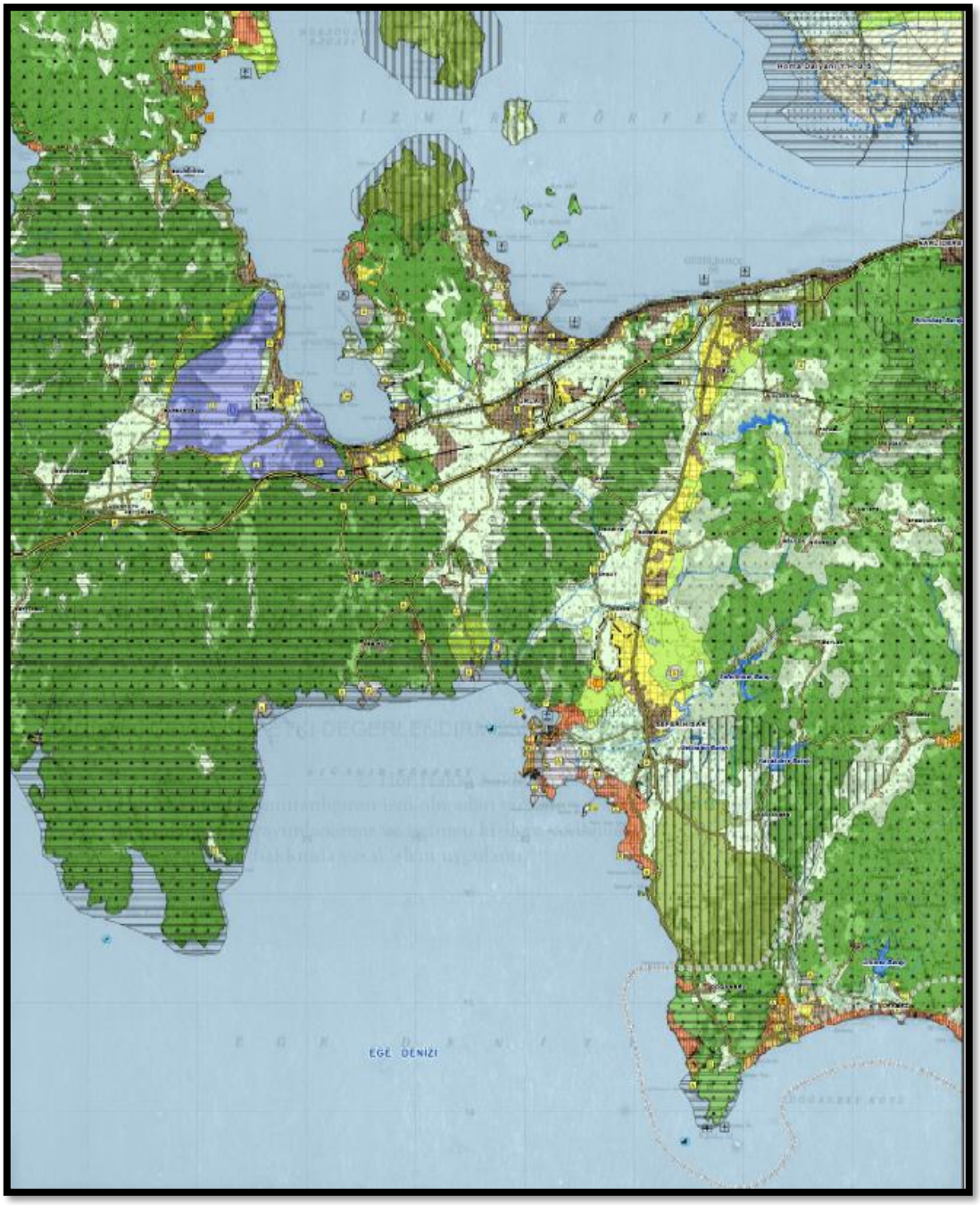

Figure 6.3 İzmir-Manisa Planning Region 1/100.000 Scale Enviromental Plan L17 (Source: (CSB 2024))

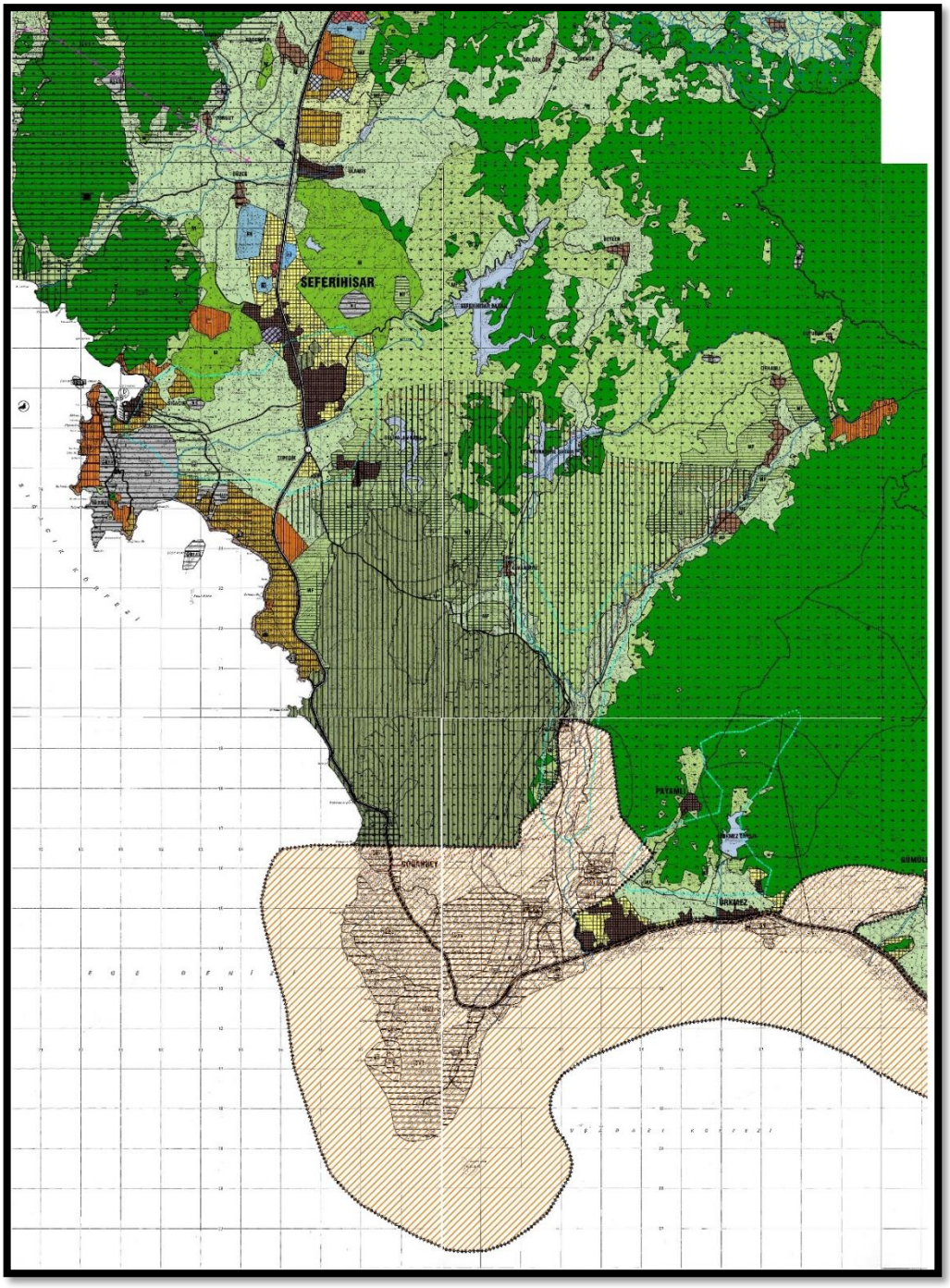

Figure 6.4 İzmir-Manisa Planning Region 1/25.000 Scale Enviromental Plan (L17-B3, L17-B4, L17-C-1, L17-C-2, L17-C-3, L17-C-4, L18-D-1, L18-D-4) (Source: (IZBB 2012)

6.3 Transportation Network

Road Transportation: Seferihisar district is 47 km away from İzmir city center, and transportation to the center is provided by road. There are two state highway lines from İzmir to the south. The first line follows the Aegean Sea coast to Seferihisar and Kuşadası; the second one reaches Aydın parallel to the İzmir-Aydın highway (IZBB 2012). Seferihisar district is 20 km away from the D-300 state highway, which starts from Çeşme and extends to Iran, and the E881 European road, which starts from Çeşme and extends to Gebze. Its proximity to the E881 highway is important, as its connection with Istanbul is strengthened. The distance to the intercity bus terminal is 67 km. In addition, the 2030 targets of the İzmir Transportation Master Plan include the highway and bicycle path connecting Seferihisar district to the center (

Figure 6.6,).

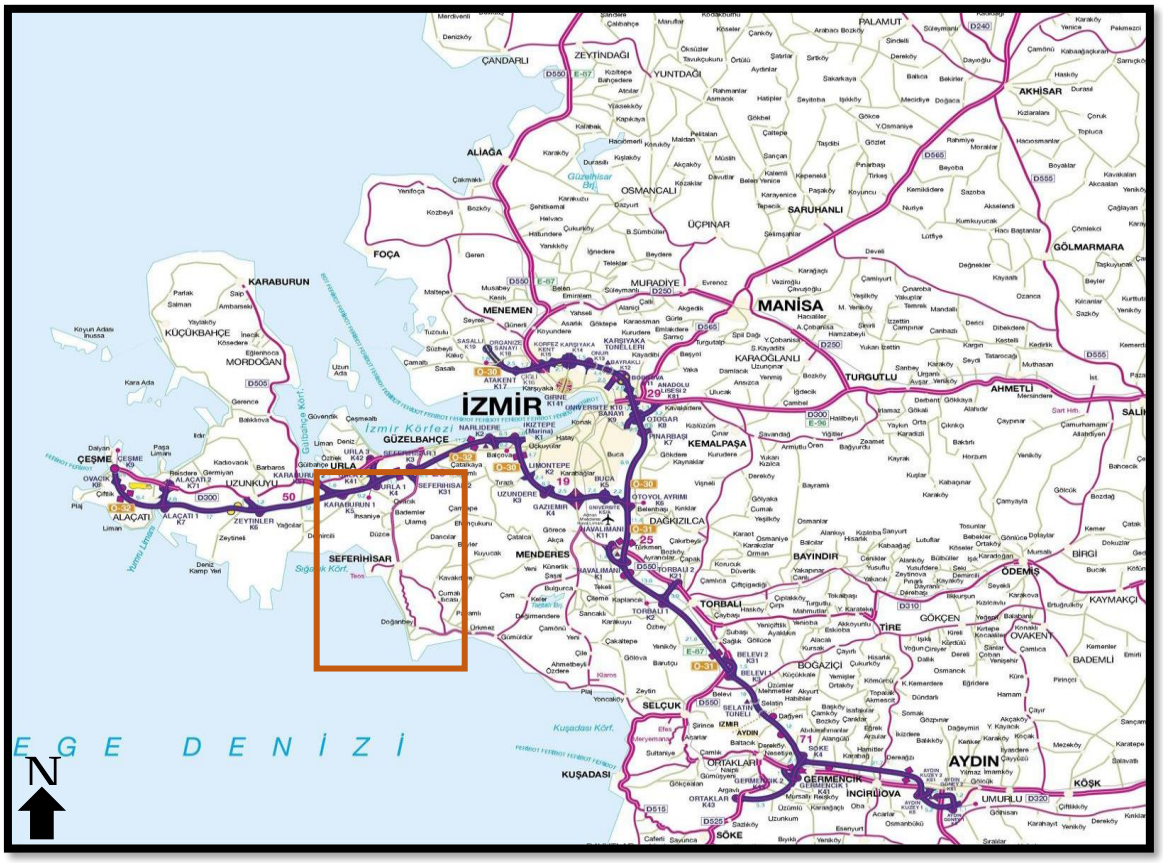

Figure 6.5 Izmir surroundings highway and motorway map. (Source: (IZBB 2012)

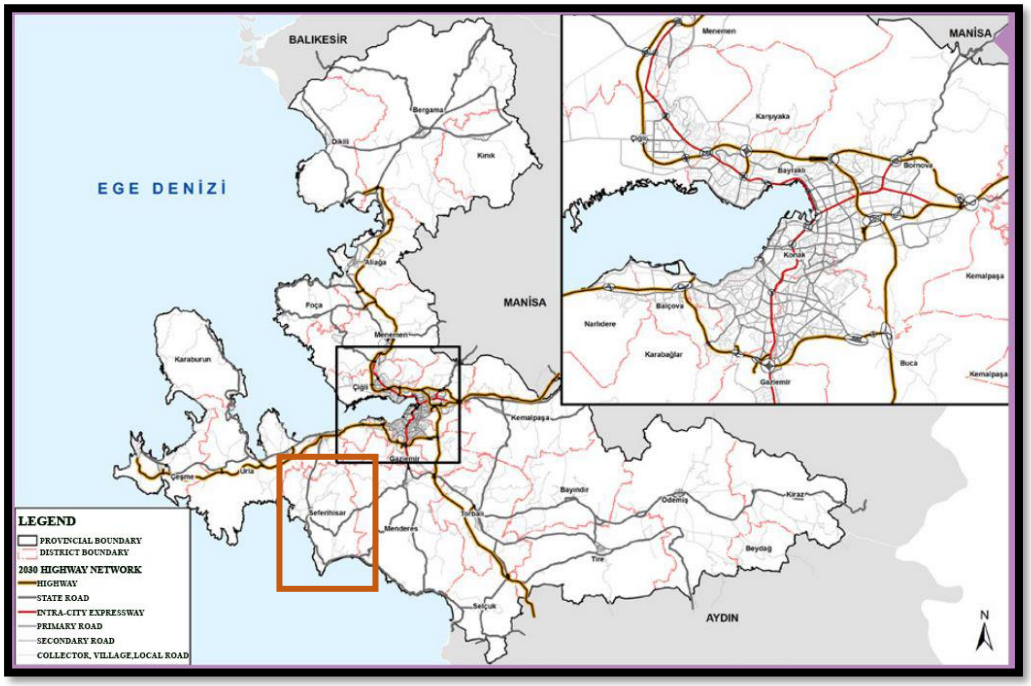

Figure 6.6 İzmir province 2030 highway network (Source: (IZBB 2019))

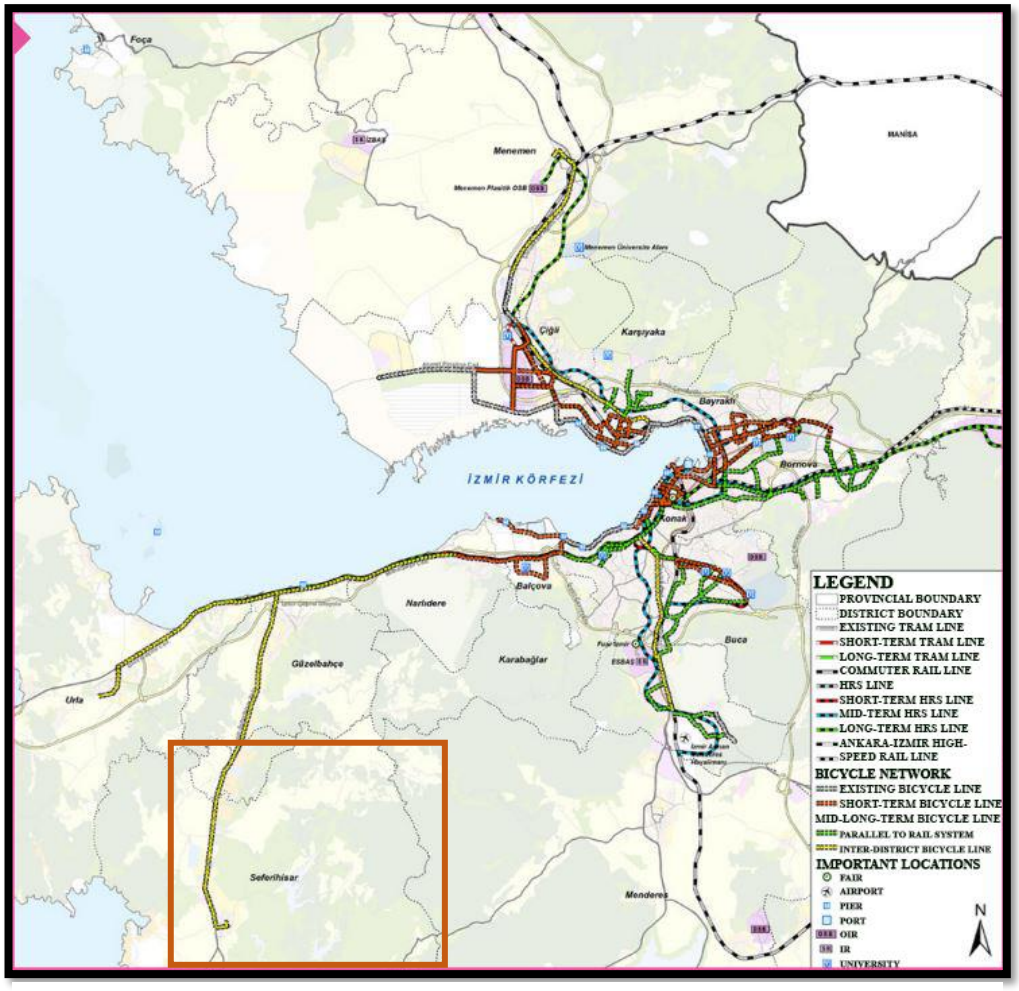

Figure 6.7 İzmir province 2030 bicycle path network (Source: (IZBB 2019))

Air Transportation: There is no airport in the study area. The nearest airport, Adnan Menderes Airport, is 45 km away.

Sea Transportation: There are many marine structures such as fishing shelters, on the coast of Seferihisar Sığacık that also serve yachts, etc. During the summer months, transportation from the center is possible by sea bus. The distance to the nearest port, Alsancak, is 55 km.

Railway Transportation: The İzmir-Aydın railway line, built in 1876, extends into the Küçük and Büyük Menderes valleys and reaches product collection centers such as Tire, Bayındır, Seferihisar, and Çivril. The district, which has no railway connection, is 45 km away from the nearest train station and 39 km away from the nearest metro station.

The expansion and improvement of transportation networks change cities' physical and economic structure, create new development areas, and determine how they

grow. Therefore, examining the current and planned transportation infrastructure of Seferihisar district is important in terms of interpreting the urban sprawl trend. In particular, the impact of the İzmir-Istanbul highway, opened in 2019, on the population mobility of the region and the idea that the planned highways and bicycle paths will strengthen this effect were taken into account in the selection of the study area.

6.4 Demographic Structure

According to the 2023 Address-Based Population Registration System results and 2022 internal migration statistics published by TURKSTAT, İzmir is the third province in Türkiye with the highest population and among the provinces that receive the most immigration (TURKSTAT 2024a).

According to the TURKSTAT Address Based Population Registration System, when comparing the population data of Seferihisar, Urla, Güzelbahçe, Çeşme, and Karaburun districts, it is evident that the population in all districts generally increased from 2007 to 2023. Seferihisar and Urla show the most significant increases, with Seferihisar's population rising from 25,830 in 2007 to 58,570 in 2023, and Urla's population growing from 48,058 in 2007 to 77,599 in 2023. Güzelbahçe's population nearly doubled, increasing from 19,255 in 2007 to 38,044 in 2023. Çeşme's population rose from 27,796 in 2007 to 50,028 in 2023, showing a notable increase. Although Karaburun had a lower population growth compared to other districts, its population still grew from 8,040 in 2007 to 13,379 in 2023. The period after 2020 saw a significant increase in population in all districts, which could be attributed to a rise in migration to rural and coastal areas due to the pandemic (TURKSTAT 2024b).

Table 6.1 Population of the districts between 2007 and 2023 (Source: (TURKSTAT 2024b)

POPULATION					
YEARS	**Seferihisar**	**Urla**	**Güzelbahçe**	**Çeşme**	**Karaburun**
2007	25830	48058	19255	27796	8040
2008	26945	49774	22138	31968	9224
2009	28603	50609	24296	32475	8889
2010	32655	52500	24462	33051	8689
2011	30890	53417	25335	33931	8848
2012	31467	54556	28469	34563	8799
2013	33588	56751	27389	35965	9092
2014	35960	59166	28470	39243	9456
2015	36335	60750	29774	39243	9403
2016	37697	62439	29835	40312	9575
2017	40785	64895	31429	41278	9812
2018	43546	66360	32592	43489	10603
2019	44526	67339	33592	44363	10759
2020	48320	69550	33727	46093	11329
2021	52507	72741	37572	48167	11927
2022	54993	74736	37753	48924	12200
2023	58570	77599	38044	50028	13379
Total Change	126.75%	61.47%	97.58%	79.98%	66.41%

Seferihisar district has the highest annual population growth rate in İzmir province at 4.63% (ITO 2023). When examining the population growth rate graph derived from TURKSTAT data (Table 6.1), it is evident that population mobility has a fluctuating pattern. However, a significant increase in the population growth rate is noticeable, particularly after 2016. This increase indicates that Seferihisar is becoming a more popular residential area. Since 2020, the population has been observed to increase by an average of 3,000 to 5,000 people annually, demonstrating the dynamic and growing nature of the region's demographic structure.

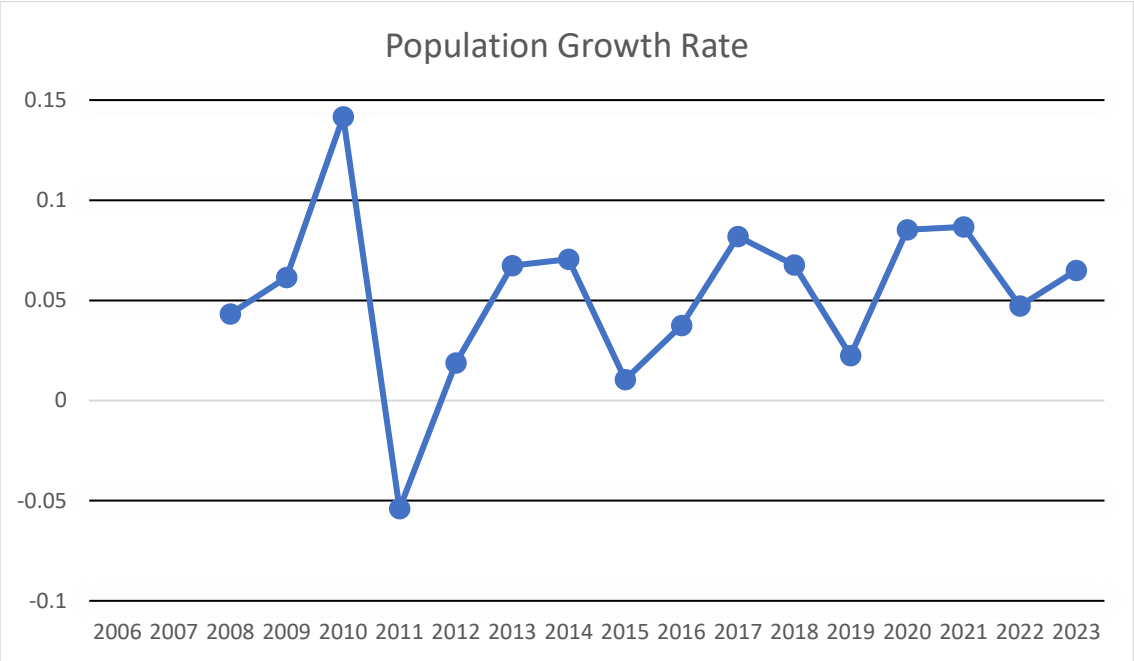

Figure 6.8 Population growth rate chart of Seferihisar (Source: (TURKSTAT 2024a)

The projected population of Seferihisar district in 2030 is determined as 142275 people in the 1/25000 Scale Environmental Plan. It is understood that a population that is approximately 4.5 times more than the population data of 2012, the date of the plan's preparation, and approximately 2 times more than the population data of 2023 is envisaged. When 1/25.000 plan is examined, it is understood that the district that will experience the highest population increase in the predicted projections is Seferihisar district. Since population growth will create a similar increase in urban areas, it is an important criterion in selecting the study area.

6.5 Economic Structure

Seferihisar's economy is generally based on two main sectors. The first of these is agriculture, and the second is tourism. Agriculture maintains its weight in Seferihisar's economy. The district's lands are covered with olive groves and citrus gardens. In recent years, there has been a significant development in greenhouse farming. Agriculture, particularly olive growing, citrus and artichoke cultivation, ornamental plant-oriented greenhouse farming, and animal husbandry, plays a significant role in the district's

economic activities. Fishing is also among the traditional sectors that continue (Izmir Governorship 2024b).

The tourism sector is an important part of Seferihisar's economy. Seferihisar attracts attention with its 60-kilometer coastline and various beautiful bays. Coastal tourism, concentrated in the Sığacık, Doğanbey-Payamlı, and Ürkmez regions, makes a significant contribution to the economy of the district. At the same time, its geothermal energy source, low-capacity thermal springs, has an important place in terms of health tourism (EGIAD 2017). Thermal springs located in the Seferihisar Doğan Bey Thermal region are: Cumalı Thermal Springs, Karakoç Thermal Springs, and Kelalan Thermal Springs (IZBB 2012). Seferihisar has also adopted a peaceful life away from the fast city life, receiving the title of Türkiye's first 'Cittaslow' (Slow City). These features make Seferihisar an attractive region both touristically and economically (ITO 2023).

The industrial and commercial life of the district is lively, with nearly 50 enterprises, including flour factories, dairies, olive oil factories, fresh fruit and vegetable packaging enterprises, and various workshops. While citrus packaging facilities from these enterprises export their products, others mostly meet the district's needs. Seferihisar Teknopark OSB was established on an area of 500 hectares and provides employment to approximately 5000 people (IZBB 2012).

Alongside economic developments, the increase in land prices in districts predominantly used for tourism and secondary housing is noteworthy. At this point, by examining data obtained from Endeksa.com, it is observed that when comparing the prices per square meter of land, vineyard, garden, olive grove, and field in the districts of Seferihisar, Urla, Güzelbahçe, Çeşme, and Karaburun between the years 2019-2024, Güzelbahçe has the lowest unit price. Güzelbahçe has lost value over time, with the unit price per square meter dropping from €74/m² in 2019 to €36/m² in 2024. The amount of change over these years is -51.35%. The district with the highest unit price is Çeşme. However, Çeşme has not shown much increase over the years, with the unit price per square meter rising from €102/m² in 2019 to €117/m² in 2024. The amount of change in this period is 14.71%. In Karaburun, the unit price per square meter increased from €26/m² in 2019 to €45/m² in 2024, marking a change of 73.08%. In Urla, the unit price per square meter increased from €44/m² in 2019 to €86/m² in 2024, reflecting a change of 95.45%. The most regular and highest increase in land unit prices in the region has been observed in the Seferihisar district. The unit price in Seferihisar increased from €10/m² in 2019 to €40/m² in 2024, showing a change of 280% over the specified period,

with an annual change rate of 77.55%. It is expected that the unit price will be €53/m² in 2025 (Endeksa 2024). This situation plays an important role in the selection of the study area. The 280% increase in the Seferihisar district is a remarkable rate compared to all the surrounding districts (Figure 6.9).

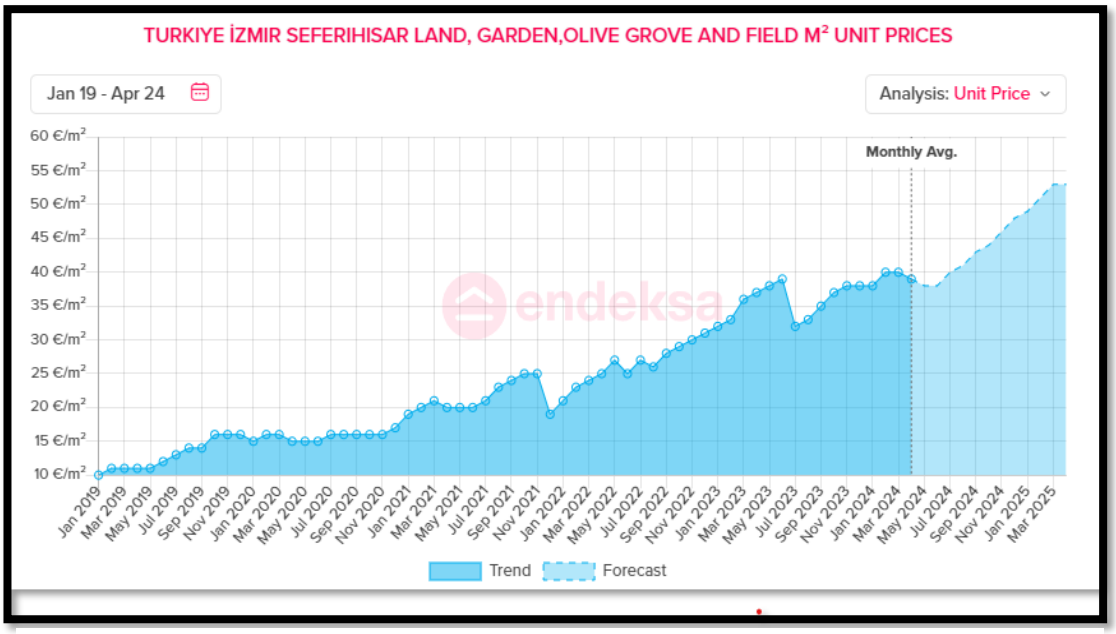

Figure 6.9 Change in unit price of land, vineyard, garden, olive grove and field in Seferihisar district (Source: (Endeksa 2024)

According to data obtained by Endeksa, residential unit prices in Seferihisar, İzmir, remained stable around 400 €/m² from January 2019 to mid-2020. Starting from mid-2020, there was a significant increase in prices, reaching approximately 600 €/m² by early 2022. This period indicates a rapid rise in prices due to increased demand or other market factors (Endeksa 2024).

From 2022 to mid-2023, prices fluctuated but continued to grow overall. By mid-2023, prices reached around 1,000 €/m² (Figure 6.10). According to forecasts for the period from mid-2023 to mid-2025, prices are expected to continue rising steadily, reaching approximately 1,500 €/m² by mid-2025 (Endeksa 2024).

The graph shows that residential prices in Seferihisar have increased strongly and steadily over the years. Significant growth has been observed especially since mid-2020, and this trend is expected to continue. This increase can be explained by the rising demand for housing, economic factors, and the attractiveness of Seferihisar as a residential area.

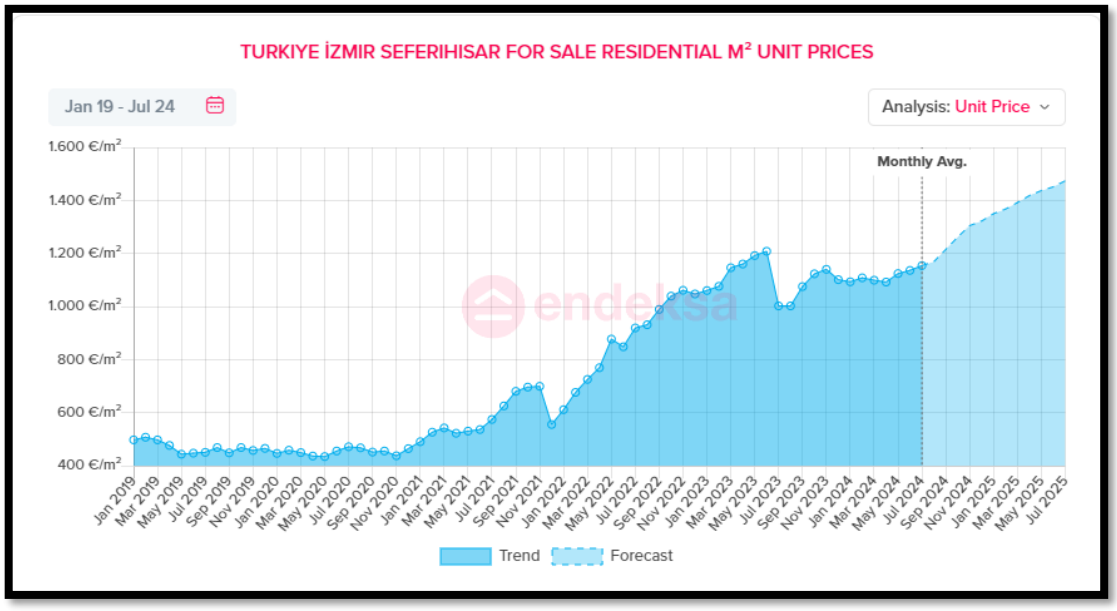

Figure 6.10 Change in unit price of land, vineyard, garden, olive grove and field in Seferihisar district (Source: (Endeksa 2024)

6.6 Physical Structure and Environmental Resources

The İzmir province features naturally formed bays along its coastline. The region's morphological structure is characterized by east-west-oriented mountains running parallel and perpendicular to the sea, depression plains between them, alluvial plains at river mouths, and occasional volcanic cones. Small coastal plains and valleys have formed in Urla and Seferihisar, creating topographically suitable areas for settlement along the Urla, Yelki, and Seferihisar axes.

The center of Seferihisar district is situated at an elevation of 18 meters above sea level, west of the Kızıldağlar and on the plains of the Kocaçay Valley. Seferihisar is situated in one of the Urla Peninsula's low depressions (Figure 6.11). This area merges with the wide depression where Ulamış, Düzce, and Turgut villages are located, gradually sloping southwest towards the Azmak Plain and eventually meeting the sea. Morphologically, Seferihisar can be divided into several units. The first distinguishable unit is the erosion surface. The slopes at the foothills of the erosion surfaces dissected by river valleys form a separate morphological unit.

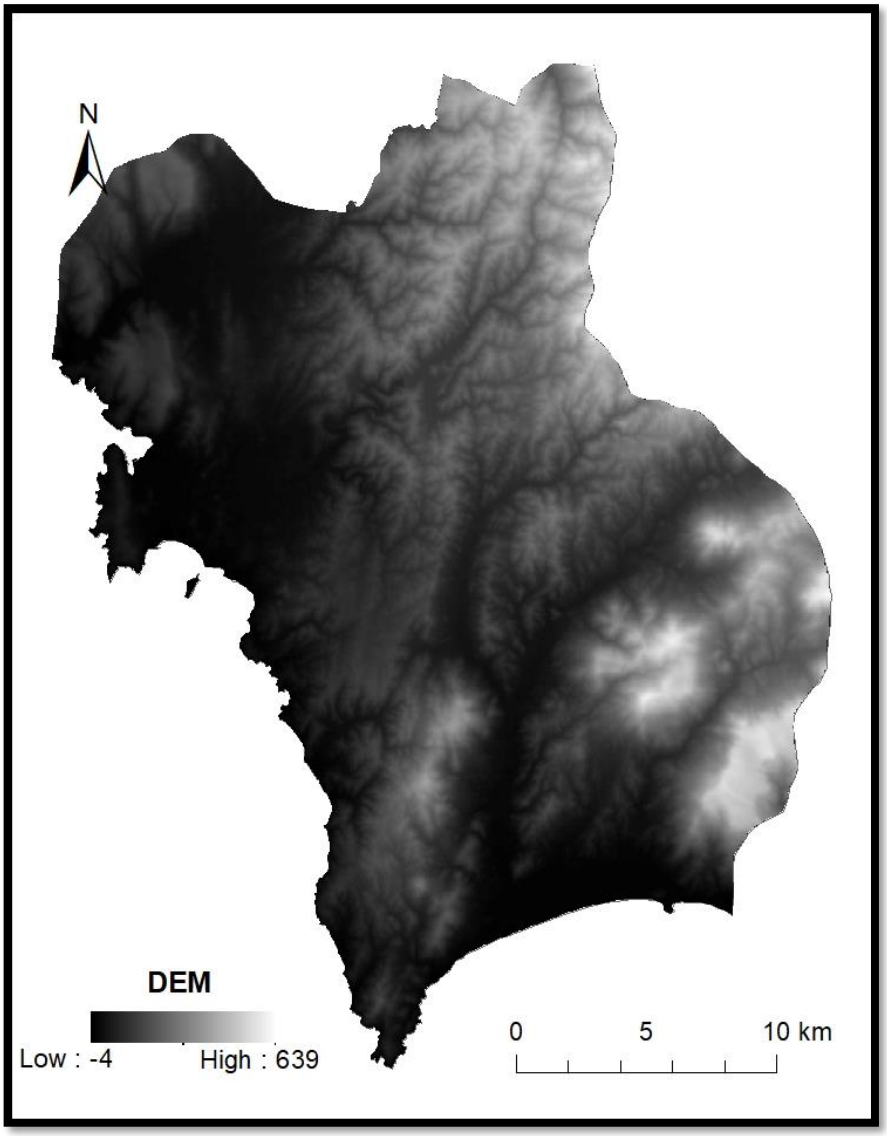

Figure 6.11 Digital Elevation Model (DEM) of Seferihisar district

Geologically, the soils of Seferihisar are composed of three units: the Upper Cretaceous aged flysch unit, the Neogene aged limestone unit, and the Quaternary aged alluvium. When examining the spatial distribution of soil classes, it is observed that the small plains around Seferihisar, Ürkmez, and Gümüldür are covered with first- and second-class soils.

Mountains and Plains: Mountains and plains play a significant role in the landforms of the Seferihisar region, which are largely shaped by river erosion and sediment deposition. Notably, the alluvial plains formed by the sedimentation of Azmak Dere, Yassı Çay, and their tributaries are prominent. The plain formed by Azmak Dere

and its tributaries is called the Azmak Plain, and another plain extends from the district center to the Teos ruins (Gülersoy 2014).

Seferihisar's coastline is another morphological unit. The Seferihisar coastline, like the other coasts of the Urla Peninsula, is indented and irregular. This irregularity can be attributed to the rise in sea levels at the end of the Quaternary glacial period and tectonic movements causing fractures. The Sığacık Plain and the coast to its south are flat and smooth, having been filled with alluvium carried by rivers, resulting in their current form. The highest elevation in the district is Çakmaktepe, at 680 meters. Other notable elevations in the area include Güney Dağı, Masal Dağı, Deli Ömer Dağları, Kovacık Dağı, Türbe Dağı, Korkmaz Dağı, and Somaklı Dağı (Gülersoy 2014).

Protected Areas: Natural protected areas in İzmir province are generally concentrated in coastal regions. One of these areas includes Seferihisar-Doğanbey and Sığacık-Hıdırlık Neighborhoods, which are designated as natural protected sites. The regions surrounding İzmir, known for their ancient cities, are designated as archaeological sites. Airai, an ancient city in Seferihisar, is one such site. Additionally, the district features numerous urban and historical protected areas, including structures like fountains, baths, and madrasahs (Karahan and Elçi 2023; IZBB 2012).

Lakes and Dams: In Seferihisar district, the dams constructed for irrigation purposes include Gelinalan and Seferihisar dams on Yassıçay, Ürkmez dam on Ürkmez stream, and Kavakdere dam on Kavak creek. The district also features Kavakçayı, a pond used for irrigation. Additionally, the 1/25,000 Plan includes small irrigation projects in Seferihisar, Ürkmez, and Ören-Bağyurdu (IZBB 2012; Karahan and Elçi 2023).

Earthquake Situation: The region is located in a first-degree earthquake zone, indicating high seismic activity. The Seferihisar Fault, which extends between Sığacık Bay and Güzelbahçe with a terrestrial length of 23 km, is active. This fault runs from the Sığacık Bay area in Seferihisar to Güzelbahçe in southwestern İzmir. Underwater data suggest that the fault continues southward along the Aegean Sea floor. The land portion of the Seferihisar Fault between Sığacık Bay and Güzelbahçe is 23 km long, and when combined with the underwater section, the fault is estimated to reach a total length of 30 km (IZBB 2012; Emre et al. 2005).

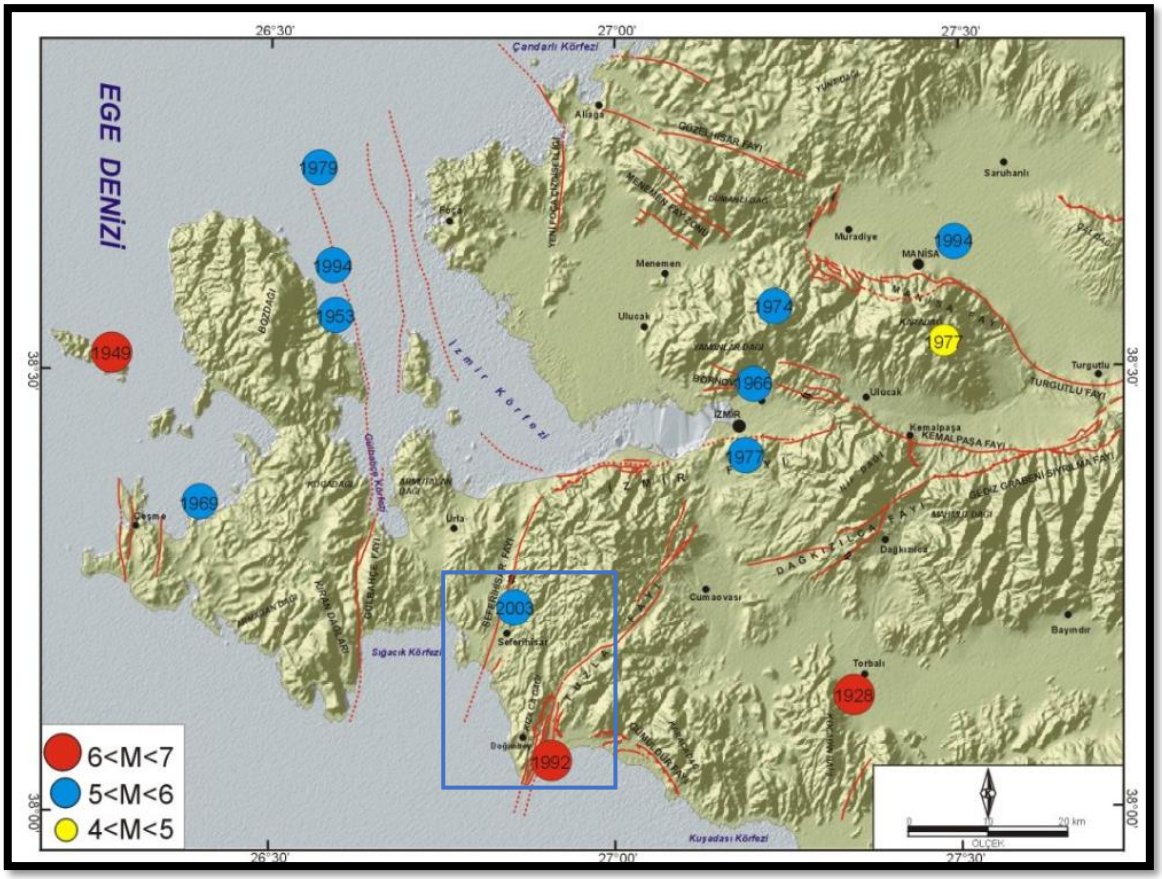

Figure 6.12 Active fault map in the immediate vicinity of İzmir (Source: (Emre et al. 2005)

6.7 Climate and Vegetation

In Seferihisar, where the Mediterranean climate prevails, summers are hot and dry, while winters are mild and rainy. Seferihisar is located in the Mediterranean macro-climate region. According to a report published by the Ministry of Environment and Climate Change in 2024, the long-term maximum temperature average in Seferihisar district is around 28.6 °C (Meteorology 2023). According to the Seferihisar meteorological station, the estimated annual average rainfall amount is around 710 mm, and the annual average temperatures range from 12.4 to 17.7 °C. The highest temperature in the region is recorded in July at 42.9 °C, while the lowest temperature is in January at -6.2 °C. The hottest months are July and August, while the coldest months are January and February (TOB 2018). Additionally, the area's annual average relative humidity is 65%; the highest humidity rate is 72% in December, and the lowest humidity rate is 53% in July. The level of relative humidity during the summer months helps to alleviate

extreme heat, contributing significantly to the development of sea tourism in the region. The dominant wind direction in the research area is NNW (North-Northwest), and especially in the summer months, these winds, which increase in frequency (364 frequency in summer months), create favorable conditions for water sports such as windsurfing and sailing (Gülersoy 2014).

The slopes and hills of the district rise from the sea towards the inland areas, displaying different exposure characteristics to the sun. Particularly, slopes facing south and west receive more sunlight throughout the day, creating a warmer and drier microclimate.

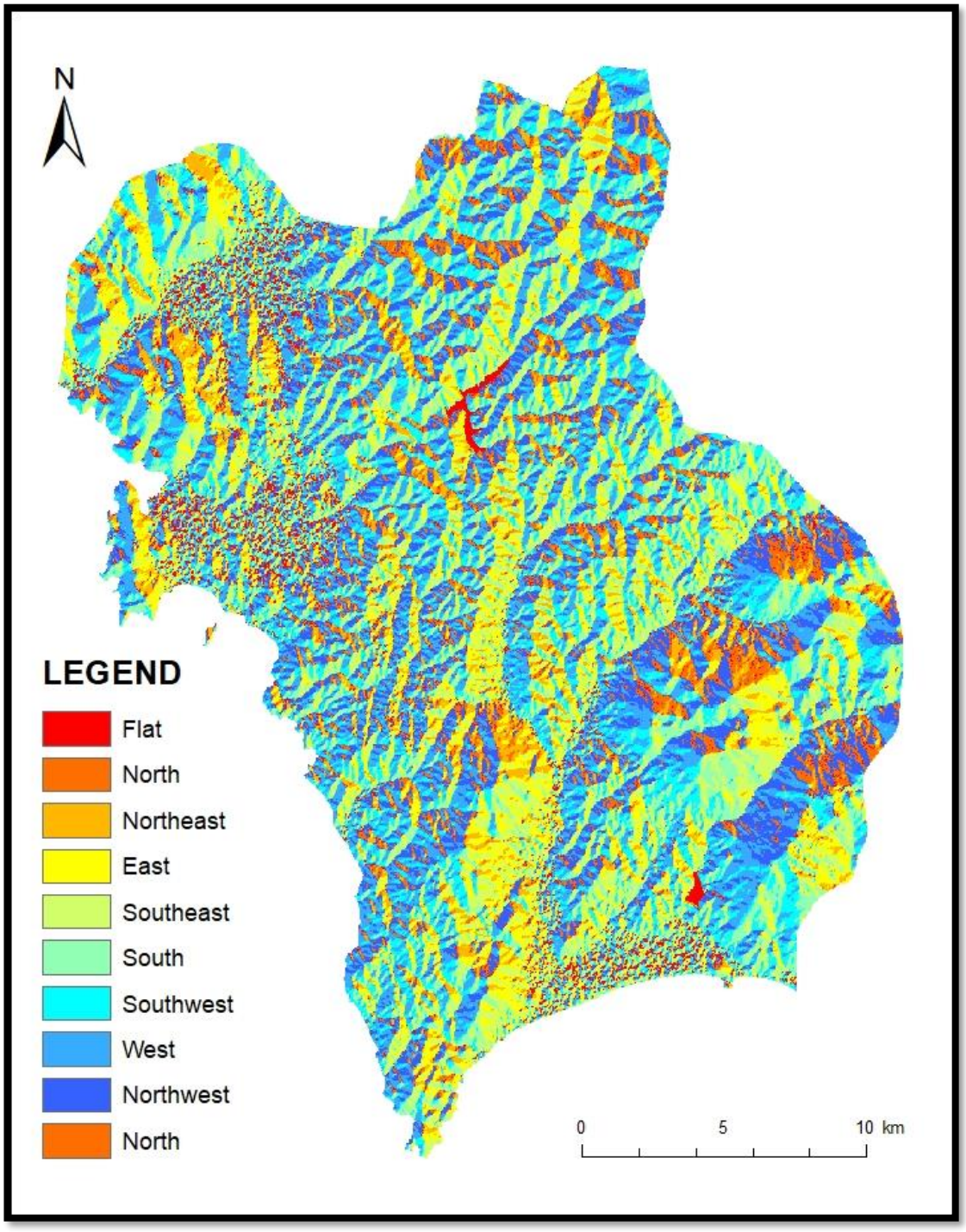

Figure 6.13 Aspect Map for Seferihisar district

CHAPTER 7

FINDINGS

In this section, the findings regarding the effects of urban sprawl on LST in Seferihisar district, based on spectral indices, land cover and LST change maps, and the 2030 land cover prediction maps, are explained. Firstly, the NDVI, NDBI, MNDWI, NDBaI values, land cover, and LST values for each year between 2017 and 2023 in Seferihisar district are presented. Secondly, the findings on the relationship between the obtained spectral indices, land cover, and LST values are presented. Thirdly, the findings related to the urban sprawl trend in Seferihisar district are presented. Finally, the results of the 2030 land cover prediction are presented.

7.1 Spectral Indices

To provide a reference for land cover classification and determine its relationship with LST, spectral indices were created for each year separately between 2017 and 2023. These indices were obtained using the spectral bands of the Landsat 8 OLI and TIRS sensors on the Google Earth Engine platform. During the visualization stage, the largest and smallest values in 2017 and 2023 were taken, and a standard range was used for each year. Additionally, tables were created to observe each year's own maximum, minimum, and mean values. In this section, the findings obtained from the analysis are explained.

7.1.1 NDVI

The purpose of calculating NDVI is to observe the presence of vegetation in the study area and its changes over the years. NDVI maps created for each year are visualized from black to white. White areas on the map indicate regions with no vegetation, while areas trending towards black indicate increasing vegetation density (Figure 7.1). When comparing NDVI values between 2017 and 2023 in the study area, the lowest value (-0.46) and the highest value (0.90) belong to the year 2023 (Figure 7.2). While high values are very close to each other, low values vary from year to year. Based on these data, it is

concluded that the vegetation density and quality in the study area have decreased in some places and increased in others. A significant increase in vegetation cover is observed in the Orhanlı region. Vegetation is concentrated in the northeast and southeast axes of the study area. Generally, areas with buildings and bare land show low vegetation density and quality (Figure 7.1).

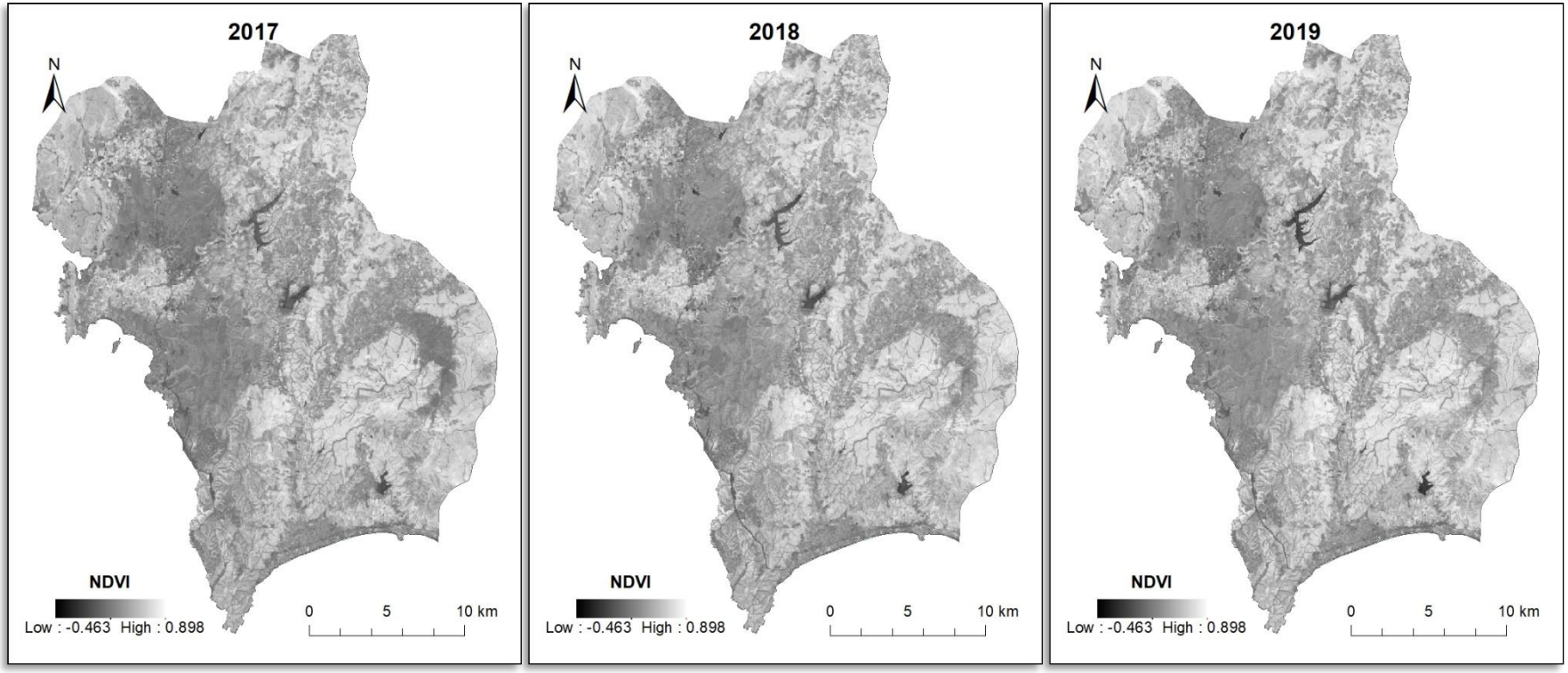

Figure 7.1 NDVI results of Seferihisar district

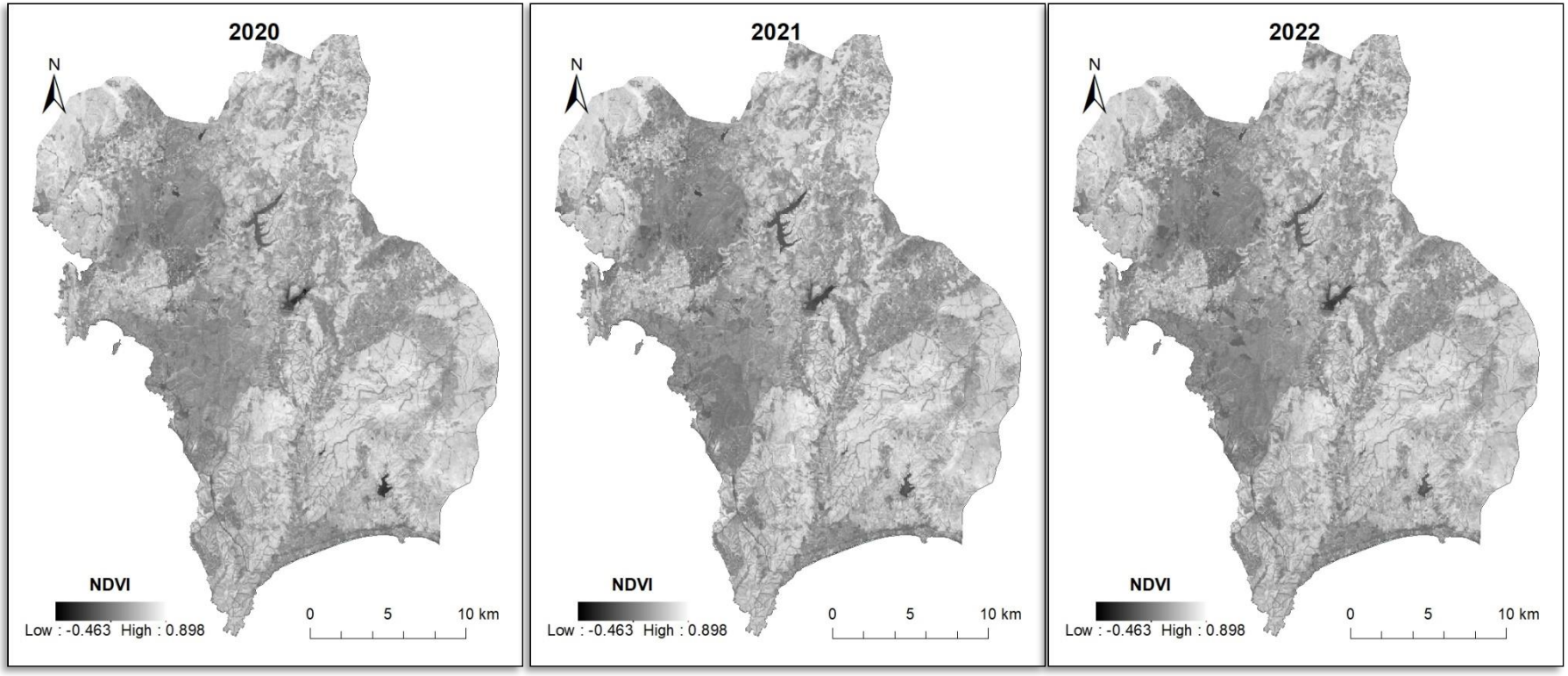

Figure 7.1 (Cont.)

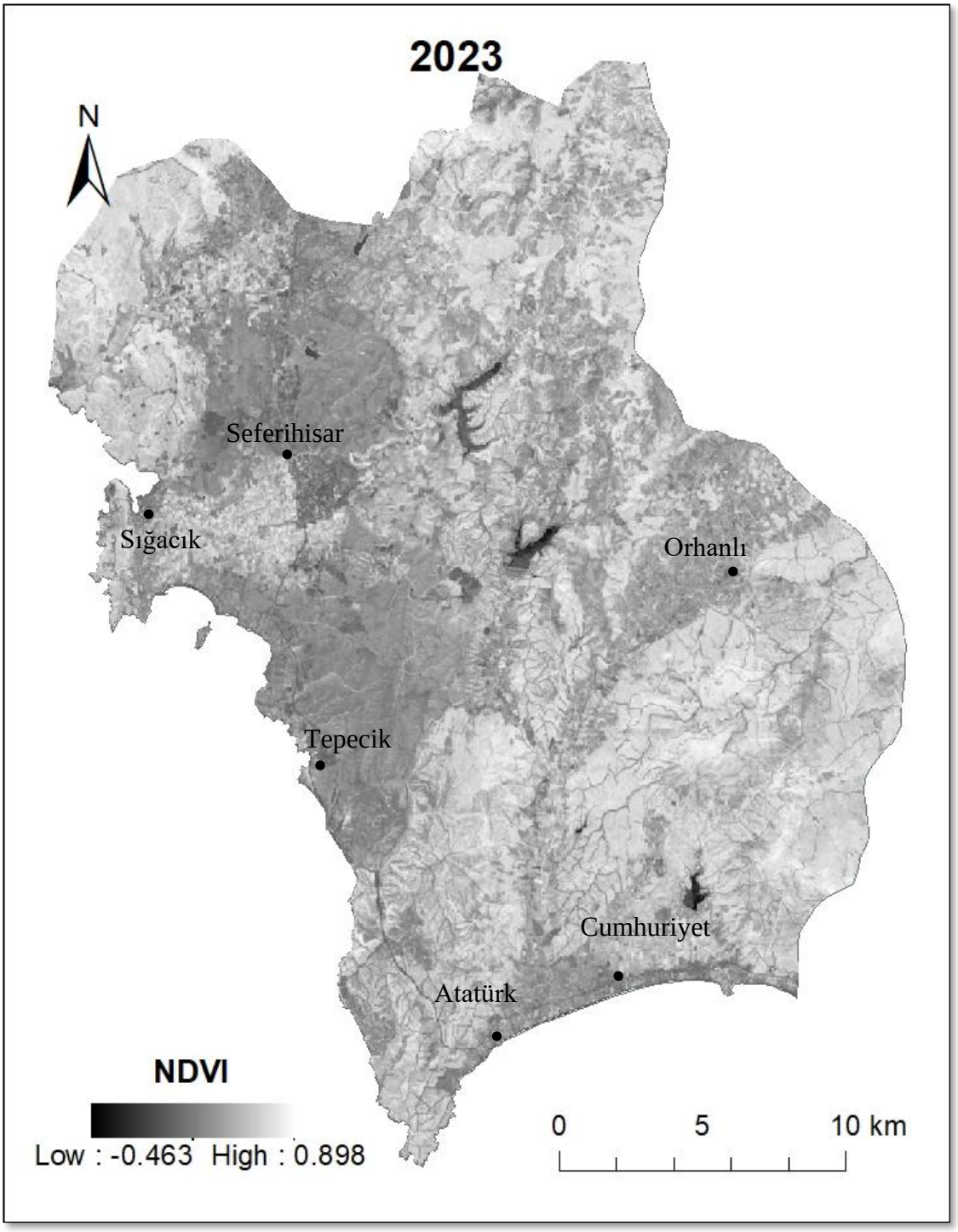

Figure 7.1 (Cont.)

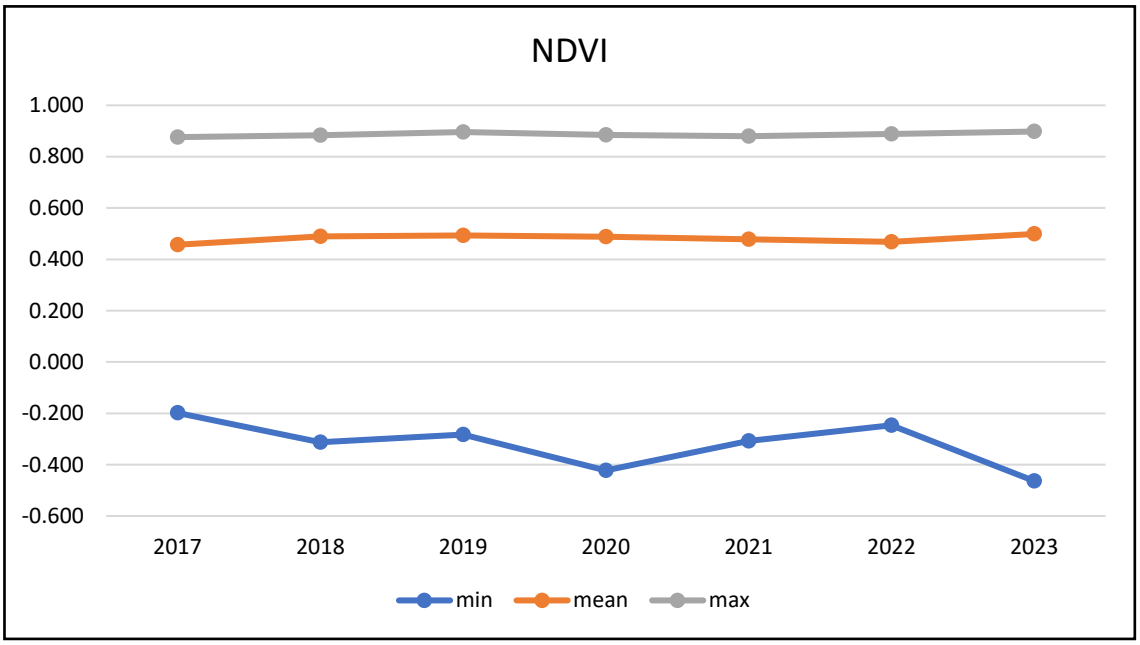

NDVI

	2017	2018	2019	2020	2021	2022	2023
min	-0.198	-0.313	-0.283	-0.423	-0.308	-0.246	-0.463
mean	0.457	0.489	0.493	0.488	0.478	0.468	0.499
max	0.876	0.883	0.896	0.885	0.880	0.889	0.898

Figure 7.2 Minimum, maximum, and mean values of NDVI

7.1.2 NDBI

The goal of calculating NDBI is to observe urban areas in the study area and their changes over the years. NDBI maps created for each year are visualized from black to white. On the map, white areas indicate healthy natural vegetation without construction, while areas trending towards black indicate increased density of urban areas and bare land. When comparing NDBI values between 2017 and 2023 in the study area, the lowest value (-0.60) is from 2019, and the highest value (0.47) is from 2023 (Figure 7.4). High values show an increasing trend over the years, while low values show a decreasing trend. Based on these data, it is concluded that urban areas are increasing while natural areas are being destroyed in the study area. In the study area, the highest NDBI values are concentrated in urban areas and bare land (Figure 7.3).

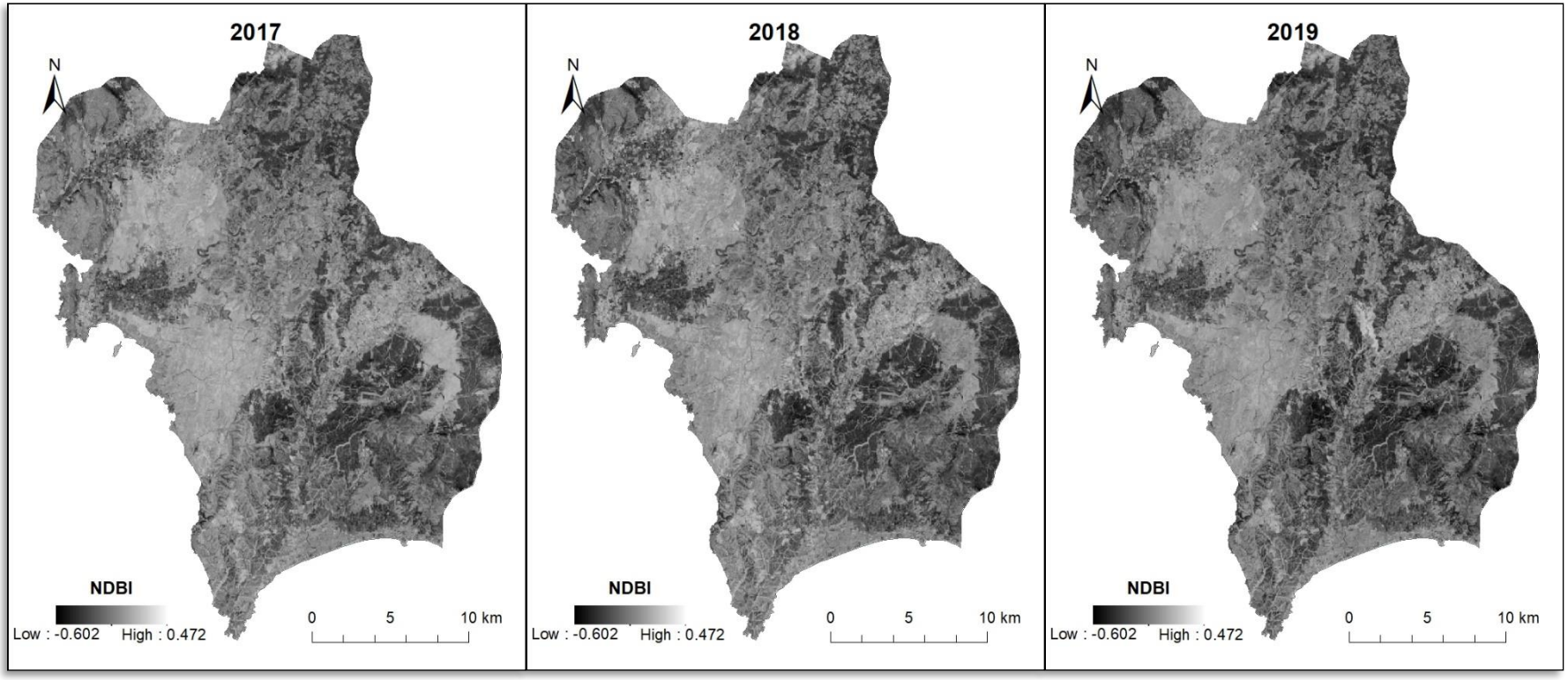

Figure 7.3 NDBI results of Seferihisar district

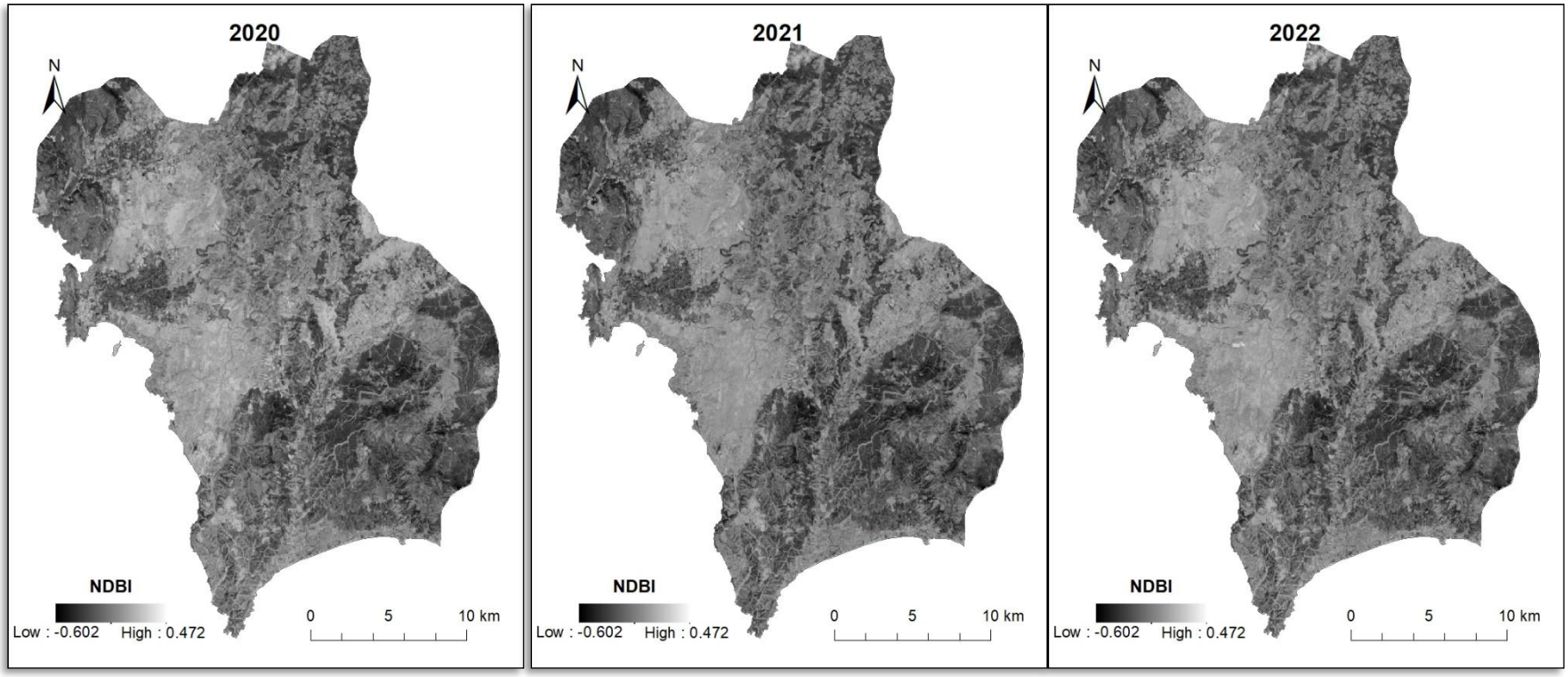

Figure 7.3 (Cont.)

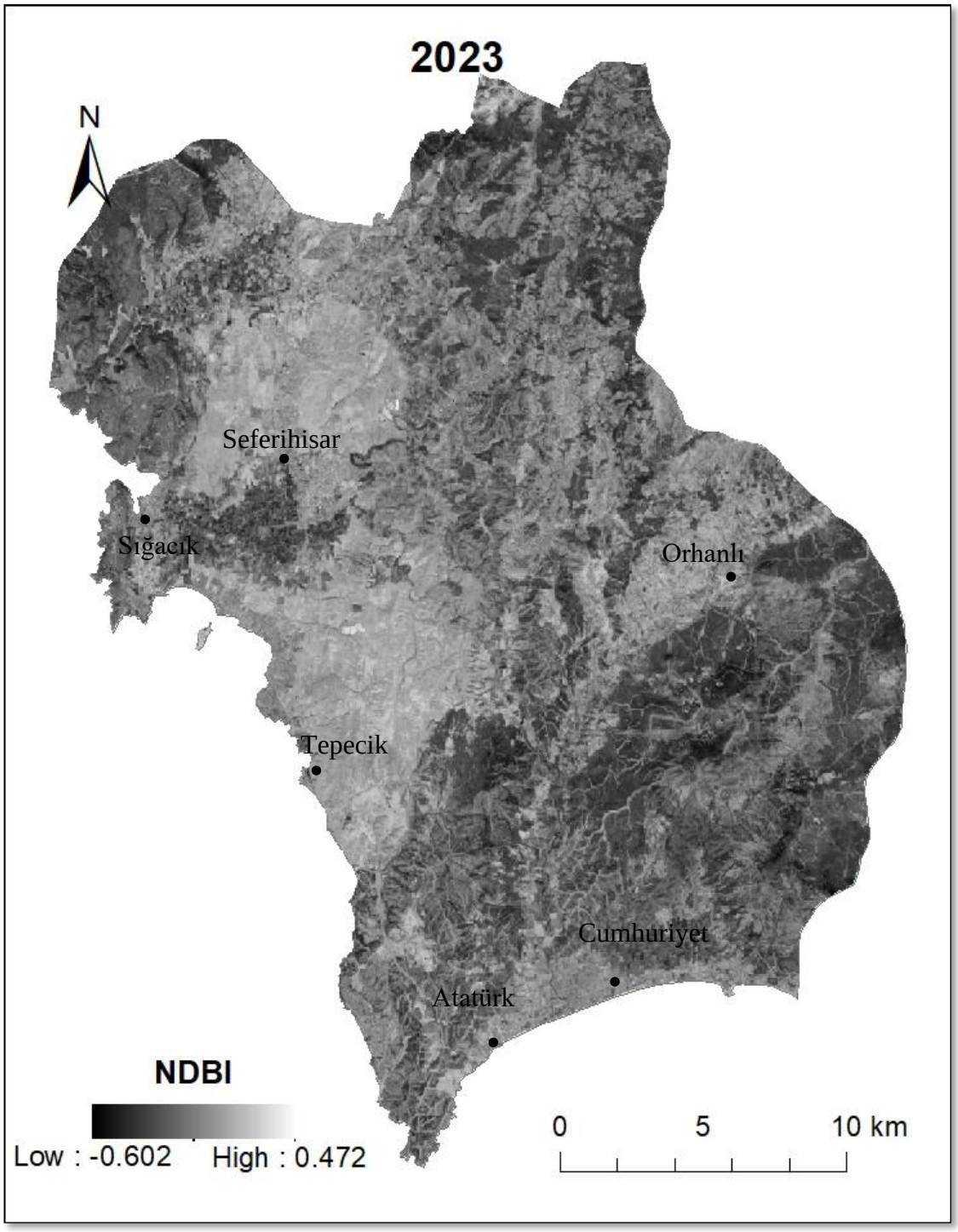

Figure 7.3 (Cont.)

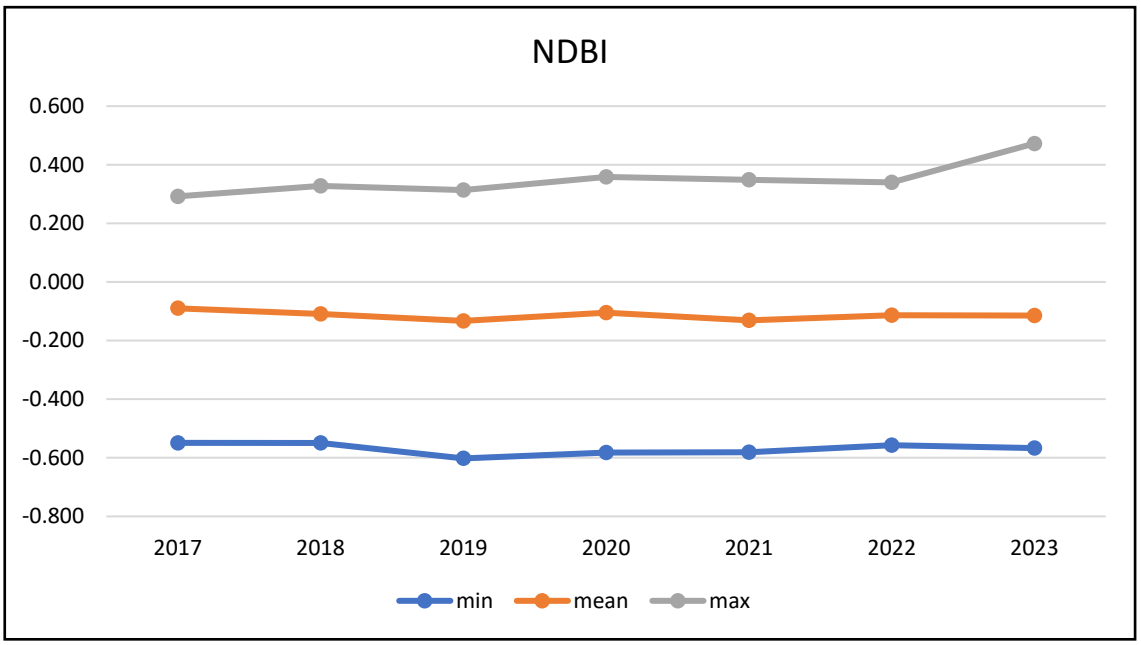

NDBI

	2017	2018	2019	2020	2021	2022	2023
min	-0.549	-0.549	-0.602	-0.582	-0.581	-0.557	-0.567
mean	-0.090	-0.109	-0.133	-0.105	-0.131	-0.113	-0.115
max	0.292	0.328	0.314	0.359	0.348	0.340	0.472

Figure 7.4 Minimum, maximum, and mean values of NDBI

7.1.3 MNDWI

The aim of computing MNDWI is to detect water bodies and moist areas in the study area and track their alterations over time. MNDWI maps produced for each year are represented from dark to light shades. Light areas on the map indicate arid regions lacking water bodies or moisture, while areas progressing towards dark shades indicate intensified presence of water bodies and moist regions (Figure 7.5). Upon comparing MNDWI values between 2017 and 2023, the lowest value (-0.66) and the highest value (0.72) are recorded in 2023 (Figure 7.6). The principal water bodies in the study area include the Seferihisar, Kavakdere, and Ürkmez dams. Additionally, the Aegean Sea is a significant water body within the study area; however, it is not included in the study area boundary and hence not depicted in the data. Based on the data acquired, it is noted that there is a visible decline in the Seferihisar, Kavakdere, and Ürkmez dams within the study area. Furthermore, areas with the least moisture content are identified as arid regions featuring bare land (Figure 7.5).

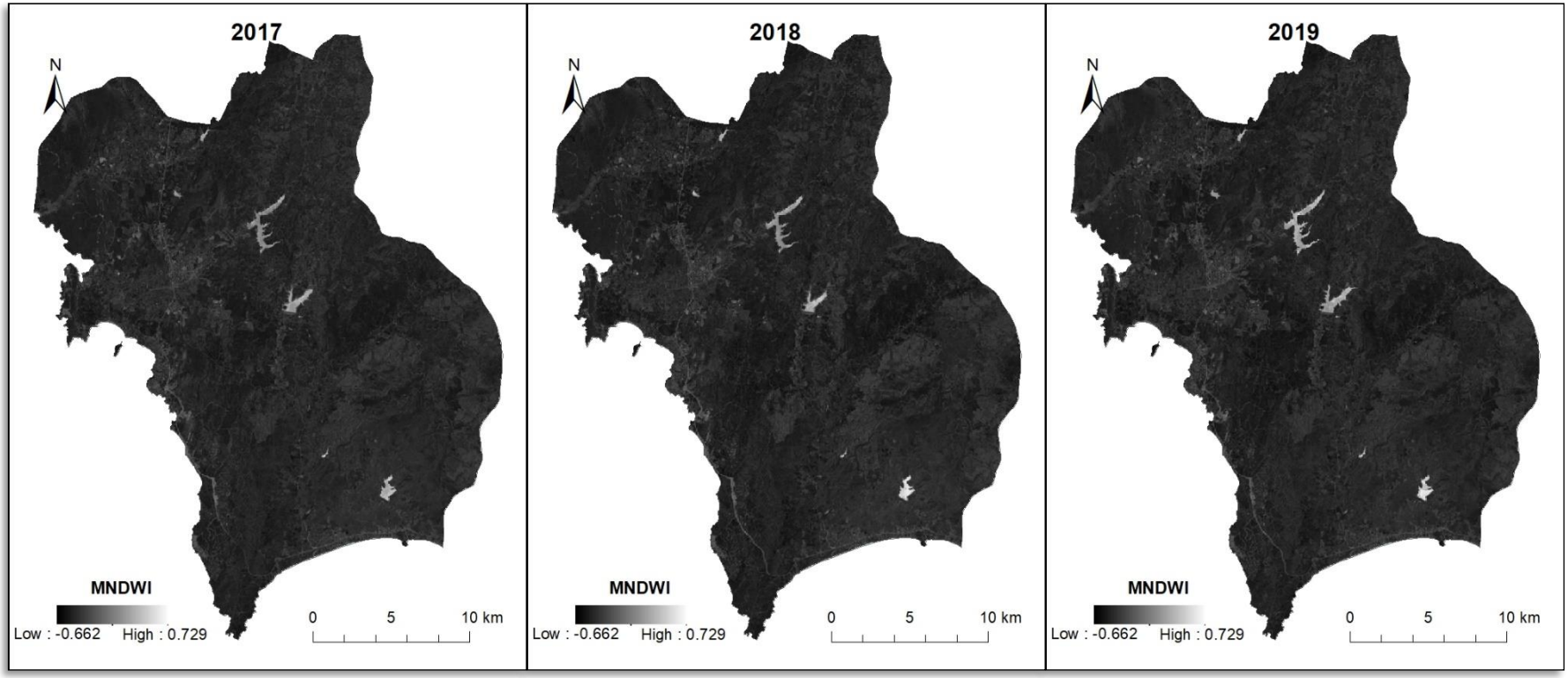

Figure 7.5 MNDWI results of Seferihisar district

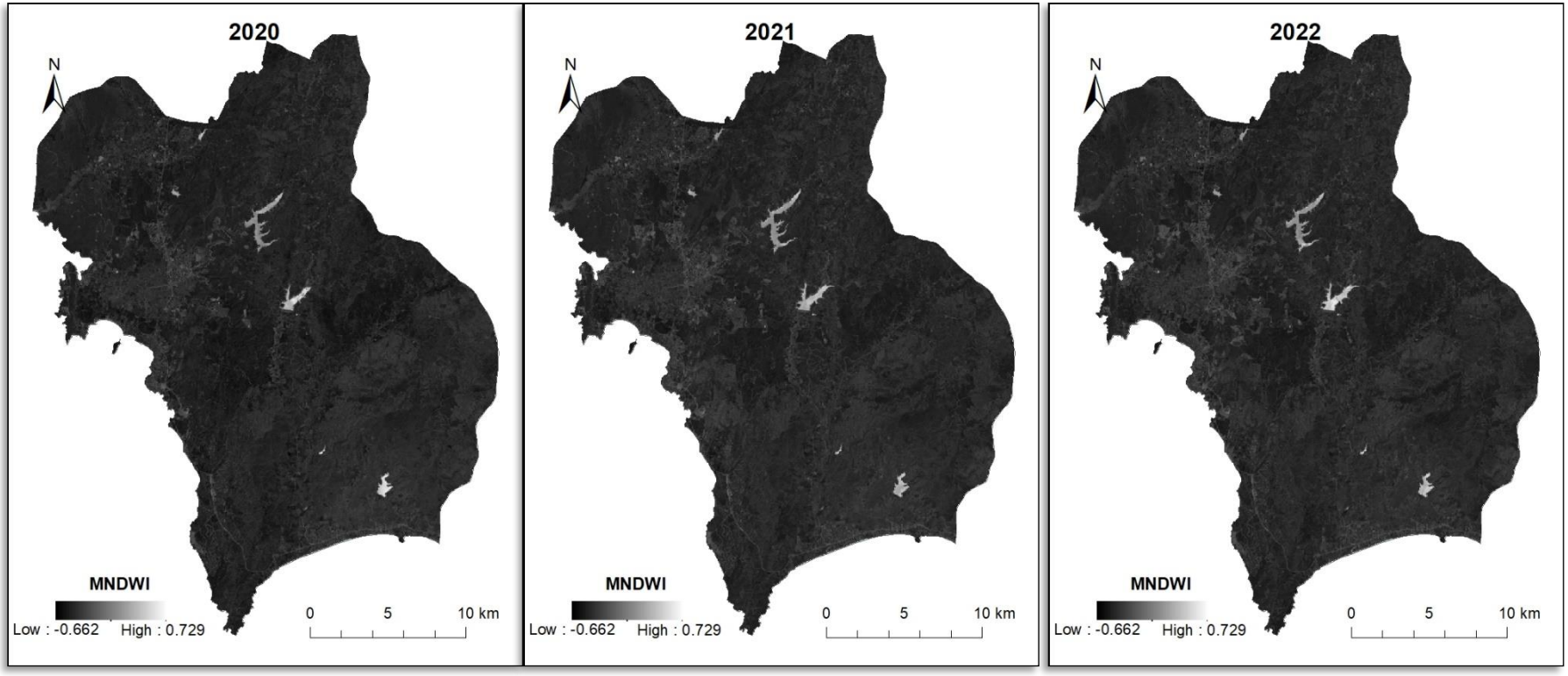

Figure 7.5 (Cont.)

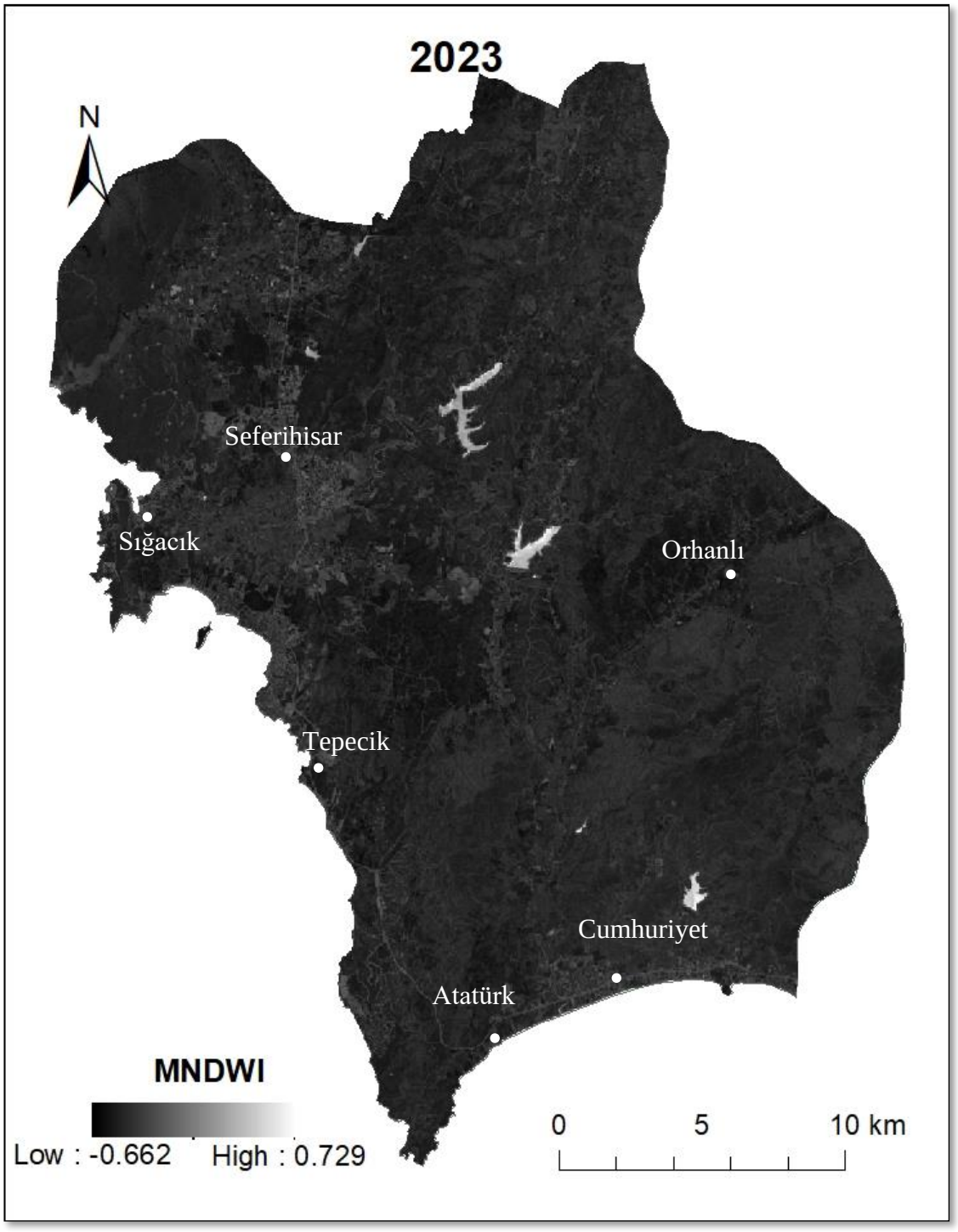

Figure 7.5 (Cont.)

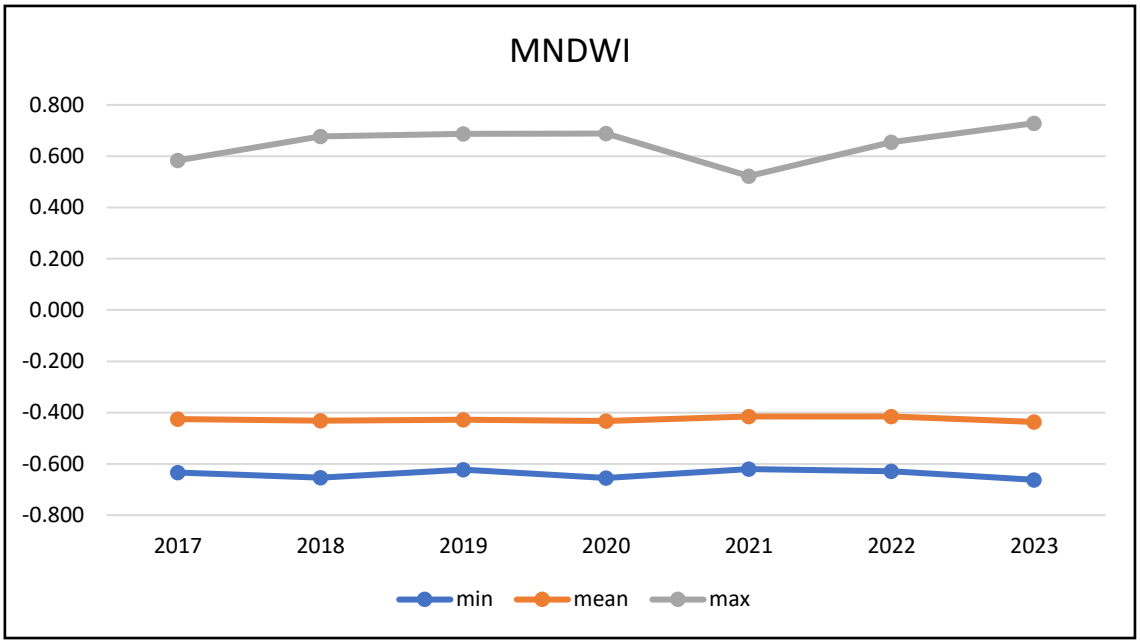

MNDWI

	2017	2018	2019	2020	2021	2022	2023
min	-0.634	-0.654	-0.623	-0.654	-0.620	-0.629	-0.662
mean	-0.425	-0.432	-0.428	-0.433	-0.416	-0.415	-0.437
max	0.583	0.678	0.687	0.688	0.522	0.654	0.729

Figure 7.6 Minimum, maximum, and mean values of MNDWI

7.1.4 NDBaI

The primary objective underlying the computation of NDBaI is to delineate and monitor bare land expanses devoid of vegetative cover within the study domain across consecutive temporal intervals. NDBaI cartographic representations, generated for each annual epoch, adopt a grayscale visualization schema, where regions tending toward darker hues signify the absence of vegetal canopy, contrasting with lighter tones emblematic of dense vegetative cover or aqueous bodies (Figure 7.7). Examination of NDBaI metrics spanning the temporal span from 2017 to 2023 reveals the nadir of this index (-0.69) occurring in both 2019 and 2023, while its zenith (0.29) is observed in 2023 (Figure 7.8). Observationally, areas proximal to the central district of Seferihisar exhibit sporadic escalations in the proportion of bare land, juxtaposed with locales contiguous to the settlement nucleus of Orhanlı manifesting a reduction in bare land ratios (Figure 7.7). The diminution of bare expanses in the Orhanlı precinct is conjectured to stem from efficacious rehabilitation endeavors following the conflagration incident in the Orhanlı woodland in 2017. Furthermore, locales characterized by urbanization evince elevated NDBaI values, indicative of shared attributes with the bare land classification.

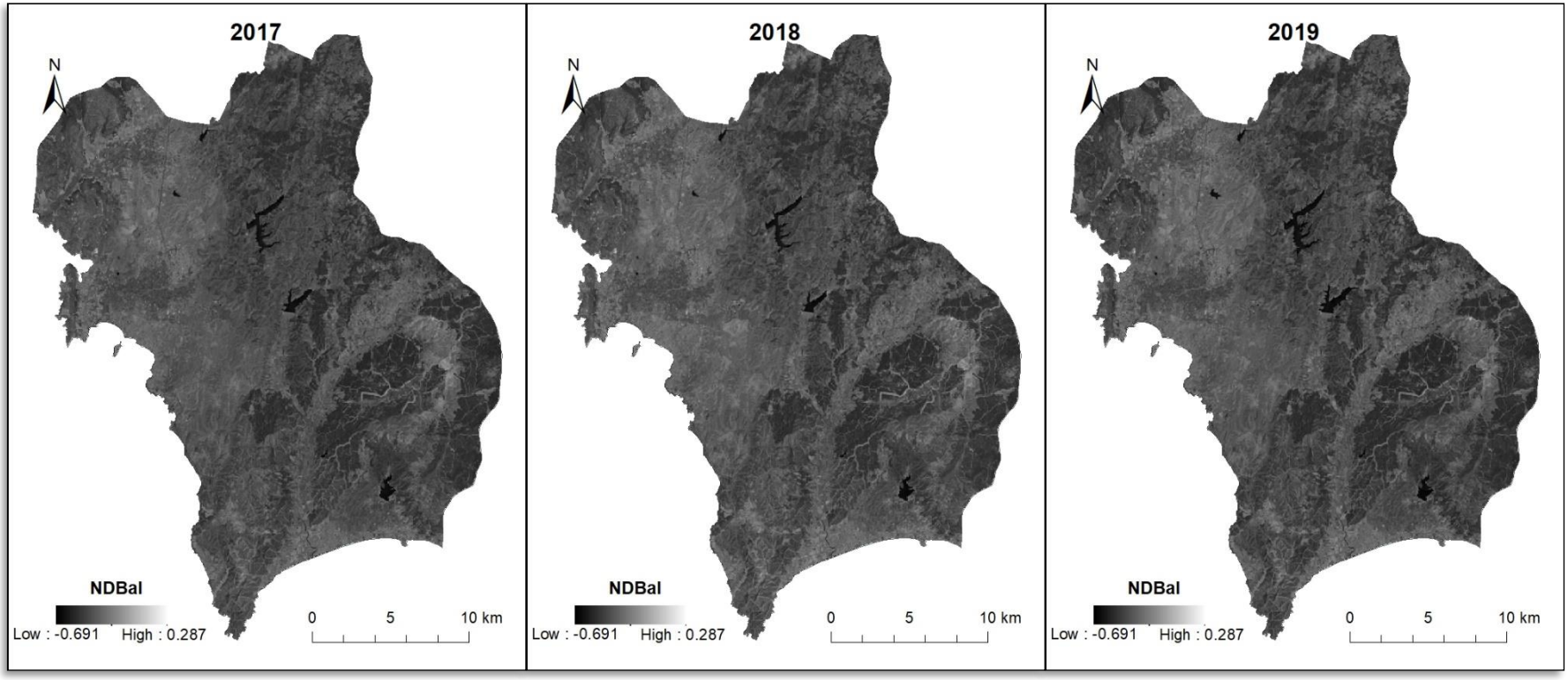

Figure 7.7 NDBaI results of Seferihisar district

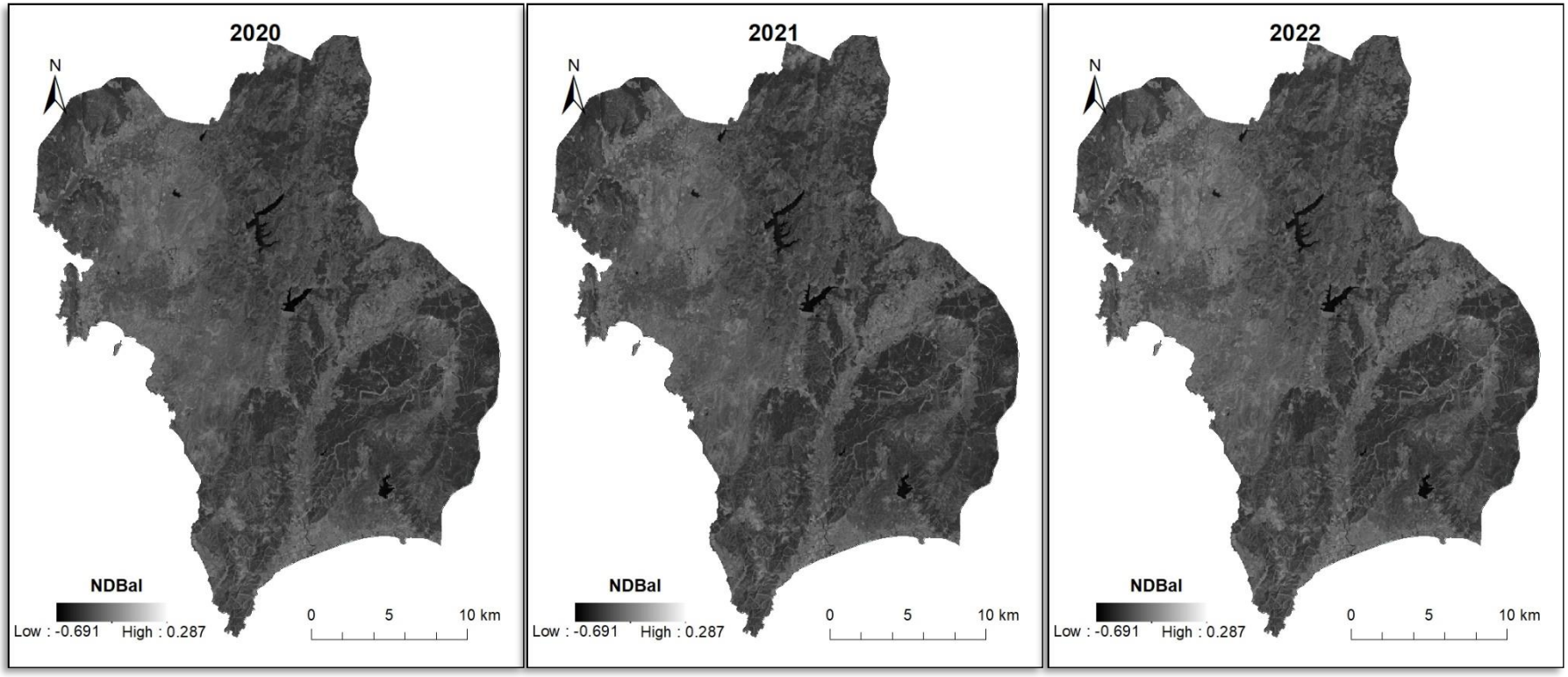

Figure 7.7 (Cont.)

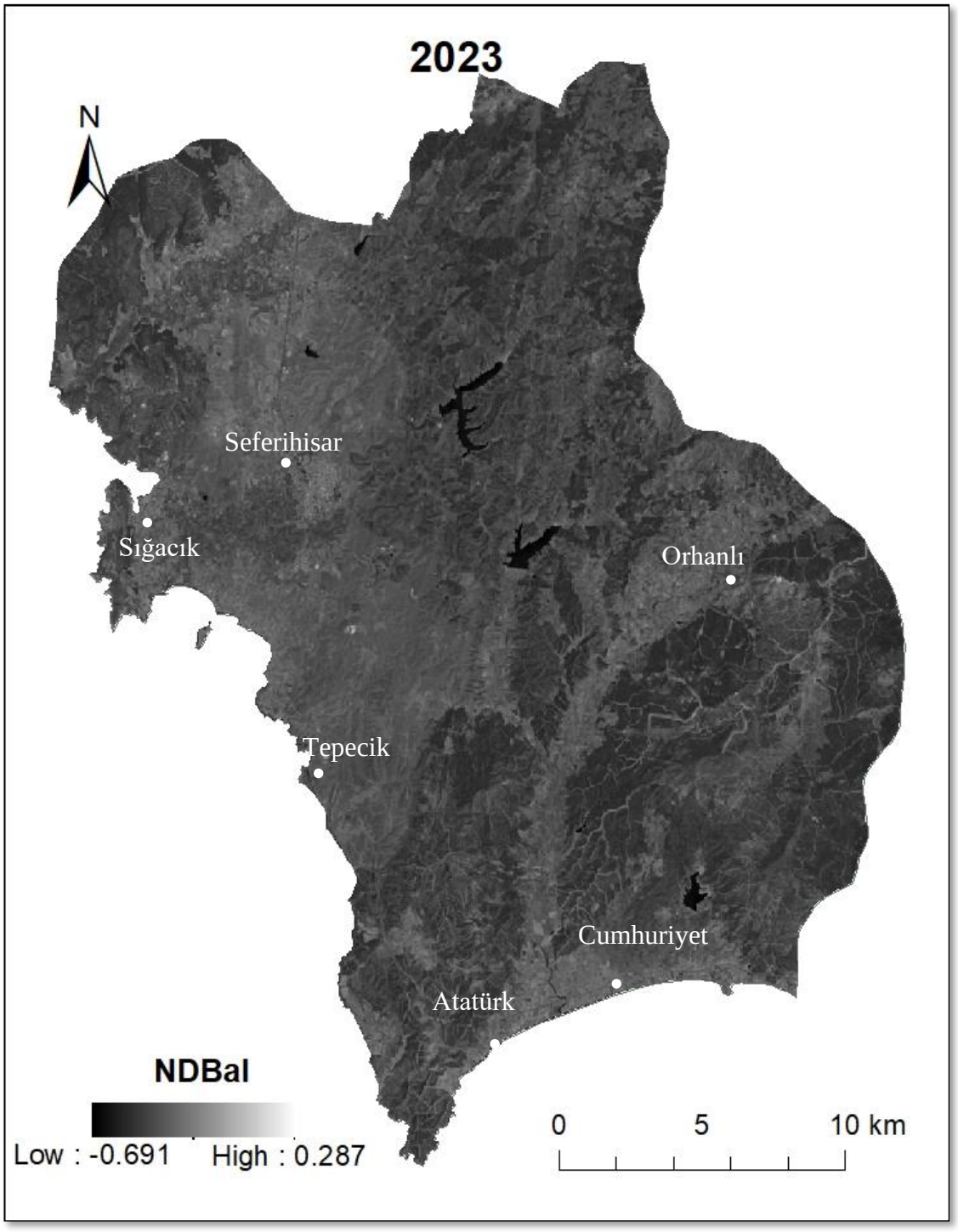

Figure 7.7 (Cont.)

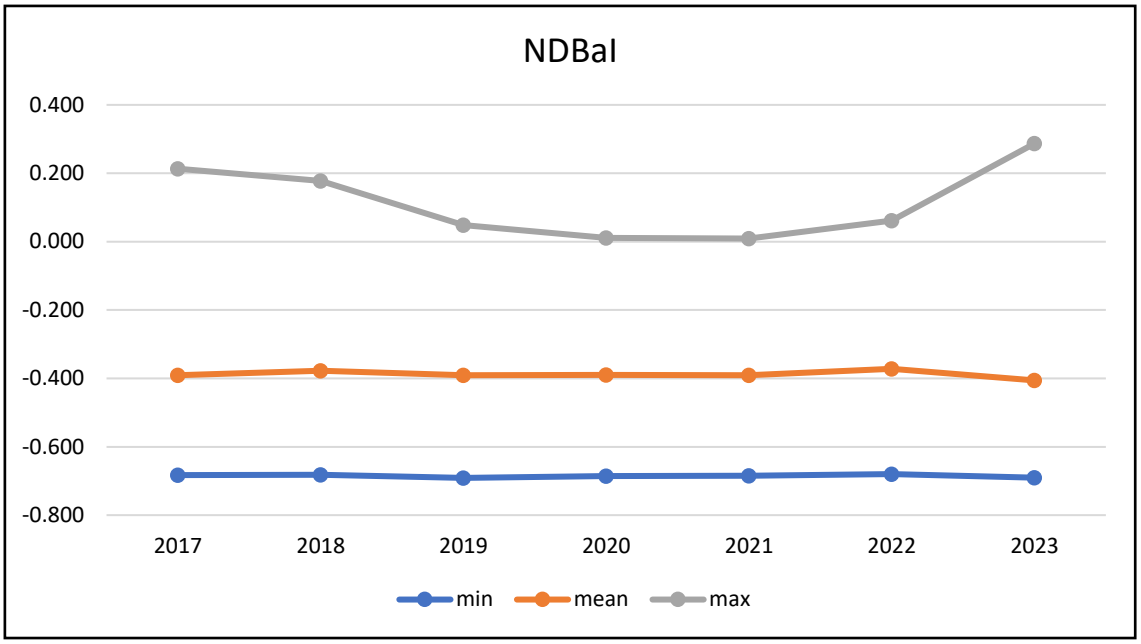

NDBaI

	2017	2018	2019	2020	2021	2022	2023
min	-0.683	-0.682	-0.691	-0.686	-0.685	-0.680	-0.691
mean	-0.391	-0.377	-0.391	-0.390	-0.391	-0.372	-0.406
max	0.213	0.177	0.048	0.011	0.009	0.062	0.287

Figure 7.8 Minimum, maximum, and mean values of NDBaI

7.2 LST

The creation of LST maps serves the purpose of identifying thermal properties across varied surface types and observing their temporal changes over the years. LST maps, generated annually from 2017 to 2023, are visually represented from red to blue, with green hues denoting areas of lowest surface temperatures and red hues indicating regions with the highest temperatures (Figure 7.9). Upon comparing LST values between 2017 and 2023, it is found that the lowest temperature (21.35°C) and the highest temperature (56.19°C) were both observed in 2019 (Figure 7.10). Analysis of the data reveals slight temperature disparities of 1-2°C between the years 2017 and 2023. Interestingly, the year 2021 records the highest mean temperature value (42.00), underscoring the spatial distribution of temperature across the area. Notably, areas abundant in vegetation and water bodies exhibit the lowest temperatures. Remarkably, a temperature decrease is observed in the Orhanlı region. Agricultural lands display varying temperature levels, influenced by farming techniques and practices. Conversely, regions characterized by bare land and urbanization correspond to areas with the highest temperatures (Figure 7.9). Overall, when the mean LST value between 2017 and 2023 is compared, it is observed that the LST has decreased with a difference of 0.711 (Figure 7.10).

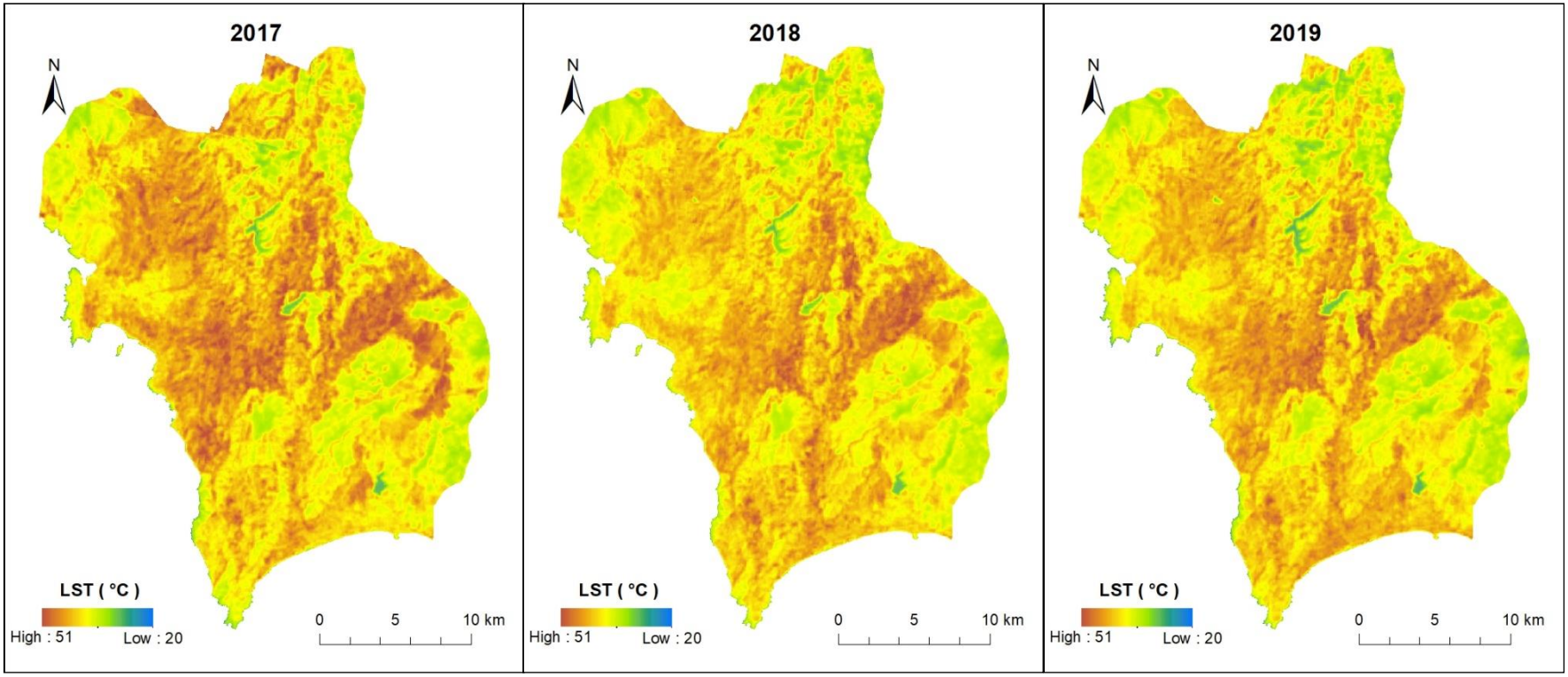

Figure 7.9 LST results of Seferihisar district

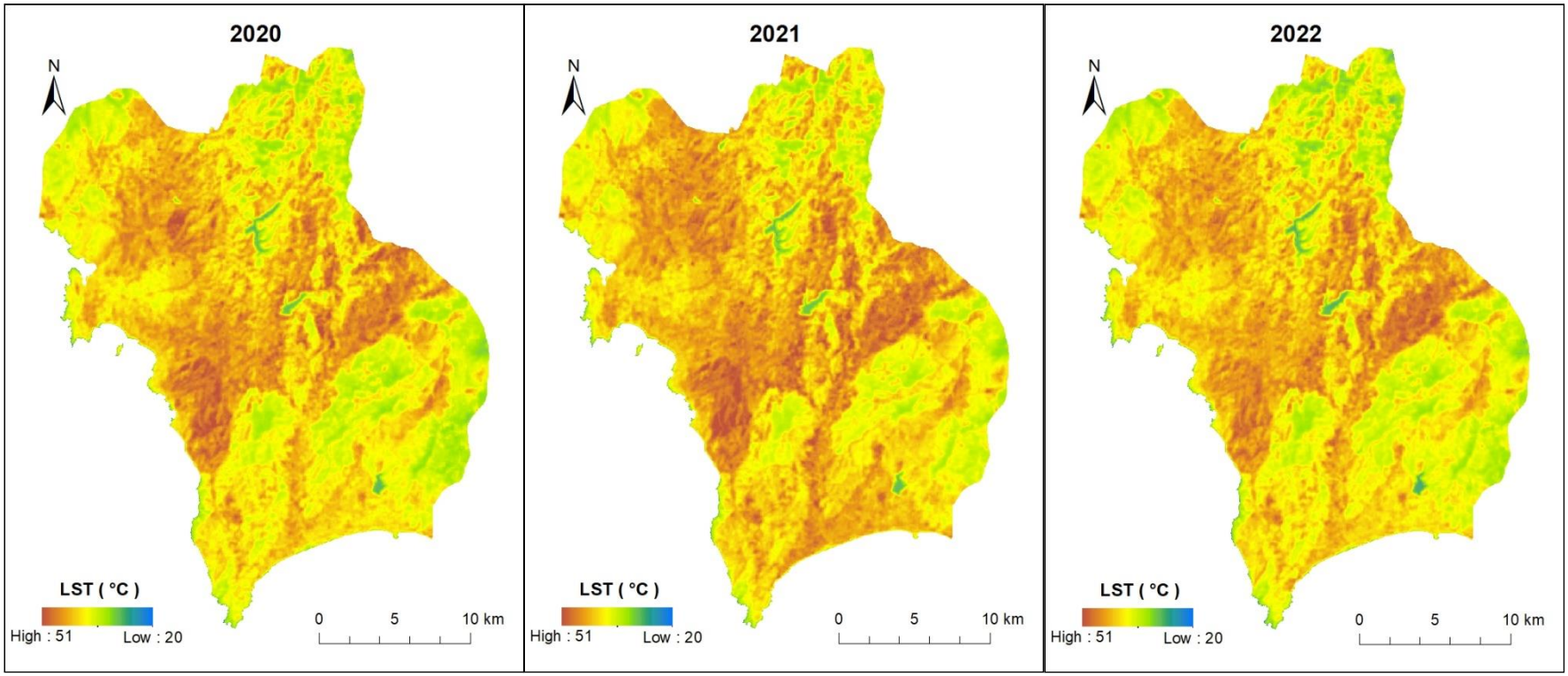

Figure 7.9 (Cont.)

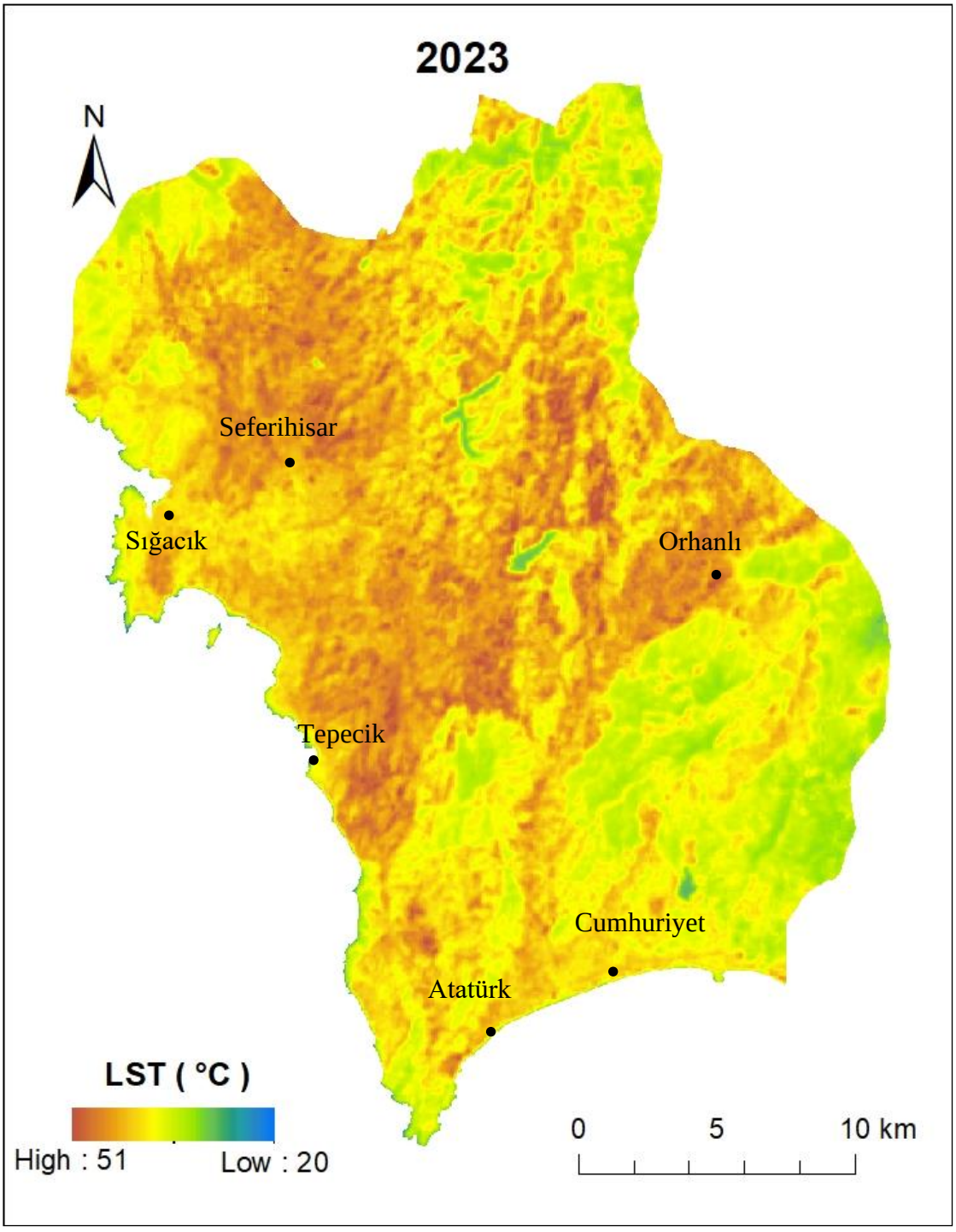

Figure 7.9 (Cont.)

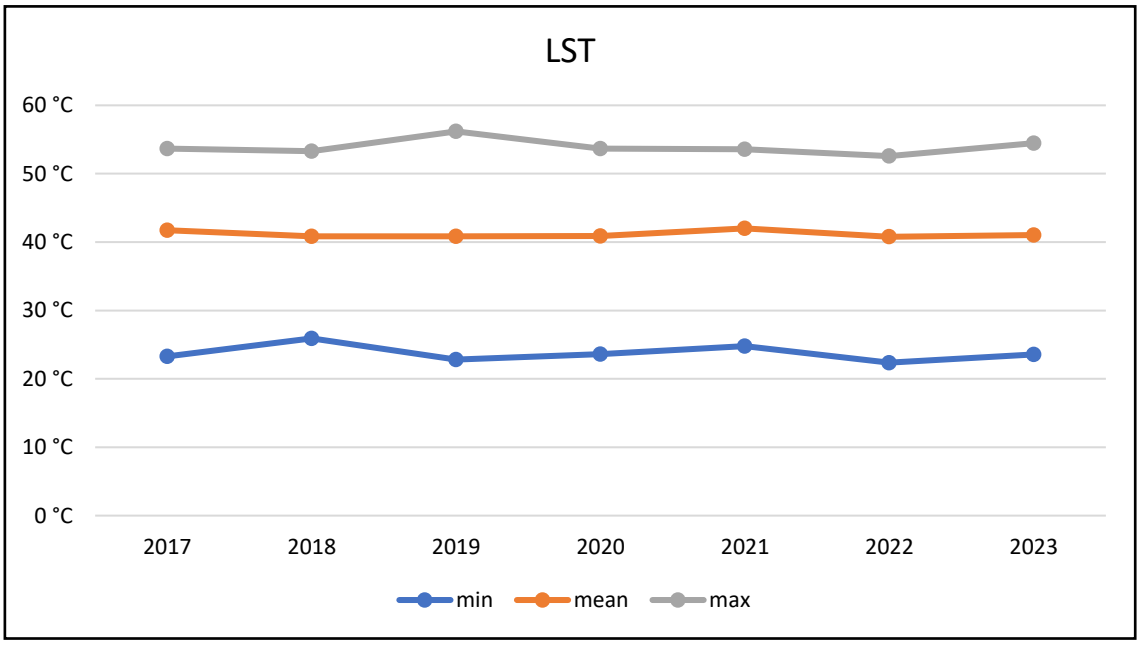

LST

	2017	2018	2019	2020	2021	2022	2023
min	23.297	25.920	22.821	23.623	24.768	22.374	23.565
mean	41.739	40.830	40.823	40.915	42.005	40.778	41.028
max	53.686	53.310	56.188	53.666	53.573	52.579	54.469

Figure 7.10 Minimum, maximum and mean values of LST

7.3 Accuracy Assessment

The algorithms used in classification studies with machine learning methods do not always provide the most accurate results. Many errors arise due to incorrect sampling, differences in correlation between bands, and indistinguishable classes when preparing the training data. Therefore, analyses are conducted with an accepted margin of error. As the accuracy rate of a classified image increases, the quality of the obtained information also improves.

In this study, the producer and user accuracies obtained from the confusion matrix for each image class in the land cover and land cover prediction studies conducted using the random forest algorithm are presented in Table 7.1.

According to the results obtained, especially for the water class, both user and producer accuracies have exhibited excellent performance across all years. This indicates that the algorithm is highly successful in accurately classifying water areas. For the bare land class, user accuracy rates vary between 72.7% and 100%, with these values being acceptable. Producer accuracy rates also show similar variability.

For the cropland class, user accuracy rates range from 55.6% to 100%, with the lowest value of 55.6% observed in 2022. Producer accuracy rates vary between 50.0% and 100%, with the lowest accuracy of 50.0% recorded in 2018 and 2023. This situation reveals that there are occasional low accuracy rates in cropland classification, and performance varies year by year. The main reason for this is the inability of the machine learning algorithm to distinguish the variability in the crops planted in cropland.

For the vegetation class, user accuracy rates generally remain high, ranging from 87.5% to 100%. Producer accuracy rates also remain high, varying between 86.7% and 100%. The lowest value of 86.7% was observed in 2022, but overall, vegetation classification has high accuracy rates.

In the built-up area class, user accuracy rates range from 70.6% to 91.6%, with the lowest accuracy observed in 2018. Producer accuracy rates vary between 60.0% and 100%, with the lowest value of 60.0% recorded in 2019. Significant accuracy fluctuations and performance declines have been observed in built-up area classification over the years.

The 2030 data generally show high accuracy rates. While 100% accuracy is achieved for water and bare land classes, high accuracy rates are also observed for other

classes. These annual data trends indicate that the algorithm performs consistently in some classes but shows variability in accuracy rates in others. This analysis can be used to evaluate the algorithm's performance and determine which classes need improvement.

Table 7.1 Random Forest accuracies

Year		Water	Bareland	Cropland	Vegetation	Build-up
2017	User	100,0%	90,9%	83,4%	92,9%	90,9%
	Producer	100,0%	90,9%	90,9%	100,0%	76,9%
2018	User	100,0%	88,8%	100,0%	100,0%	70,6%
	Producer	100,0%	88,8%	50,0%	100,0%	100,0%
2019	User	100,0%	83,4%	100,0%	100,0%	75,0%
	Producer	100,0%	90,9%	100,0%	100,0%	60,0%
2020	User	100,0%	90,0%	87,5%	87,5%	91,6%
	Producer	100,0%	90,0%	77,8%	100,0%	91,6%
2021	User	100,0%	72,7%	78,6%	94,7%	76,4%
	Producer	100,0%	72,7%	61,1%	100,0%	92,9%
2022	User	100,0%	100,0%	55,6%	100,0%	87,5%
	Producer	100,0%	82,4%	83,4%	86,7%	100,0%
2023	User	100,0%	90,0%	100,0%	91,6%	75,0%
	Producer	100,0%	90,0%	55,6%	100,0%	100,0%
2030	User	100,0%	100,0%	88,4%	92,9%	87,5%
	Producer	100,0%	90,0%	73,5%	92,9%	93,3%

Additionally, the overall accuracy values, which evaluate the total classification accuracy of the produced maps, and the kappa coefficient values, which assess the

model's performance considering the probability of random correct classification, are provided in Table 7.2.

In 2019, this rate reached its highest level at 91.9%, while in 2021, it remained at its lowest level at 83.3%. In 2017, 2020, 2022, and 2023, the accuracy rate varied between 88% and 91%, and in 2030, it was recorded at 88.9%. This indicates that the model generally demonstrated a stable performance in terms of accuracy.

The kappa coefficient reached its highest value at 89.4% in 2019 and its lowest at 78.5% in 2021. In other years, this coefficient varied between 84% and 88%. In 2023 and 2030, the kappa coefficient was recorded at 84.7% and 84.8%, respectively.

The overall analysis of the table reveals that 2019 was the most successful year in terms of both overall accuracy and the kappa coefficient. On the other hand, 2021 stands out as the year with the lowest performance in both metrics. The data for 2030 shows that the overall accuracy and the kappa coefficient are similar to those in 2023. All results have sufficient rates to conduct the analysis.

Table 7.2 Random Forest overall accuracy and Kappa Coefficients

Year	Overall Accuracy	Kapa Coefficient
2017	90,6%	88,0%
2018	87,5%	84,2%
2019	91,9%	89,4%
2020	90,5%	87,8%
2021	83,3%	78,5%
2022	90,0%	87,3%
2023	88,1%	84,7%
2030	88,9%	84,8%

7.4 Land Cover Classification

In order to observe the dynamics of land cover transformation and urban expansion and to lay the foundation for land cover prediction, supervised classification was employed within the study area to delineate land cover categories. Land cover was classified into five distinct classes based on the classification system outlined by the Food and Agriculture Organization (FAO). The analysis unveiled substantial alterations across all land cover categories between the years 2017 and 2023. The general area of the study has seen agricultural lands and bare lands decrease, being replaced by built-up and vegetation areas. The built-up areas have predominantly expanded towards the north. (Figure 7.11).

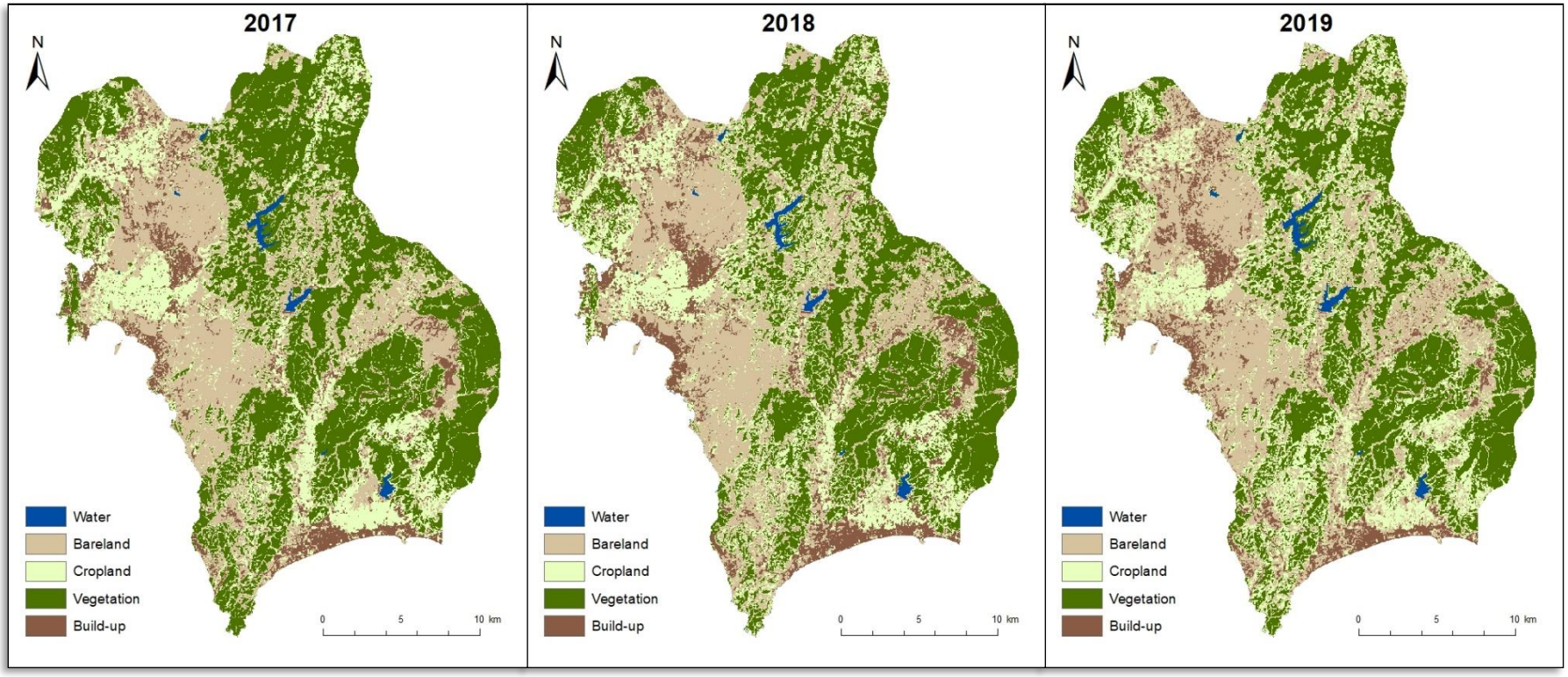

Figure 7.11 Land cover classification results of Seferihisar district

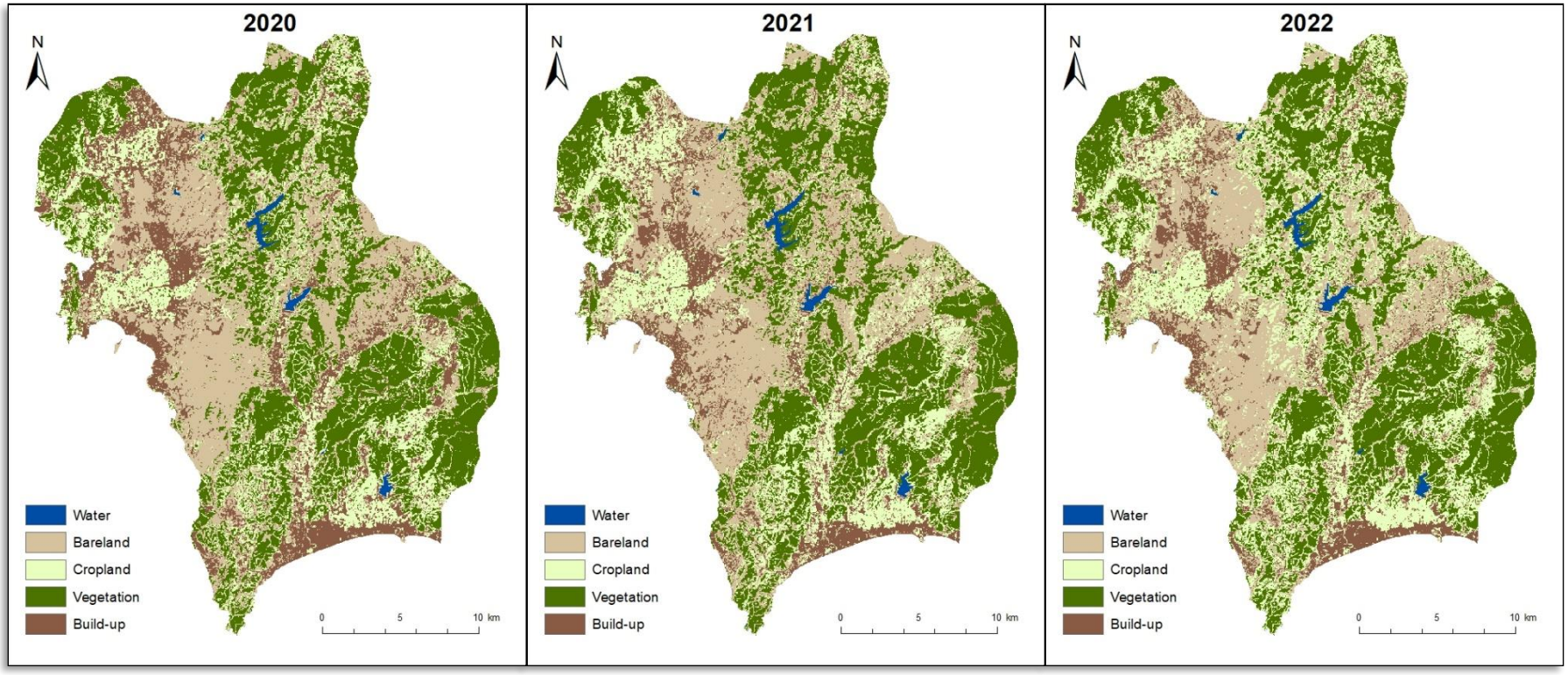

Figure 7.11 (Cont.)

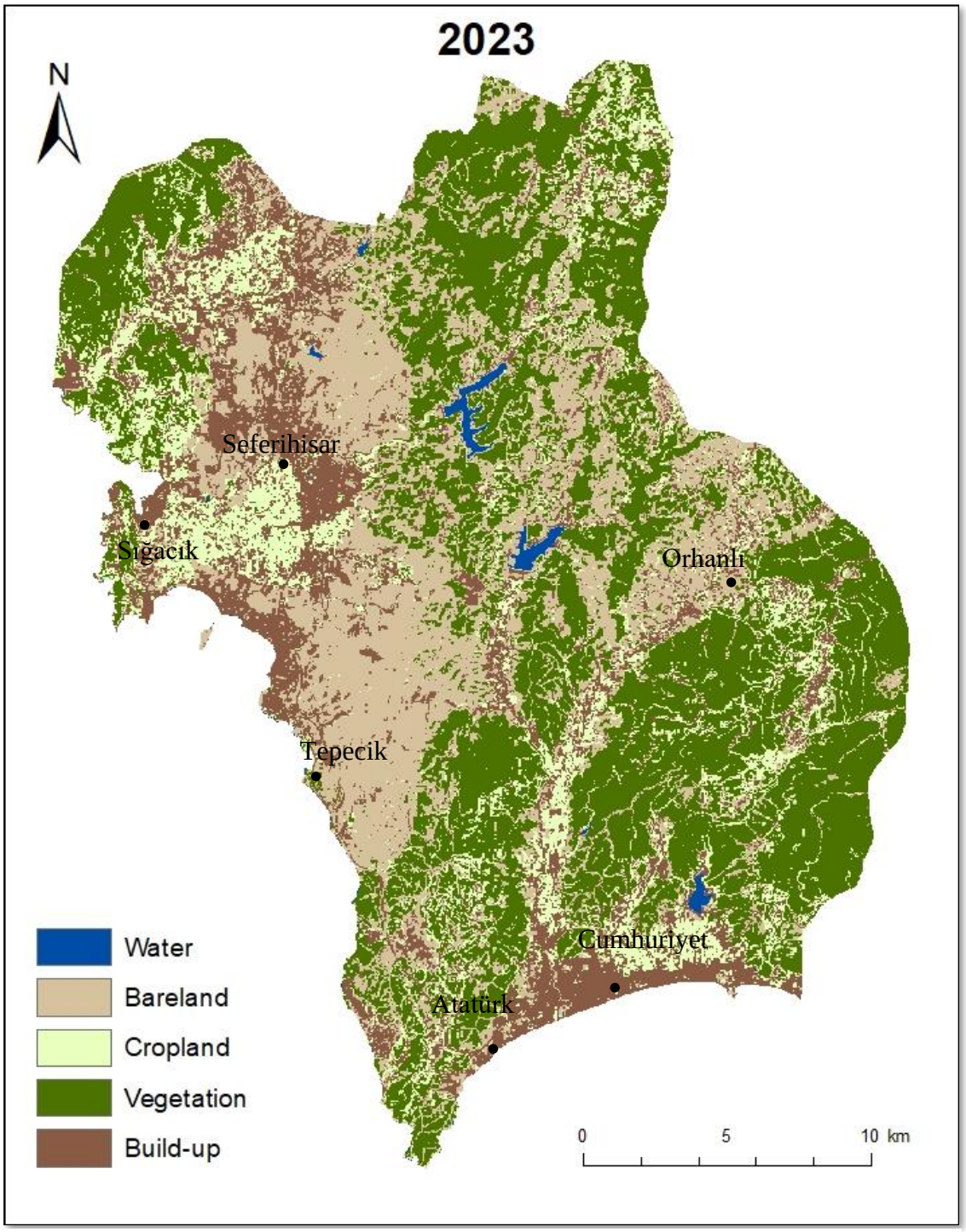

Figure 7.11 (Cont.)

When examining the changes in land cover classes between 2017 and 2023, it is evident that the built-up class experienced the most significant change, with an increase of up to 8.9%. The vegetation class exhibited a general declining trend until 2022, but in 2023, it experienced a notable increase of 6.69%. In contrast, the cropland class showed an increasing trend until 2022, but then experienced a decrease of 15.48% in 2023. The bare land class displayed fluctuating changes over the years. While water bodies witnessed an increase between 2018 and 2022, there was a slight decrease of 0.11% in 2023. The year 2020 recorded the lowest extent of water bodies. Throughout all years, the vegetation class consistently held the highest percentage in the study area, followed by the bare land class. By 2023, the final distribution of land cover classes in the area was as follows: 0.63% water bodies, 27.95% bare land, 14.83% cropland, 40.46% vegetation, and 16.13% built-up. The sizes of land cover classes (in hectares) and their proportions to the total area are summarized in Table 7.3.

Table 7.3 Size of land cover type and its ratio to total area

	2017	2018	2019	2020	2021	2022	2023
Water	2.51km²	2.83km²	3.05km²	2.34km²	3.09km²	2.90km²	2.47km²
	0.64%	0.72%	0.78%	0.60%	0.79%	0.74%	0.63%
Bare Land	115.58km²	122.17km²	130.63km²	111.71km²	116.28km²	92.75km²	109.64km²
	29.46%	31.14%	33.30%	28.47%	29.64%	23.64%	27.95%
Cropland	84.35km²	89.49km²	95.11km²	83.62km²	88.06km²	118.91km²	58.20km²
	21.50%	22.81%	24.24%	21.31%	22.44%	30.31%	14.83%
Vegetation	161.53km²	139.05km²	134.11km²	135.83km²	138.52km²	132.48km²	158.75km²
	41.17%	35.44%	34.18%	34.62%	35.31%	33.77%	40.46%
Built-up	28.35km²	38.79km²	29.43km²	58.83km²	46.38km²	45.29km²	63.27km²
	7.23%	9.89%	7.50%	14.99%	11.82%	11.54%	16.13%
Total	392.33km²	392.33km²	392.33km²	392.33km²	392.33km²	392.33km²	392.33km²

7.5 Relationship between Spectral Indices, Land Cover and LST

To determine the factors influencing LST, a Pearson Correlation Analysis was conducted between spectral indices and LST using the IBM-SPSS statistical program. The analysis utilized data obtained from 3000 random points extracted from the 2023-year maps of all variables. According to the findings of the analysis, a strong negative correlation (-0.690) was observed between LST and NDVI. It can be inferred that areas with high NDVI values tend to have lower LST values. Additionally, a strong positive correlation (0.765) was found between LST and NDBI, indicating that areas with high NDBI values also exhibit high LST values. Furthermore, a weak negative correlation (-0.219) was observed between LST and MNDWI. The scarcity of water surfaces and/or the quality of water within the study area may contribute to the weak correlation, as LST values tend to be lower over clean water surfaces and higher over polluted water surfaces.

Table 7.4 Pearson Correlation (r) between spectral indices and LST

CORRELATIONS

	LST	NDVI	NDBI	MNDWI	NDBaI
LST	1	-,690**	,765**	-,219**	,650**
NDVI	-,690**	1	-,899**	-,234**	-,730**
NDBI	,765**	-,899**	1	-,190**	,786**
MNDWI	-,219**	-,234**	-,190**	1	-,208**
NDBaI	,650**	-,730**	,786**	-,208**	1

**. Correlation is significant at the 0.01 level (2-tailed).

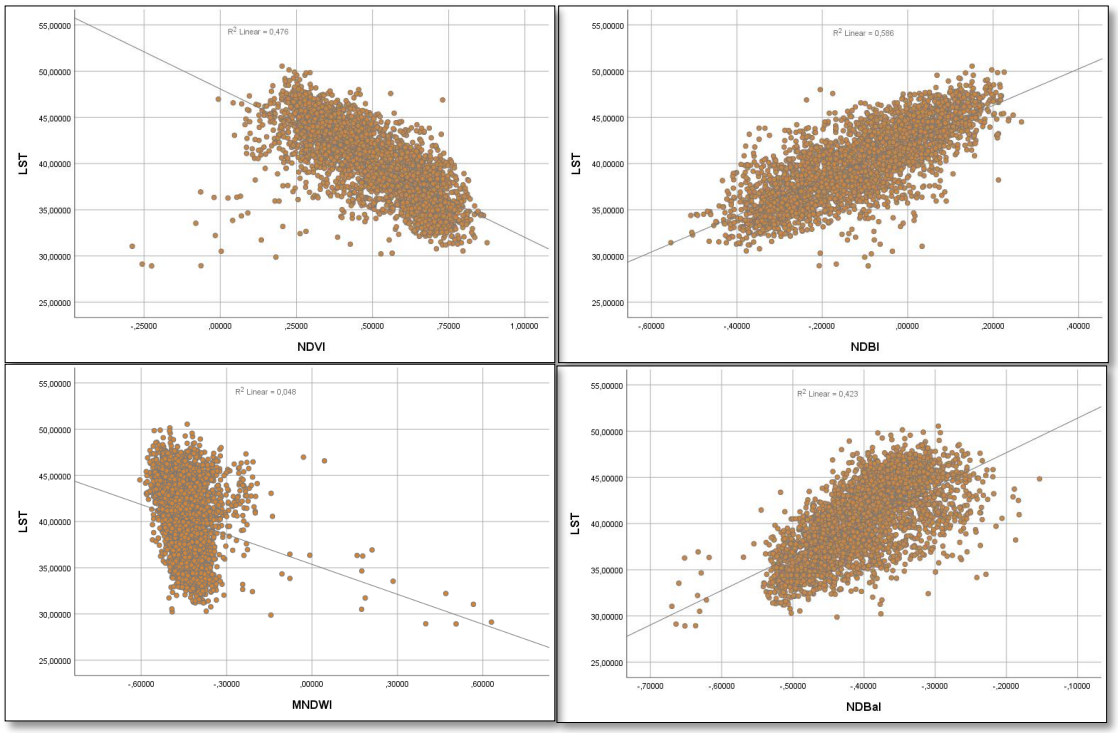

Figure 7.12 Scatter chart between spectral indices and LST

To examine how LST is influenced by changes in land cover, mean, and standard deviation values of temperature were obtained for each land cover class to determine the relationship between land cover classes and LST. According to the obtained data, it is generally observed that LST values tend to decrease in all classes. The classes with the highest LST values throughout all years are built-up and bare land, while the class with the lowest LST values is water. The average surface temperature of water areas increased from 32.394°C in 2017 to 33.352°C in 2023, indicating a significant increasing trend in surface temperatures between these years. The standard deviation (SD) varies over the years and reached its highest level in 2023 at 3.222. The average surface temperature of bare lands showed a slight decrease from 45.153°C in 2017 to 44.144°C in 2023. Although there were slight fluctuations in surface temperatures over the years, overall, a stable trend was observed. The standard deviation values remained relatively constant and did not show significant changes. The average surface temperature of agricultural lands decreased from 41.807°C in 2017 to 40.940°C in 2023. A notable decrease was observed in 2020 (40.284°C), but it increased again in 2021 to 42.422°C. The standard deviation values are generally close to each other and do not show significant changes.

The average surface temperature of vegetation areas decreased from 39.077°C in 2017 to 38.165°C in 2023, indicating a continuous decreasing trend in this category. The standard deviation values are very close to each other, showing minimal changes. The average surface temperature of built-up areas showed a slight decrease from 43.552°C in 2017 to 43.325°C in 2023. Although there were small fluctuations in surface temperatures over the years, a generally stable trend was observed. The standard deviation values also remained relatively constant in a similar manner.

Table 7.5 Change of LST values in land cover classes

Land Cover Type	LST (°C)	2017	2018	2019	2020	2021	2022	2023
Water	Mean	32.394	33.084	31.741	31.723	32.478	31.344	33.352
	SD	2.592	2.876	2.576	2.345	2.746	2.680	3.222
Bare Land	Mean	45.153	43.487	43.576	44.374	44.795	44.471	44.144
	SD	2.929	2.706	2.663	2.988	2.814	2.618	2.843
Cropland	Mean	41.807	40.623	40.766	40.284	42.422	40.968	40.940
	SD	2.723	2.674	2.584	2.411	2.777	2.661	2.594
Vegetation	Mean	39.077	38.404	37.860	37.696	38.826	37.499	38.165
	SD	2.940	2.924	2.938	2.805	2.632	2.648	2.908
Built-up	Mean	43.552	42.159	43.172	43.007	44.305	42.872	43.325
	SD	3.014	2.653	2.809	2.770	2.844	2.721	2.960
Total Area	**Mean**	**41.739**	**40.830**	**40.823**	**40.915**	**42.005**	**40.778**	**41.028**

7.6 Prediction of Land Cover

According to the 2030 land cover prediction results created using land cover classifications and DEM data from 2017 and 2023, the water areas, which were 2.47 km² (0.63%) in 2023, decreased to 1.74 km² (0.44%) in 2030. This indicates a significant reduction in water areas. Bare land increased from 109.64 km² (27.95%) in 2023 to 114.42 km² (29.16%) in 2030, revealing an increase in the amount of bare land.

Agricultural land, which was 58.20 km² (14.83%) in 2023, decreased to 15.66 km² (3.99%) in 2030. This drastic decrease in agricultural land indicates that agricultural areas are being converted into built-up areas. Vegetation areas, which were 158.75 km² (40.46%) in 2023, decreased slightly to 152.93 km² (38.98%) in 2030, indicating a slight reduction in vegetation areas.

Settlement areas increased from 63.27 km² (16.13%) in 2023 to 107.56 km² (27.42%) in 2030. This significant increase in built-up areas is an important point to consider in terms of potential future risks. The spatial comparison of the land cover prediction with the 2023 land cover classification is summarized in Table 7.6.

Table 7.6 Size of 2023 and 2030 land cover type and its ratio to total area

Land Cover Type	**2023**	**2030**
Water	2.47 km^2	1.74 km^2
	0.63%	0.44%
Bare Land	109.64 km^2	114.42 km^2
	27.95%	29.16%
Cropland	58.20 km^2	15.66 km^2
	14.83%	3.99%
Vegetation	158.75 km^2	152.93 km^2
	40.46%	38.98%
Built-up	63.27 km^2	107.56 km^2
	16.13%	27.42%
Total	392.33 km^2	392.33 km^2

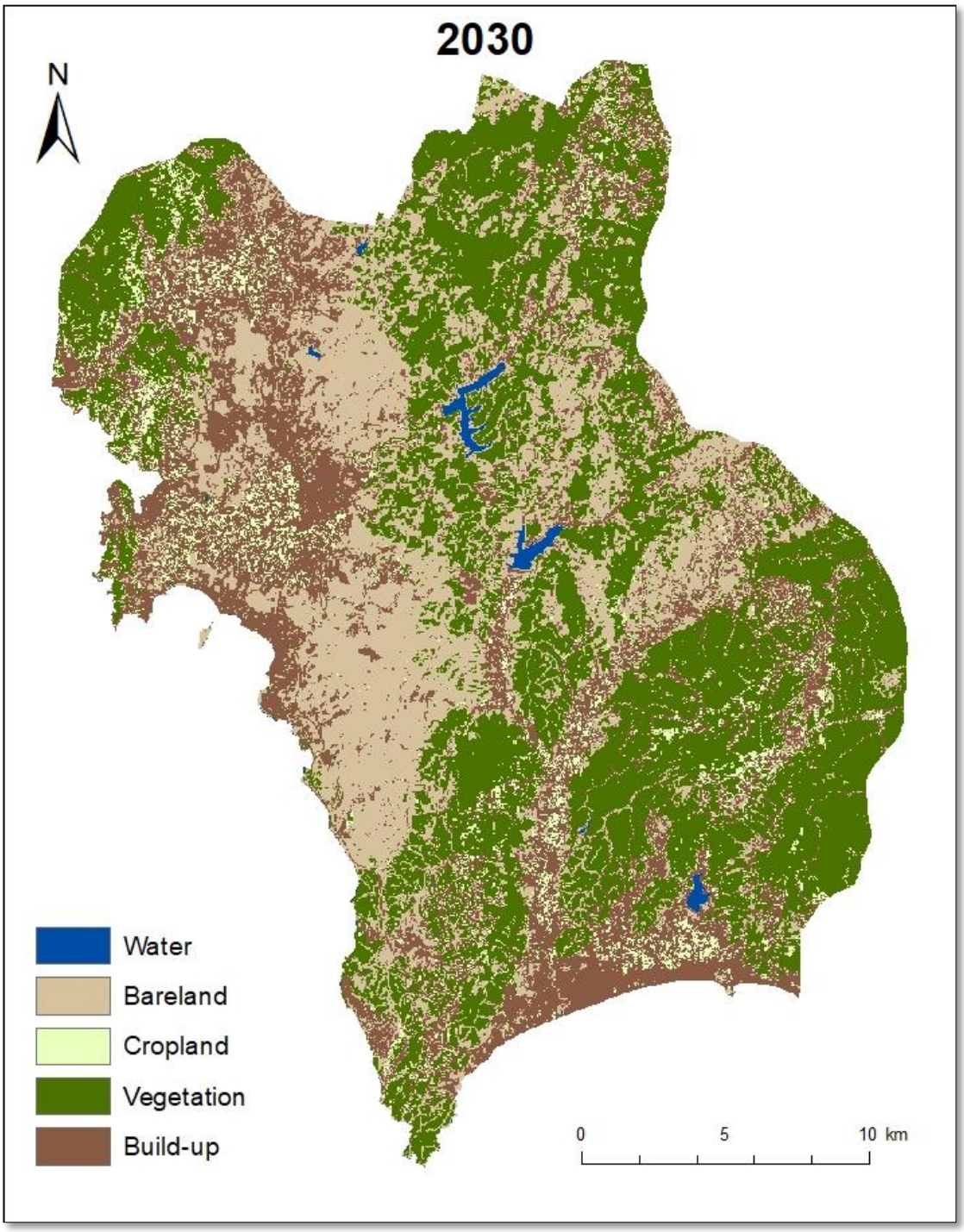

Figure 7.13 2030 Land cover prediction of Seferihisar district

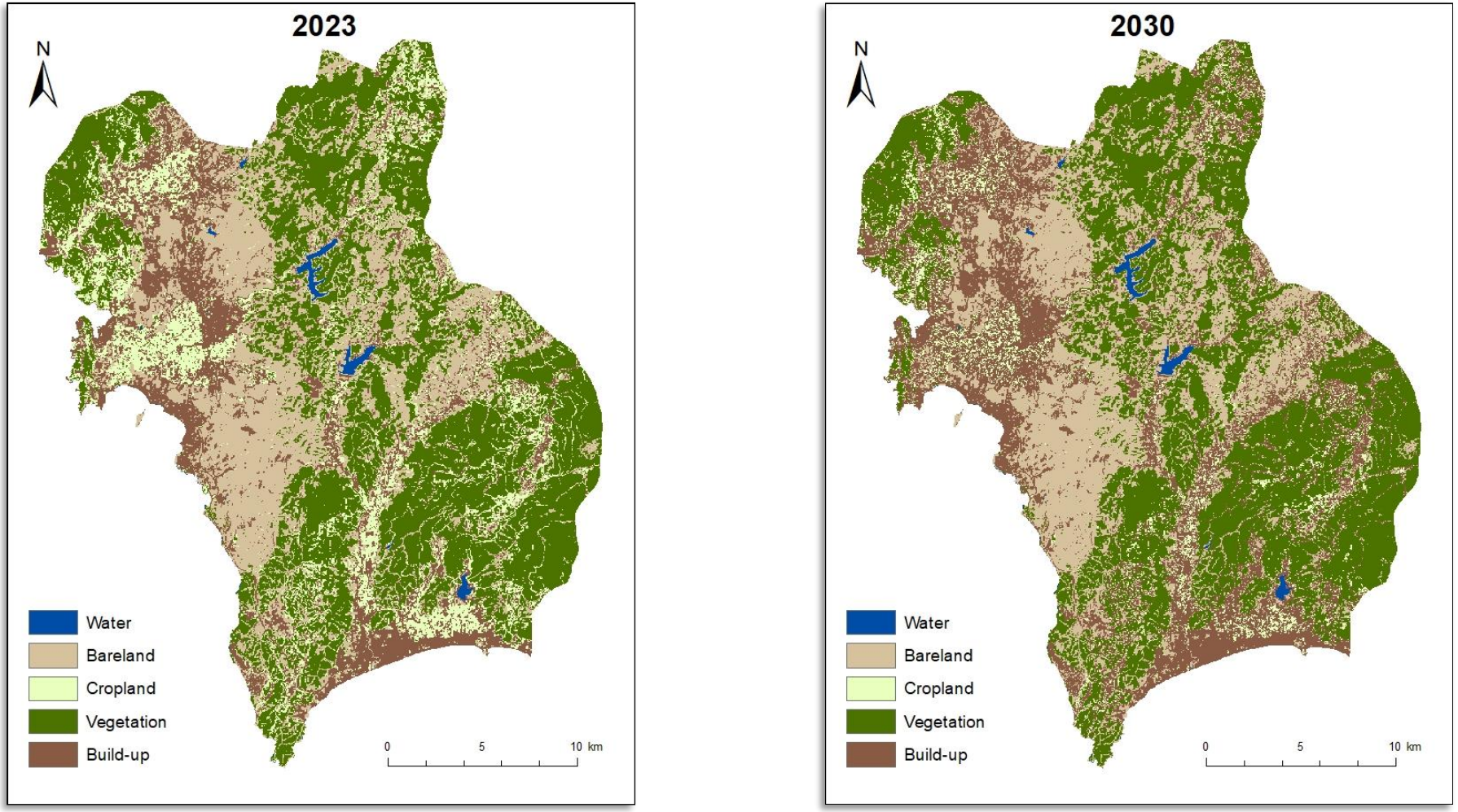

Figure 7.14 2023-2030 landcover comparison

As a result of numerical data and spatial observations, built-up areas have replaced vegetation and cropland in the study area. The expansion of built-up areas has generally occurred towards the north of the study area. In addition to this expansion, an increase in construction density is observed in coastal regions. This density is particularly increasing in the Atatürk, Cumhuriyet, and Sığacık neighborhoods. As the density increases, built-up areas are progressing towards the Orhanlı neighborhood. Additionally, built-up areas have predominantly developed over agricultural lands. One of the main reasons for this is the elevation data used in producing the land cover prediction map. The region with barren land in the Çolakibrahimbey and Turabiye neighborhoods has a high slope, so there is no increase in built-up areas in this region (Figure 7.14).

CHAPTER 8

DISCUSSION AND CONCLUSION

8.1 Discussion

In this study, conducted within the framework of urban sprawl, the relationship between spatial parameters and temperature values was established using remote sensing data, focusing specifically on the Seferihisar district. This section will evaluate the findings of the study, discuss the answers to the research questions, and compare these results with existing literature. This part is crucial to understand how the new findings obtained from the study area are positioned within the literature. Firstly, the significant findings of the research will be summarized, and their implications will be explained. Secondly, the findings will be compared with other studies in the literature, highlighting the similarities and differences. Subsequently, the potential risks that may be encountered in the study area in the future will be evaluated, and solutions to these risks will be proposed.

The analyses revealed that changes in land cover significantly impact LST. In Seferihisar district, a strong positive correlation was identified between LST and both the Normalized Difference Built-up Index (NDBI) and the Normalized Difference Bareness Index (NDBaI). This indicates that as NDBI and NDBaI values increase, LST values also increase, aligning with the findings in the literature (Bala and Dar 2024; Dewan and Corner 2012; Sun, Wu, and Tan 2012; Xiao and Weng 2007). The proximity of bare lands to built-up areas has led to very high temperature values in these regions. Conversely, a strong negative correlation was found between LST and the Normalized Difference Vegetation Index (NDVI). This suggests, consistent with previous studies (Saleem et al. 2020; Xiao and Weng 2007; Zhou, Huang, and Cadenasso 2011), that areas with dense vegetation have lower LST values, indicating that vegetation can reduce LST. The findings from the examination of changes in land cover further support this, as areas with improved vegetation showed a decrease in temperature values. Although a decrease in water presence in the area was observed, the insufficient water data led to a weak

correlation between the Modified Normalized Difference Water Index (MNDWI) and LST (Şentürk and Çubukçu 2022).

When compared with the studies examined in the literature, the findings obtained in this study show a significant degree of similarity. As a result of this similarity, it should be emphasized that in the planning studies to be carried out to reduce LST in the Seferihisar district, the relationship between the indices and LST must be taken into account.

According to the results obtained from the land cover maps, an increase in built-up areas is observed in the Seferihisar district, while all other land cover classes show a decrease. Additionally, when examining the relationship between LST and land cover, high LST values are noticeable in built-up and bare land classes, whereas low LST values are observed in vegetation, cropland, and water areas. Another noteworthy point is the direction of urban sprawl. In the study area, significant sprawl has been observed in built-up areas over the past seven years. The lower LST values in the coastal regions of this sprawl compared to areas near bare land provide important information about the significance of the direction of sprawl. In this regard, studies in the literature provide similar information (Buo et al. 2021; Guo et al. 2020; Neog 2023).

The results obtained from studies examining the relationship between urban sprawl and LST are consistent with the findings of this study. At this point, it becomes evident that in sustainable urban planning and LST reduction studies, attention should be paid to changes in land cover classes and their combinations with each other.

According to the 2030 land cover prediction results, while decreases are observed in the vegetation, cropland, and water classes, there is a significant increase in the built-up and bare land classes (Figure 8.1). The most noteworthy finding at this point is the observed conversion of agricultural land into built-up areas. According to the 2030 land cover prediction, built-up areas generally occupy agricultural lands and bare lands. The fact that vegetation areas are not being significantly encroached upon by other land cover classes is among the positive outcomes of the analysis. Similar to the results of this study, other land cover prediction studies (Asif et al. 2023; Baig et al. 2022; Jalayer et al. 2022; Leta, Demissie, and Tränckner 2021; Wang, Munkhnasan, and Lee 2021) generally observe an increase in built-up areas and indicate that this increase in built-up areas will lead to a decrease in vegetation and agricultural lands.

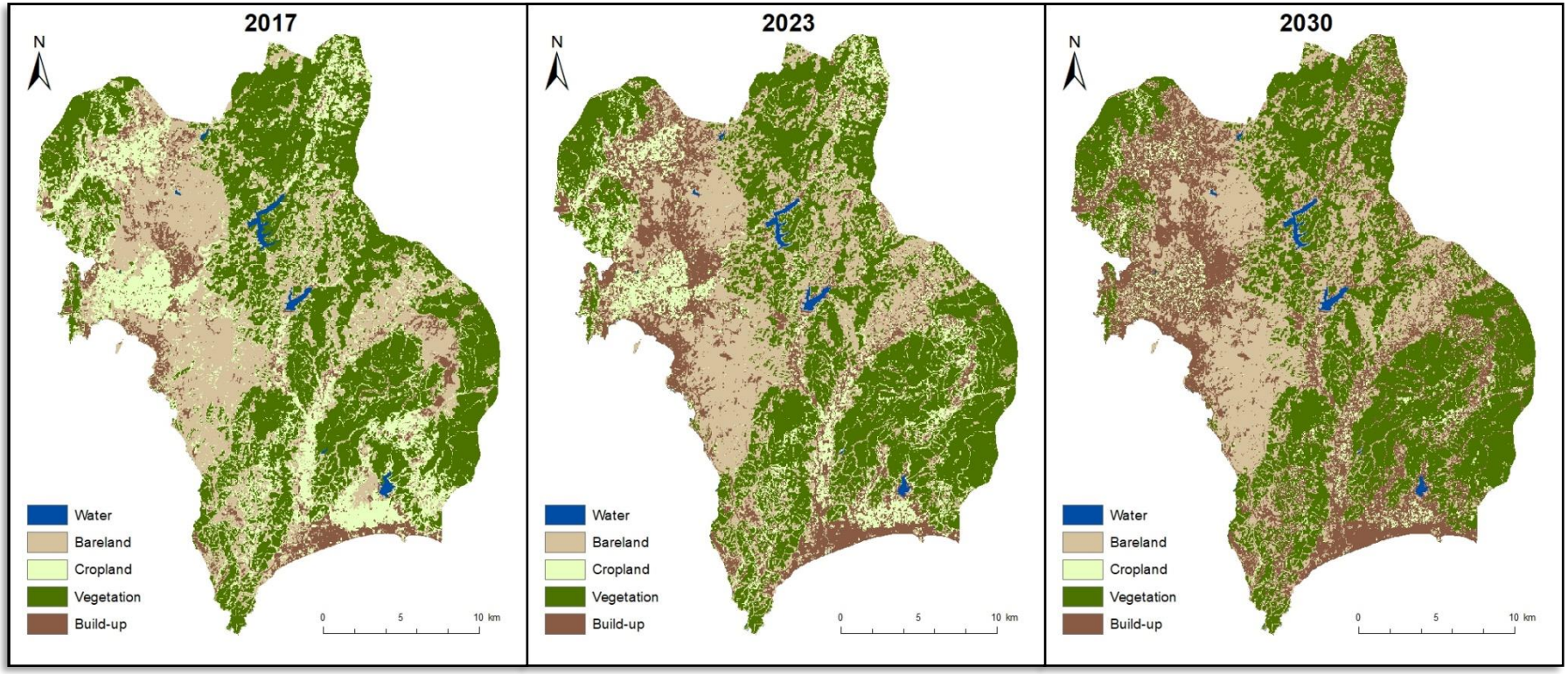

Figure 8.1 2017-2023-2030 land cover comparison

In light of this information, when examining the land cover prediction for the year 2030 for the Seferihisar district, it is evident that Seferihisar will face intense urbanization, which may lead to increases in LST. Another risk the district faces is a significant decrease in cropland areas. This situation implies both ecological and economic damage.

In addition to the impact of land cover on LST, the spatial configuration of land cover classes relative to each other is also important. This underscores the significance of considering the relationships between spaces when undertaking planning efforts aimed at reducing LST. To alleviate urban areas from intense heat pressure, a comprehensive approach should integrate vegetation, water bodies, and built-up areas. Given the proximity of bare lands and built-up areas in the study area, where the highest temperatures are recorded, it is imperative to establish green belts between bare lands and built-up areas. Additionally, new urban settlement areas should be established on habitable barren lands, without destroying agricultural lands and vegetation. However, when the analyses of the 1/25,000 scale environmental layout plan are examined (Figure 8.2), it is observed that the surroundings of the built-up areas are generally covered by areas with slopes exceeding 40%, agricultural lands, and protected areas. Therefore, when urban sprawl can no longer proceed adjacent to these residential areas, the risk of leapfrog sprawl, a type of urban expansion, should be considered. At this point, according to the analysis made in the 1/25,000 scale plan (Figure 8.4), in terms of leapfrog sprawl, a part of the Orhanlı neighborhood stands out due to its barre land quality and low slope. The leap could occur on the habitable barre lands of the Orhanlı neighborhood. However, considering the positive effects of improvements in the area's vegetation, it is important that the leap occurs without damaging the natural vegetation. This leap should occur in a controlled manner, taking into account land cover changes and LST values. During urbanization, structures should be arranged rationally, maintaining a distance from one another, and designed to create cooler areas by distributing vegetation and water bodies appropriately. Moreover, measures tailored to local conditions should be implemented to ensure the coordinated development of regional climates.

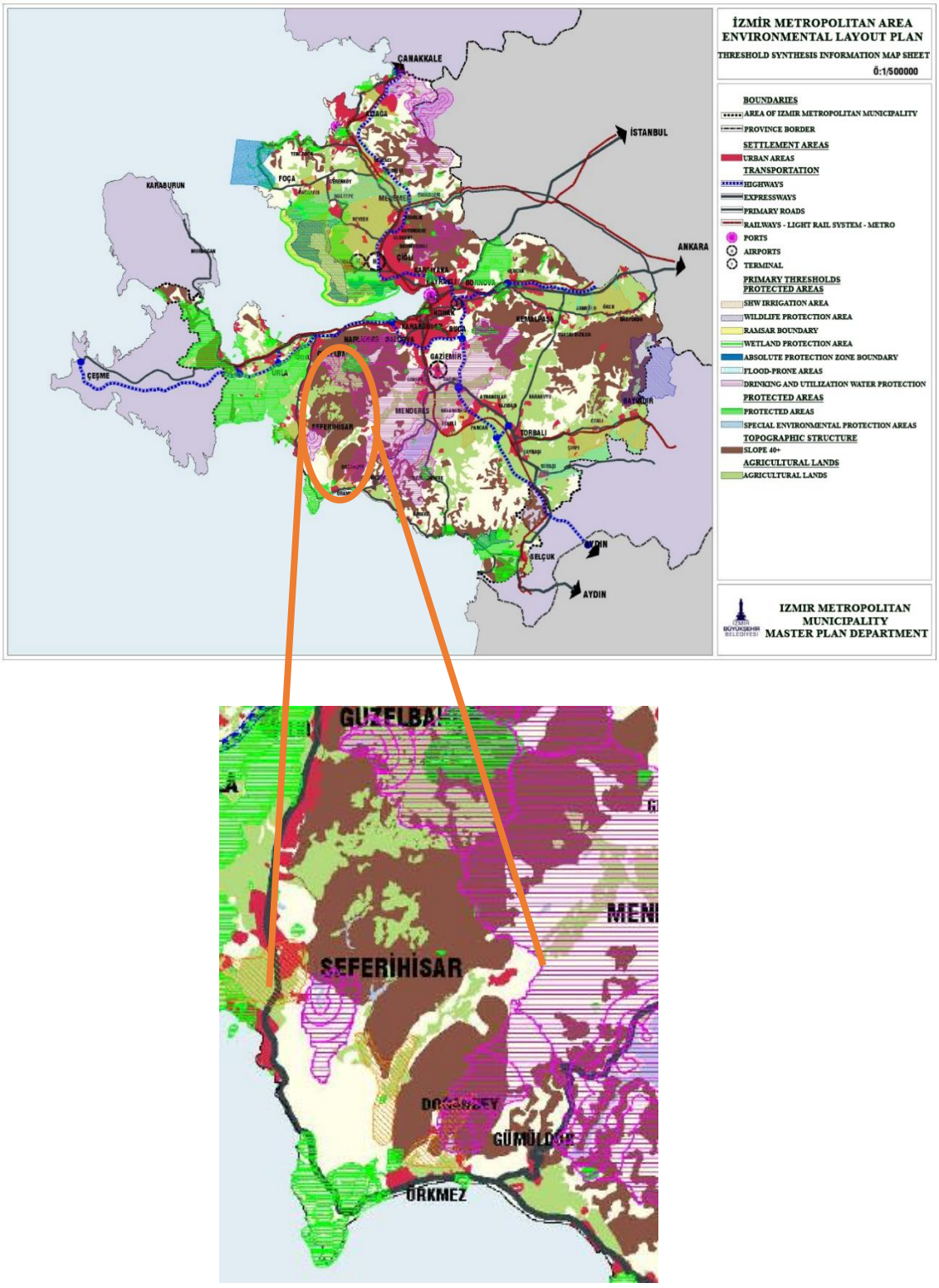

Figure 8.2 Izmir Metropolitan Area Environmental Layout Plan - threshold synthesis information map sheet

In addition, it would be beneficial to interpret the 1/25,000 scale plan decisions of the study area in light of the results obtained from this study. At this point, in the plan, the largest residential development areas are located in the district center (Turabiye, Camikebir, Hıdırlık, Tepecik, and Çolakibrahimbey neighborhoods) (Figure 8.3). Residential development is relatively low in the remaining settlement areas. However, the 'Preferred Use Areas' designated in Sığacık and Hıdırlık neighborhoods (Figure 8.3) and the 'Tourism Center Areas' designated in Atatürk and Cumhuriyet neighborhoods (Figure 8.5) create potential built-up areas and will indirectly/directly trigger urban sprawl in the region. As a result, consistent with the 2030 land cover prediction map created in this study, the cropland in Tepecik neighborhood (Figure 8.3) is at risk of transforming into built-up areas. The study recommends developing ecosystem-based adaptation policies to protect the existing forest cover and cropland, rehabilitate and improve the existing green spaces within and around the residential areas, and prevent urban sprawl, considering other legal frameworks.

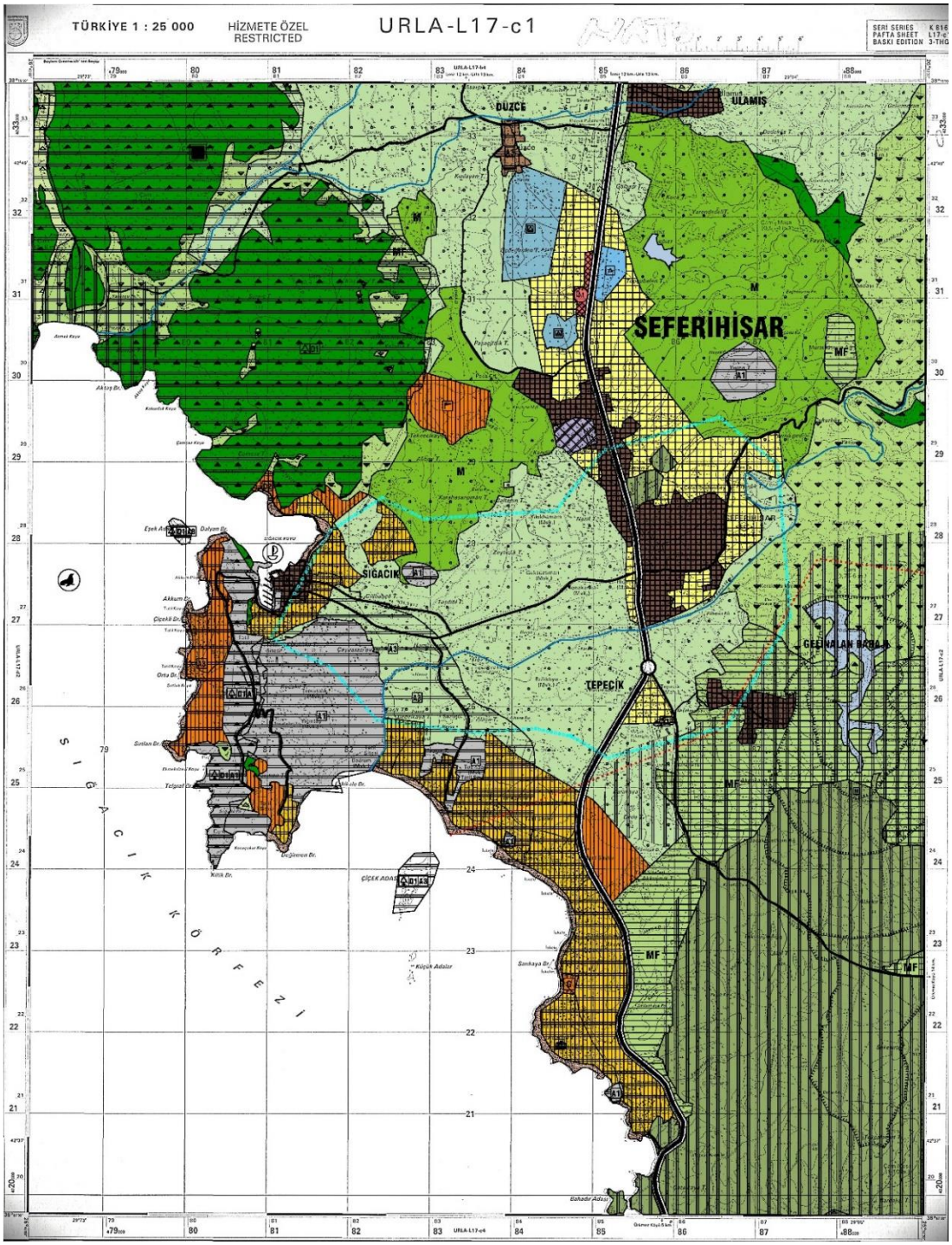

Figure 8.3 1/25000 Scale Environmental Plan L17-c1 map sheet (Source: (IZBB 2012)

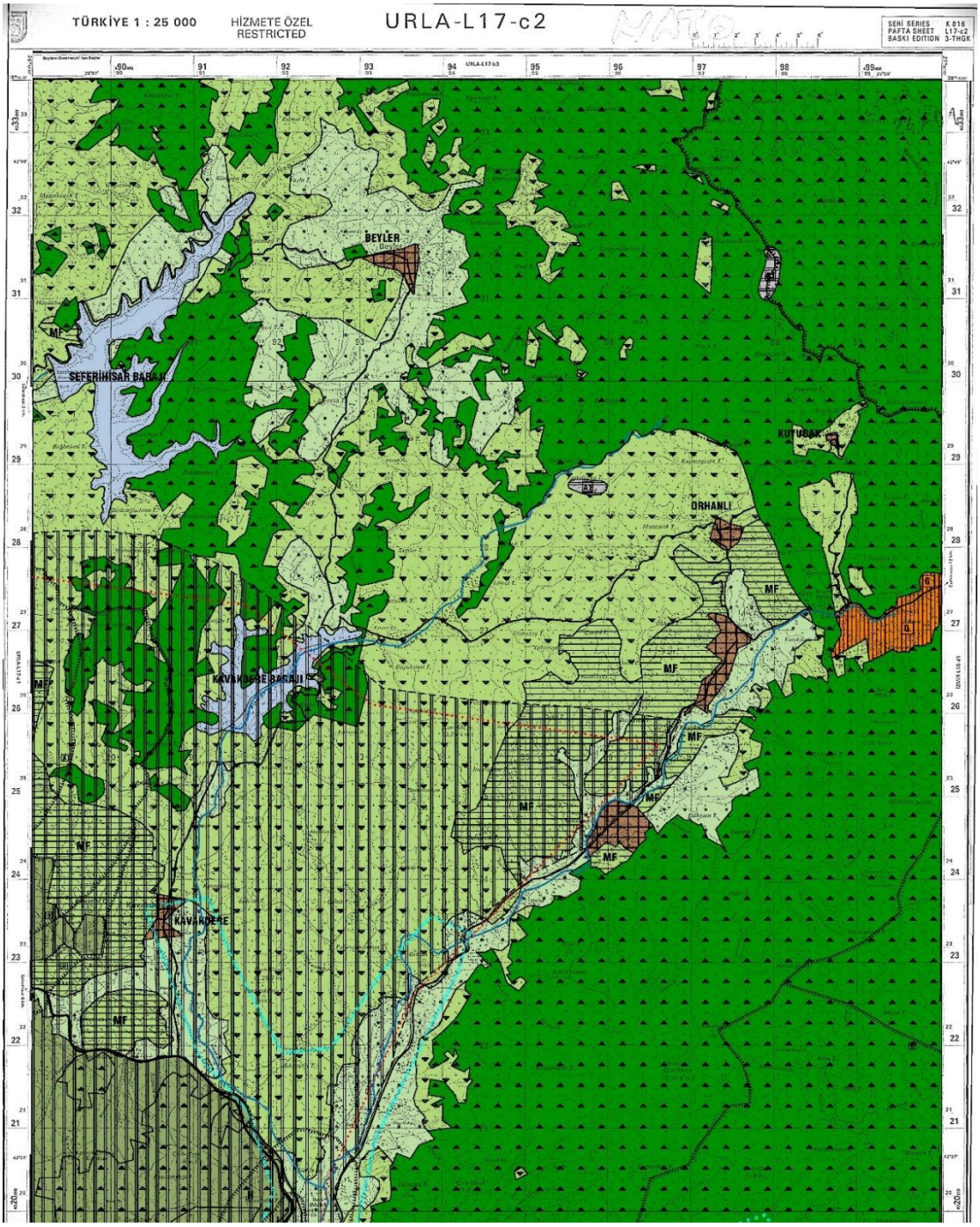

Figure 8.4 1/25000 Scale Environmental Plan L17-c2 map sheet (Source: (IZBB 2012)

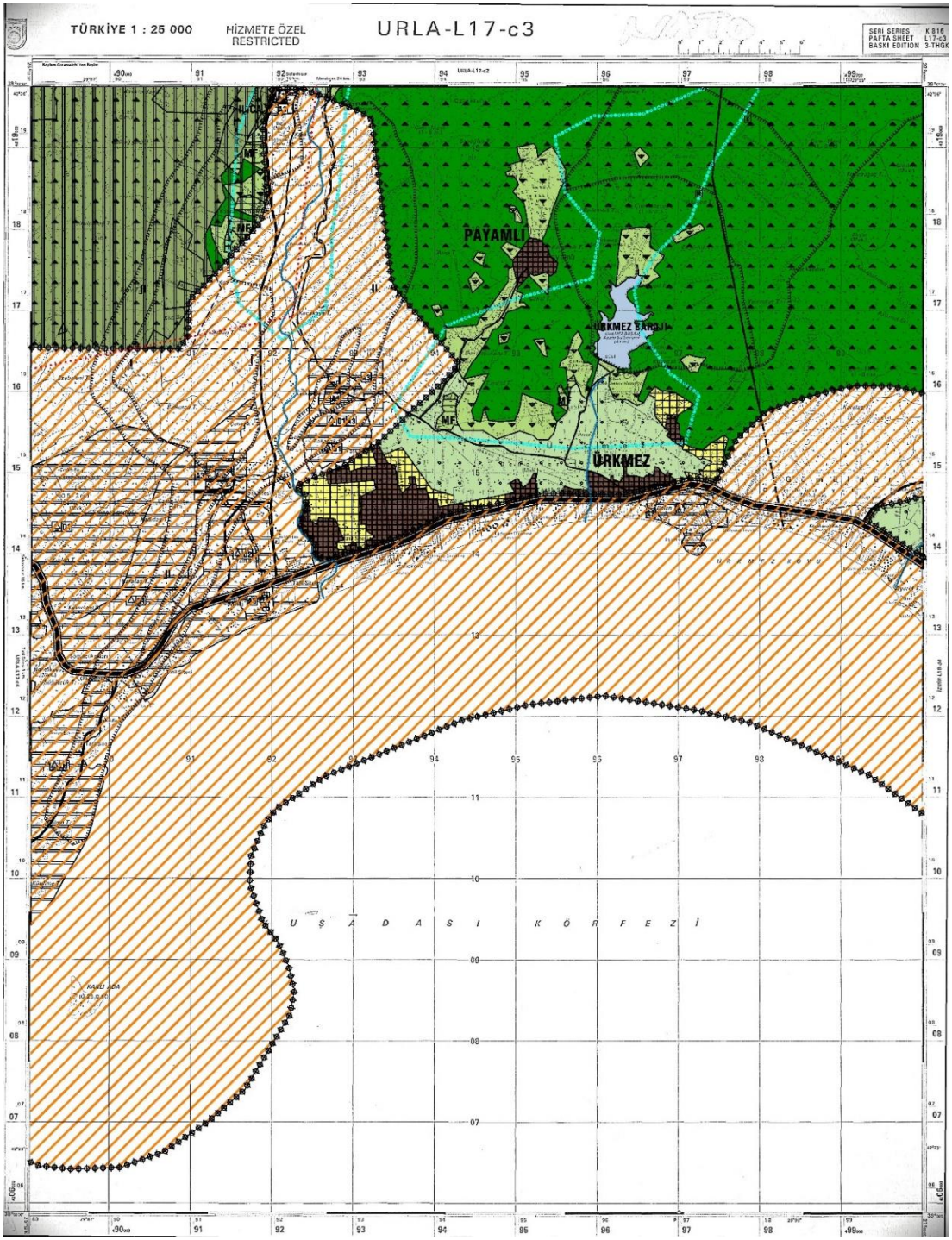

Figure 8.5 1/25000 Scale Environmental Plan L17-c3 map sheet (Source: (IZBB 2012)

8.2 Conclusion

This study focuses on the physical impacts of urban sprawl and examines how changes in land cover due to urban sprawl affect LST. Utilizing spectral indices, land cover, and LST change maps, the study investigates the effects of urban sprawl on LST in the Seferihisar district. Additionally, by predicting land cover for the year 2030, the study addresses potential risks that may arise in the future.

The findings provide valuable insights into the relationship between urban sprawl and climate conditions, particularly how changes in land cover impact LST. Firstly, the spectral indices, including NDVI, NDBI, MNDWI, and NDBaI, were analyzed for each year from 2017 to 2023. Collectively, these indices painted a comprehensive picture of land cover changes over the years. The NDVI results indicated a decrease in vegetation density and quality in some areas, while areas like Orhanlı showed a significant increase in vegetation density and quality. This variability was found to have a strong negative correlation with LST values within the study area. The NDBI, representing built-up areas, indicated an increase in impervious surfaces, and this increase was projected to be even more pronounced in the 2030 land cover prediction. This increase is expected to raise LST. Similarly, a strong positive relationship between bare land cover and LST was identified. These findings suggest that focusing on built-up and bare land areas in planning efforts is crucial for reducing LST. The MNDWI, representing water areas, showed a decrease in water surfaces, but due to the limited water surface data in the area, a weak relationship with LST was identified.

The LST analysis revealed that urban sprawl contributes to increasing temperatures, with built-up areas showing higher LST values compared to vegetated areas. This indicates that urban areas tend to be warmer than their rural surroundings due to the concentration of impervious surfaces and the reduction of vegetation, consistent with the UHI effect observed in the study area. The results from the land cover prediction map were evaluated in this context. As a result of this evaluation, the risks that will affect the study area in the coming years were highlighted, and suggestions were made on how to take precautions against these risks. In this context, all the findings obtained contain important information that can be used in sustainable planning studies and strategies.

In conclusion, this study underscores the significant impact of urban sprawl on LST and emphasizes the need for sustainable urban planning practices to mitigate the

adverse effects of urbanization. By providing a detailed analysis of land cover changes and their climatic impacts, this research offers valuable insights for policymakers and urban planners aiming to develop strategies for more resilient and climate-adaptive urban environments. The findings strengthen the importance of preserving vegetation and managing urban growth to promote a sustainable future for rapidly urbanizing areas like the Seferihisar district.

This research significantly contributes to urban climate studies by establishing a clear link between urban sprawl and increasing LST. The methodology, combining remote sensing data with statistical analyses, provides a robust framework for monitoring and predicting land cover changes and their climatic impacts. Additionally, the execution of land cover prediction studies on the GEE platform is a notable contribution to the study. The use of GEE and SPSS for data processing and analysis ensured accurate and reliable results.

One limitation of this study is its focus on the summer months (June–August) to minimize seasonal variability. While this approach enhances data consistency, it may overlook the effects of urban sprawl on LST during other seasons. Furthermore, the study's restriction to the Seferihisar district limits the generalizability of the findings to other regions with different climatic and geographical conditions. Another limitation is the use of data from the Landsat 8 satellite. Although these data facilitated the analyses, the 30-meter resolution posed challenges in delineating precise spatial boundaries in the results.

Future research could consider year-round analyses to capture seasonal variations in LST and their relationships with urban sprawl. Expanding the study to encompass multiple districts or regions with diverse characteristics would enhance the understanding of urban sprawl's impact across different environmental contexts. Moreover, incorporating socioeconomic factors into the analyses could provide a more holistic view of the driving forces behind urban sprawl and its environmental consequences. Obtaining higher-resolution data or comparing this data with remote sensing data where possible could lead to more accurate results.

REFERENCES

Alberti, Marina, and John M Marzluff. 2004. “Ecological Resilience in Urban Ecosystems: Linking Urban Patterns to Human and Ecological Functions.” Vol. 7.

Anniballe, Roberta, Stefania Bonafoni, and Manuele Pichierri. 2014. “Spatial and Temporal Trends of the Surface and Air Heat Island over Milan Using MODIS Data.” *Remote Sensing of Environment* 150:163–71. https://doi.org/10.1016/j.rse.2014.05.005.

Anyamba, Assaf, J. Estes, K. Kline, and E. Collins. 2015. “Remote Sensing.” In *International Encyclopedia of the Social & Behavioral Sciences: Second Edition*, 419–24. Elsevier Inc. https://doi.org/10.1016/B978-0-08-097086-8.72046-0.

Arellano, Blanca, and Josep Roca. 2018. “Can Urban Design Mitigate the UHI Effect?” https://www.researchgate.net/publication/330858743.

Asif, Muhammad, Jamil Hasan Kazmi, Aqil Tariq, Na Zhao, Rufat Guluzade, Walid Soufan, Khalid F. Almutairi, Ayman El Sabagh, and Muhammad Aslam. 2023. “Modelling of Land Use and Land Cover Changes and Prediction Using CA-Markov and Random Forest.” *Geocarto International* 38 (1). https://doi.org/10.1080/10106049.2023.2210532.

AtlasBig. 2024. “İzmir Seferihisar’ın Mahalleleri - AtlasBig.Com.” 2024. https://atlasbig.com.tr/izmir-seferihisarin-mahalleleri.

Baig, Mohammed Feras, Muhammad Raza Ul Mustafa, Imran Baig, Husna Binti Takaijudin, and Muhammad Talha Zeshan. 2022. “Assessment of Land Use Land Cover Changes and Future Predictions Using CA-ANN Simulation for Selangor, Malaysia.” *Water (Switzerland)* 14 (3). https://doi.org/10.3390/w14030402.

Bala, Sanju, and Sajad Nabi Dar. 2024. “Dynamics of Land Use Land Cover and Its Impact on Land Surface Temperature: A Study of Faridabad District, India.” *GeoJournal* 89 (1). https://doi.org/10.1007/s10708-024-11011-y.

Bhandari, Nimesh, Purna Bahadur Saud, and Susan Mahatara. 2023. “"LULC and Urban Expansion Intensity Analysis in Dhangadhi.” https://doi.org/10.13140/RG.2.2.27702.06723.

Bhatta, Basudeb. 2010. “Analysis of Urban Growth and Sprawl from Remote Data.” http://www.springer.com/series/7712.

Branea, Ana-Maria, Marius Stelian Gaman, Stefana Badescu, Branea Ana-Maria, Danciu Mihai-Ionut, Găman Marius Stelian, and Bădescu Ștefana. 2016. “Challanges Regarding the Study of Urban Heat Islands. Ruleset for Researchers CHALLENGES REGARDING THE STUDY OF URBAN HEAT ISLANDS. RULESET FOR RESEARCHERS.” https://www.researchgate.net/publication/309740257.

Brueckner, Jan K. 2000. “URBAN SPRAWL: DIAGNOSIS AND REMEDIES.” *INTERNATIONAL REGIONAL SCIENCE REVIEW*. Vol. 23. Brueckner / URBAN SPRAWL.

Bruegmann, Robert. 2005. *Sprawl : A Compact History*. University of Chicago Press.

Buo, Isaac, Valentina Sagris, Iuliia Burdun, and Evelyn Uuemaa. 2021. “Estimating the Expansion of Urban Areas and Urban Heat Islands (UHI) in Ghana: A Case Study.” *Natural Hazards* 105 (2): 1299–1321. https://doi.org/10.1007/s11069-020-04355-4.

Çağlak, Savaş, Tamer Özlü, and Süleyman Toy. 2019. “İklim Verilerinin Deniz Etkisi Altında Kentsel Kırsal Farklılığı, Samsun Kenti Örneği.” *Iğdır Üniversitesi Fen Bilimleri Enstitüsü Dergisi* 9 (1): 330–38. https://doi.org/10.21597/jist.447421.

Castells, Manuel. 2010. *The Rise of the Network Society*. Second. Willey-Blackwell.

Chandra, Shankar N Ramaseri, Jon B Christopherson, and Kimberly A Casey. 2020. *2020 Joint Agency Commercial Imagery Evaluation—Remote Sensing Satellite Compendium*. US Geological Survey.

Chen, Xiao Ling, Hong Mei Zhao, Ping Xiang Li, and Zhi Yong Yin. 2006. “Remote Sensing Image-Based Analysis of the Relationship between Urban Heat Island and Land Use/Cover Changes.” *Remote Sensing of Environment* 104 (2): 133–46. https://doi.org/10.1016/j.rse.2005.11.016.

Chettry, Vishal. 2023. “A Critical Review of Urban Sprawl Studies.” *Journal of Geovisualization and Spatial Analysis*. Springer Nature. https://doi.org/10.1007/s41651-023-00158-w.

Chin, Nancy. 2002. “CENTRE FOR ADVANCED SPATIAL ANALYSIS UNEARTHING THE ROOTS OF URBAN SPRAWL: A CRITICAL ANALYSIS OF FORM, FUNCTION AND METHODOLOGY.” www.casa.ucl.ac.uk.

Claverie, Martin, Junchang Ju, Jeffrey G. Masek, Jennifer L. Dungan, Eric F. Vermote, Jean Claude Roger, Sergii V. Skakun, and Christopher Justice. 2018. “The Harmonized Landsat and Sentinel-2 Surface Reflectance Data Set.” *Remote Sensing of Environment* 219 (December):145–61. https://doi.org/10.1016/j.rse.2018.09.002.

Copernicus. 2024. “S2 Applications.” 2024. https://sentiwiki.copernicus.eu/web/s2-applications.

CSB. 2024. “İzmir-Manisa Planlama Bölgesi 1/100.000 Ölçekli Çevre Düzeni Planı.” 2024. https://mpgm.csb.gov.tr/izmir-manisa-planlama-bolgesi-1-100.000-olcekli-cevre-duzeni-plani-i-82265.

Deilami, Kaveh, Md Kamruzzaman, and Yan Liu. 2018. “Urban Heat Island Effect: A Systematic Review of Spatio-Temporal Factors, Data, Methods, and Mitigation Measures.” *International Journal of Applied Earth Observation and Geoinformation*. Elsevier B.V. https://doi.org/10.1016/j.jag.2017.12.009.

Demircan, Neslihan, and Süleyman Toy. 2018. “TÜRKİYE KENTSEL İKLİM DEĞİŞİKLİĞİ LİTERATÜRÜ TURKISH URBAN CLIMATE CHANGE LITERATURE.” https://www.researchgate.net/publication/326683154.

Demirkesen, Ali Can, and Fatih Evrendilek. 2017. “Compositing Climate Change Vulnerability of a Mediterranean Region Using Spatiotemporally Dynamic Proxies for Ecological and Socioeconomic Impacts and Stabilities.” *Environmental Monitoring and Assessment* 189 (1). https://doi.org/10.1007/s10661-016-5750-0.

Dewan, Ashraf M, and Robert J Corner. 2012. “THE IMPACT OF LAND USE AND LAND COVER CHANGES ON LAND TEMPERATURE IN A RAPIDLY URBANIZING MEGACITY.” In *IEEE International Geoscience and Remote Sensing Symposium*, 6337–39. IEEE.

Dincer, Seyma Elif, Furkan Akdemir, Hayri Ulvi, and Hidir Duzkaya. 2019. “Assessing Urban Sprawl Effect of Transportation Investments Using Remote Sensing Data and GIS Methods: The Case of Ankara Protocol Road.” In *IOP Conference Series: Materials Science and Engineering*. Vol. 471. Institute of Physics Publishing. https://doi.org/10.1088/1757-899X/471/9/092079.

Dissanayake, D. M.S.L.B., Takehiro Morimoto, Manjula Ranagalage, and Yuji Murayama. 2019. “Land-Use/Land-Cover Changes and Their Impact on Surface Urban Heat Islands: Case Study of Kandy City, Sri Lanka.” *Climate* 7 (8). https://doi.org/10.3390/cli7080099.

EarthData. 2024a. “Data Processing Levels | Earthdata.” 2024. https://www.earthdata.nasa.gov/engage/open-data-services-and-software/data-and-information-policy/data-levels.

———. 2024b. “Sensors | Earthdata.” 2024. https://www.earthdata.nasa.gov/sensors.

———. 2024c. “What Is Remote Sensing? And Sensors| Earthdata.” 2024. https://www.earthdata.nasa.gov/learn/backgrounders/remote-sensing.

Ebi, K L, L O Mearns, and B Nyenzi. 2003. “Weather and Climate: Changing Human Exposures.”

Ebrahimy, Hamid, Babak Mirbagheri, Ali Akbar Matkan, and Mohsen Azadbakht. 2021. “Per-Pixel Land Cover Accuracy Prediction: A Random Forest-Based Method with Limited Reference Sample Data.” *ISPRS Journal of Photogrammetry and Remote Sensing* 172 (February):17–27. https://doi.org/10.1016/j.isprsjprs.2020.11.024.

EEA. 2016. “Urban Sprawl in Europe — Scattered Urban Areas Continue to Expand — Joint EEA-FOEN Report.”

EGIAD. 2017. “EKONOMİK VE DEMOGRAFİK GÖSTERGELERLE İZMİR.”

Elmarakby, Esraa, Marwa Khalifa, Abeer Elshater, and Samy Afifi. 2020. “Spatial Morphology and Urban Heat Island: Comparative Case Studies.” In *Architecture and Urbanism: A Smart Outlook*, 441–54. Springer International Publishing. https://doi.org/10.1007/978-3-030-52584-2_31.

Emre, Ömer, Selim Özalp, Ahmet Doğan, Volkan Özaksoy, Cengiz Yıldırım, and Fikret Göktaş. 2005. “İZMİR YAKIN ÇEVRESİNİN DİRİ FAYLARI VE DEPREM POTANSİYELLERİ MADEN TETKİK VE ARAMA GENEL MÜDÜRLÜĞÜ.”

Endeksa. 2024. “İzmir Seferihisar Satılık Arazi Fiyatları.” 2024. https://www.endeksa.com/tr/analiz/turkiye/izmir/seferihisar/endeks/satilik/arazi.

EPA. 2008. “Reducing Urban Heat Islands: Compendium of Strategies: Heat Island Reduction Activities.” https://www.epa.gov/heat-islands/heat-.

Erell, Evyatar, David Pearlmutter, and Terry Williamson. 2012. *Urban Microclimate-Designing the Spaces Between Buildings*.

Ersoy Tonyaloğlu, Ebru, Adnan Menderes Üniversitesi, Ziraat Fakültesi, and Peyzaj Mimarlığı Bölümü. 2019. “KENTLEŞMENİN KENTSEL TERMAL ÇEVRE ÜZERİNDEKİ ETKİSİNİN DEĞERLENDİRİLMESİ, EFELER VE İNCİRLİOVA (AYDIN) ÖRNEĞİ.” *Araştırma Makalesi Turkish Journal of Landscape Research*. Vol. 2.

ESRI. 2024a. “How Zonal Statistics Tools Work—ArcGIS Pro | Documentation.” 2024. https://pro.arcgis.com/en/pro-app/latest/tool-reference/spatial-analyst/how-zonal-statistics-works.htm.

———. 2024b. “Indices Gallery—ArcGIS Pro | Documentation.” 2024. https://pro.arcgis.com/en/pro-app/latest/help/data/imagery/indices-gallery.htm.

Ewing, Reid. 1997. “Is Los Angeles-Style Sprawl Desirable?” *Journal of the American Planning Association* 63 (1): 107–26. https://doi.org/10.1080/01944369708975728.

———. 2008. “Characteristics, Causes, and Effects of Sprawl: A Literature Review.”

Ewing, Reid, Rolf Pendall, and Don Chen. 2003. “Measuring Sprawl and Its Transportation Impacts.”

Feranec, Jan, Monika Kopecka, Daniel Szatmari, Juraj Holec, Pavel Stastny, Robert Pazur, and Hana Babalova. 2019. “A Review of Studies Involving the Effect of Land Cover and Land Use on the Urban Heat Island Phenomenon, Assessed by Means of the MUKLIMO Model.” *Geografie* 124 (1):383–101.

Frenkel, Amnon, and Maya Ashkenazi. 2008. “Measuring Urban Sprawl: How Can We Deal with It?” *Environment and Planning B: Planning and Design* 35 (1): 56–79. https://doi.org/10.1068/b32155.

Galster, George, Royce Hanson, Michael R. Ratcliffe, Harold Wolman, Stephen Coleman, and Jason Freihage. 2001. “Wrestling Sprawl to the Ground: Defining and Measuring an Elusive Concept.” *Housing Policy Debate* 12 (4): 681–717. https://doi.org/10.1080/10511482.2001.9521426.

Garipağaoğlu, Nuriye. 2010. “Investigation Of Urbanization in Turkey According to Number of Cities, Urban Population Criteria and Geographical Distribution.” *Marmara Coğrafya Dergisi* 22 (July):1–42.

GDM. 2024. “GDM | General Directorate of Mapping - National Mapping Agency.” 2024. https://www.harita.gov.tr/il-ve-ilce-yuzolcumleri.

GEE. 2024. “FAQ – Google Earth Engine.” 2024. https://earthengine.google.com/faq/.

Glaeser, Edward L, and Matthew E Kahn. 2004. “SPRAWL AND URBAN GROWTH.” *Handbook of Regional and Urban Economics* 4:2481–2527. https://doi.org/10.1016/S0169-7218(04)07056-X.

Gorelick, Noel, Matt Hancher, Mike Dixon, Simon Ilyushchenko, David Thau, and Rebecca Moore. 2017. “Google Earth Engine: Planetary-Scale Geospatial Analysis for Everyone.” *Remote Sensing of Environment* 202 (December):18–27. https://doi.org/10.1016/J.RSE.2017.06.031.

Gülersoy, Ali Ekber. 2014. “Sayı: 31, Ss.” *Nisan*.

Guo, Andong, Jun Yang, Xiangming Xiao, Jianhong Xia (Cecilia), Cui Jin, and Xueming Li. 2020. “Influences of Urban Spatial Form on Urban Heat Island Effects at the Community Level in China.” *Sustainable Cities and Society* 53 (February). https://doi.org/10.1016/j.scs.2019.101972.

Harvey, Robert O, and W A V Clark. 1965. “The Nature and Economics of Urban Sprawl.” Vol. 41. https://www.jstor.org/stable/3144884.

İneç, Zekeriya F. 2023. “Dinamik Web Haritalamada Yeni Bir Dönem: Google Earth Engine.” *Kamu Yönetimi Enstitüsü Sosyal Bilimler Dergisi*, no. 4, 233–58. https://dergipark.org.tr/tr/pub/turkav.

IPCC. 2019. “Global Warming of 1.5°C.” www.environmentalgraphiti.org.

———. 2023. “IPCC, 2023: Climate Change 2023: Synthesis Report.” Edited by Paola Arias, Mercedes Bustamante, Ismail Elgizouli, Gregory Flato, Mark Howden, Carlos Méndez-Vallejo, Joy Jacqueline Pereira, et al. https://doi.org/10.59327/IPCC/AR6-9789291691647.

ITO. 2023. “EKONOMİK GÖSTERGELERLE İZMİR Hazırlayan: Erdem Alptekin İş Geliştirme Müdürlüğü Araştırma ve Geliştirme Uzmanı.”

IZBB. 2012. “İZMİR BÜYÜKŞEHİR BELEDİYESİ İMAR ve ŞEHİRCİLİK DAİRESİ BAŞKANLIĞI NAZIM PLAN ŞUBE MÜDÜRLÜĞÜ 1/25000 ÖLÇEKLİ İZMİR BÜYÜKŞEHİR BÜTÜNÜ ÇEVRE DÜZENİ PLANI AÇIKLAMA RAPORU EYLÜL 2012.”

———. 2019. “İZMİR ULAŞIM ANA PLANI.”

Izmir Governorship. 2024a. “İzmir Hakkında.” 2024. http://izmir.gov.tr/izmir-hakkinda.

———. 2024b. “Seferihisar.” 2024. http://www.izmir.gov.tr/seferihisar.

Jaeger, Jochen A.G., René Bertiller, Christian Schwick, and Felix Kienast. 2010. “Suitability Criteria for Measures of Urban Sprawl.” *Ecological Indicators* 10 (2): 397–406. https://doi.org/10.1016/j.ecolind.2009.07.007.

Jaeger, Jochen A.G., and Christian Schwick. 2014. “Improving the Measurement of Urban Sprawl: Weighted Urban Proliferation (WUP) and Its Application to Switzerland.” *Ecological Indicators* 38 (March):294–308. https://doi.org/10.1016/j.ecolind.2013.11.022.

Jaiswal, Tanushri, Dalchand Jhariya, and Surjeet Singh. 2023. “Spatio-Temporal Analysis of Changes Occurring in Land Use and Its Impact on Land Surface Temperature.” *Environmental Science and Pollution Research* 30 (49): 107199–218. https://doi.org/10.1007/s11356-023-26442-2.

Jalayer, Sepideh, Alireza Sharifi, Dariush Abbasi-Moghadam, Aqil Tariq, and Shujing Qin. 2022. “Modeling and Predicting Land Use Land Cover Spatiotemporal Changes: A Case Study in Chalus Watershed, Iran.” *IEEE Journal of Selected Topics*

in Applied Earth Observations and Remote Sensing 15:5496–5513. https://doi.org/10.1109/JSTARS.2022.3189528.

Jensen, R R, J D Gatrell, and D Mclean. 2007. *Geo-Spatial Technologies in Urban Environments: Policy, Practice and Pixels*. Edited by R R Jensen, J D Gatrell, and D McLean. Second Edition. Springer Science & Business Media.

Johnson, Craig, Noah Toly, and Heike Schroeder. 2015. "The Urban Climate Challenge."

Karahan, S. M., and S. Elçi. 2023. "Assessment of Future Water Demand in a Semiarid Region of Turkey: A Case Study of Tahtali–Seferihisar Basin." *Sustainable Water Resources Management* 9 (2). https://doi.org/10.1007/s40899-023-00817-2.

Karaman, Kasım. 2003. "TÜRKİYE'DE ŞEHİRLEŞME OLGUSU ve GECEKONDU SORUNU."

Keleş, Ruşen. 1961. *Şehir ve Bölge Planlaması Bakımından Şehirleşme Hareketleri*. Siyasal Bilgiler Fakültesi.

Kent. 2024. "Pearson Correlation - SPSS Tutorials - LibGuides at Kent State University." Kent State University. 2024. https://libguides.library.kent.edu/SPSS/PearsonCorr.

Koko, Auwalu Faisal, Zexu Han, Yue Wu, Ghali Abdullahi Abubakar, and Muhammed Bello. 2022. "Spatiotemporal Land Use/Land Cover Mapping and Prediction Based on Hybrid Modeling Approach: A Case Study of Kano Metropolis, Nigeria (2020–2050)." *Remote Sensing* 14 (23). https://doi.org/10.3390/rs14236083.

Lee, Jae Kang, Tri Dev Acharya, and Dong Ha Lee. 2018. "Exploring Land Cover Classification Accuracy of Landsat 8 Image Using Spectral Index Layer Stacking in Hilly Region of South Korea." *Sensors and Materials* 30 (12): 2927–41. https://doi.org/10.18494/SAM.2018.1934.

Leta, Megersa Kebede, Tamene Adugna Demissie, and Jens Tränckner. 2021. "Modeling and Prediction of Land Use Land Cover Change Dynamics Based on Land Change Modeler (Lcm) in Nashe Watershed, Upper Blue Nile Basin, Ethiopia." *Sustainability (Switzerland)* 13 (7). https://doi.org/10.3390/su13073740.

Li, S., and X. Chen. 2014. "A New Bare-Soil Index for Rapid Mapping Developing Areas Using Landsat 8 Data." In *International Archives of the Photogrammetry, Remote Sensing and Spatial Information Sciences - ISPRS Archives*, 40:139–44. International Society for Photogrammetry and Remote Sensing. https://doi.org/10.5194/isprsarchives-XL-4-139-2014.

Marsh, William M. 2010. *Landscape Planning Environmental Applications Fifth Edition*. Fifth. John Wiley & Sons.

Marshall, Stephen. 2005. “Urban Pattern Specification.”

Masson, Valéry, Aude Lemonsu, Julia Hidalgo, and James Voogt. 2020. “Annual Review of Environment and Resources Urban Climates and Climate Change.” https://doi.org/10.1146/annurev-environ-012320.

Meteorology, CSB. 2023. “2023 YILI İKLİM DEĞERLENDİRMESİ.”

NASA LANDSAT. 2024. “Landsat 8 | Landsat Science.” 2024. https://landsat.gsfc.nasa.gov/satellites/landsat-8/.

NASA MODIS. 2024. “MODIS Web.” 2024. https://modis.gsfc.nasa.gov/about/specifications.php.

Nechyba, Thomas J, and Randall P Walsh. 2004. “Urban Sprawl.”

Neelin, J. David. 2011. *Climate Change and Climate Modeling*. Cambridge University Press.

Neog, R. 2023. “Monitoring Land Use Dynamics, Urban Sprawl, and Land Surface Temperature in Dimapur Urban Area, Nagaland, India.” *International Journal of Environmental Science and Technology* 20 (7): 7519–32. https://doi.org/10.1007/s13762-022-04378-3.

Nimish, G., H. A. Bharath, and A. Lalitha. 2020. “Exploring Temperature Indices by Deriving Relationship between Land Surface Temperature and Urban Landscape.” *Remote Sensing Applications: Society and Environment* 18 (April). https://doi.org/10.1016/j.rsase.2020.100299.

Oke, Tim. 2006. “Towards Better Scientific Communication in Urban Climate.” *Theoretical and Applied Climatology* 84 (1–3): 179–90. https://doi.org/10.1007/s00704-005-0153-0.

Oke, Timothy. 1982. “The Energetic Basis of the Urban Heat Island.” *Quart. J. R. Met. Soc*. Vol. 108.

———. 1991. “CLIMATE OF CITIES.”

———. 1995. “THE HEAT ISLAND OF THE URBAN BOUNDARY LAYER: CHARACTERISTICS, CAUSES AND EFFECTS.”

Okumuş, Erdem, Deniz. 2022. “KENTSEL MİKRO İKLİMİN İYİLEŞTİRİLMESİNE YÖNELİK KENT DOKULARINDA ISI ADASI ETKİ DEĞERLENDİRME VE AZALTIM STRATEJİLERİ GELİŞTİRME MODELİ: İSTANBUL ÖRNEĞİ.”

Öncel, Hale, and Sinan Levend. 2023. “The Effects of Urban Growth on Natural Areas: The Three Metropolitan Areas in Türkiye.” *Environmental Monitoring and Assessment* 195 (7). https://doi.org/10.1007/s10661-023-11383-7.

Özbalmumcu, Mahmut, and Mustafa Erdoğan. 2001. “SATELLITE IMAGING SYSTEMS FOR REMOTE SENSING.” *Harita Dergisi* 125 (6): 59–82.

Pickett, S. T.A., M. L. Cadenasso, J. M. Grove, Christopher G. Boone, Peter M. Groffman, Elena Irwin, Sujay S. Kaushal, et al. 2011. “Urban Ecological Systems: Scientific Foundations and a Decade of Progress.” *Journal of Environmental Management*. Academic Press. https://doi.org/10.1016/j.jenvman.2010.08.022.

Pirenne, Henri. 1946. *Medieval Cities_ Their Origins and the Revival of Trade*. *Henri Pirenne*. Fourth. Princeton University Press.

Rasul, Azad. 2023. “Artificial Intelligence-Enabled Assessment of Urban Growth Impacts on Land Surface Temperature in a Hot Desert Climate: A Case Study of Baghdad City.” https://doi.org/10.20944/preprints202207.0248.v2.

Roth, Matthias, and Winston T.L. Chow. 2012. “A Historical Review and Assessment of Urban Heat Island Research in Singapore.” *Singapore Journal of Tropical Geography* 33 (3): 381–97. https://doi.org/10.1111/sjtg.12003.

Saleem, Sajid Muhammad, Rashid Sajid Ahmad, Shafiq Ur Rehman, and Muhammad Asif Javed. 2020. “Impact Assessment of Urban Development Patterns on Land Surface Temperature by Using Remote Sensing Techniques: A Case Study of Lahore, Faisalabad and Multan District.” *Environmental Science and Pollution Research* 27. https://doi.org/10.1007/s11356-020-10050-5/Published.

Sales, Marcio H.R., Sytze De Bruin, Carlos Souza, and Martin Herold. 2022. “Land Use and Land Cover Area Estimates from Class Membership Probability of a Random Forest Classification.” *IEEE Transactions on Geoscience and Remote Sensing* 60. https://doi.org/10.1109/TGRS.2021.3080083.

Sassen, Saskia. 1991. *THE GLOBAL CITY*. New York, London, Tokyo: Princeton University Press.

Schwarz, Nina, Uwe Schlink, Ulrich Franck, and Katrin Großmann. 2012. “Relationship of Land Surface and Air Temperatures and Its Implications for Quantifying Urban Heat Island Indicators - An Application for the City of Leipzig (Germany).” *Ecological Indicators* 18 (July):693–704. https://doi.org/10.1016/j.ecolind.2012.01.001.

Şentürk, Yasemin, and Kemal Mert Çubukçu. 2022. “INVESTIGATING COOLING CAPACITY OF URBAN COOL AREAS, CASE OF İZMİR.” *Çevre, Şehir ve İklim Dergisi* 1:106–26. https://orcid.org/0000-0003-3604-7014.

Shafizadeh-Moghadam, Hossein, Morteza Khazaei, Seyed Kazem Alavipanah, and Qihao Weng. 2021. “Google Earth Engine for Large-Scale Land Use and Land Cover Mapping: An Object-Based Classification Approach Using Spectral, Textural and Topographical Factors.” *GIScience and Remote Sensing* 58 (6): 914–28. https://doi.org/10.1080/15481603.2021.1947623.

Shetty, Aishwarya, Pruthviraj Umesh, and Amba Shetty. 2022. “An Exploratory Analysis of Urbanization Effects on Climatic Variables: A Study Using Google Earth Engine.” *Modeling Earth Systems and Environment* 8 (1): 1363–78. https://doi.org/10.1007/s40808-021-01157-w.

Sjoberg, Gideon. 1955. “THE PREINDUSTRIAL CITY.” http://www.journals.uchicago.edu/t-and-c.

Sobrino, José A., Juan C. Jiménez-Muñoz, and Leonardo Paolini. 2004. “Land Surface Temperature Retrieval from LANDSAT TM 5.” *Remote Sensing of Environment* 90 (4): 434–40. https://doi.org/10.1016/j.rse.2004.02.003.

Somuncu, Deniz Hilal. 2021. “KENTSEL ISI ADASI ETKİSİNİN YEREL İKLİM BÖLGELERİ SINIFLANDIRMA SİSTEMİ KULLANILARAK İRDELENMESİ: ANKARA KENT MERKEZİ ÖRNEĞİ.”

Streutker, David R. 2003. “Satellite-Measured Growth of the Urban Heat Island of Houston, Texas.” *Remote Sensing of Environment* 85 (3): 282–89. https://doi.org/10.1016/S0034-4257(03)00007-5.

Sudhira, H. S., T. V. Ramachandra, and K. S. Jagadish. 2004. “Urban Sprawl: Metrics, Dynamics and Modelling Using GIS.” *International Journal of Applied Earth Observation and Geoinformation* 5 (1): 29–39. https://doi.org/10.1016/j.jag.2003.08.002.

Sun, Qinqin, Zhifeng Wu, and Jianjun Tan. 2012. “The Relationship between Land Surface Temperature and Land Use/Land Cover in Guangzhou, China.” *Environmental Earth Sciences* 65 (6): 1687–94. https://doi.org/10.1007/s12665-011-1145-2.

Tekeli, İlhan. 2009. *Modernizm, Modernite ve Türkiye’nin Kent Planlama Tarihi* . Vol. 8. Tarih Vakfı Yurt Yayınları.

Thorns, David C. 2002. *The Transformation of Cities: Urban Theory and Urban Life*.

TOB. 2018. “TAŞKIN VE KURAKLIK YÖNETİMİ DAİRESİ BAŞKANLIĞI.”

Toy, Süleyman, and Zeynep Eren. 2023. “SUGGESTIONS FOR THE PARAMETRIZATION OF URBAN CHARACTERISTICS TO INCREASE THE

CLIMATE – RESILIENCE OF CITIES IN TÜRKİYE.” *Çevre, Şehir ve İklim Dergisi* 4 (July):324–47. https://orcid.org/0000-0002-3679-280X.

Türkeş, Murat. 2001. “Hava, Iklim, Şiddetli Hava Olayları ve Küresel Isınma.” *Devlet Meteoroloji Şleri Genel Müdürlüğü*. Vol. 1.

TURKSTAT. 2024a. “TÜİK Kurumsal.” 2024. https://data.tuik.gov.tr/Bulten/Index?p=Ic-Goc-Istatistikleri-2022-49727 and https://data.tuik.gov.tr/Bulten/Index?p=Adrese-Dayali-Nufus-Kayit-Sistemi-Sonuclari-2023-49684.

TURKSTAT, GIP. 2024b. “TÜİK - Coğrafi İstatistik Portalı.” 2024. https://cip.tuik.gov.tr/?il=35.

UNFCC. 2006. “United Nations Framework Convention on Climate Change Handbook.” UNFCCC Climate Change Secretariat.

USGS. 2024a. “What Is Remote Sensing and What Is It Used For?” Https://Www.Usgs.Gov/Faqs/What-Remote-Sensing-and-What-It-Used. May 22, 2024.

———. 2024b. “What Is Remote Sensing and What Is It Used for? | U.S. Geological Survey.” 2024. https://www.usgs.gov/faqs/what-remote-sensing-and-what-it-used and https://www.usgs.gov/faqs/what-are-band-designations-landsat-satellites.

Üstün Topal, Tuğba. 2023. “Evaluation Of The Relationship Between Spatial-Temporal Changes Of Land Use/Land Cover (Lulc) And Land Surface Temperature (Lst): A Case Study Of Nilüfer, Bursa.” *Türkiye Peyzaj Araştırmaları Dergisi* 6 (1): 56–74. https://doi.org/10.51552/peyad.1346845.

Voogt, J. A., and T. R. Oke. 2003. “Thermal Remote Sensing of Urban Climates.” *Remote Sensing of Environment* 86 (3): 370–84. https://doi.org/10.1016/S0034-4257(03)00079-8.

Wang, Lei, Yao Lu, and Yunlong Yao. 2019. “Comparison of Three Algorithms for the Retrieval of Land Surface Temperature from Landsat 8 Images.” *Sensors (Switzerland)* 19 (22). https://doi.org/10.3390/s19225049.

Wang, Shenmin, Qifang Ma, Haiyong Ding, and Hanwei Liang. 2018. “Detection of Urban Expansion and Land Surface Temperature Change Using Multi-Temporal Landsat Images.” *Resources, Conservation and Recycling* 128 (January):526–34. https://doi.org/10.1016/j.resconrec.2016.05.011.

Wang, Sonam Wangyel, Lamchin Munkhnasan, and Woo Kyun Lee. 2021. “Land Use and Land Cover Change Detection and Prediction in Bhutan’s High Altitude City of

Thimphu, Using Cellular Automata and Markov Chain." *Environmental Challenges* 2 (January). https://doi.org/10.1016/j.envc.2020.100017.

Weng, Qihao. 2009. "Thermal Infrared Remote Sensing for Urban Climate and Environmental Studies: Methods, Applications, and Trends." *ISPRS Journal of Photogrammetry and Remote Sensing*. https://doi.org/10.1016/j.isprsjprs.2009.03.007.

WHO. 2003. "Climate Change and Human Health : Risks and Responses." World Health Organization.

Wirth, Louis. 1938. "Urbanism as a Way of Life." *American Journal of Sociology*. Vol. 44. https://www.jstor.org/stable/2768119.

WMO. 2020. "The Global Climate in 2015-2019."

Xiao, Honglin, and Qihao Weng. 2007. "The Impact of Land Use and Land Cover Changes on Land Surface Temperature in a Karst Area of China." *Journal of Environmental Management* 85 (1): 245–57. https://doi.org/10.1016/j.jenvman.2006.07.016.

Xu, Hanqiu. 2006. "Modification of Normalised Difference Water Index (NDWI) to Enhance Open Water Features in Remotely Sensed Imagery." *International Journal of Remote Sensing* 27 (14): 3025–33. https://doi.org/10.1080/01431160600589179.

Yaşar, Ceren Gamze. 2010. "POLITICS OF URBAN SPRAWL: THE CASE OF ANKARA." THE PROGRAM OF URBAN POLICY PLANNING AND LOCAL GOVERNMENTS.

Yin, Chaohui, Man Yuan, Youpeng Lu, Yaping Huang, and Yanfang Liu. 2018. "Effects of Urban Form on the Urban Heat Island Effect Based on Spatial Regression Model." *Science of the Total Environment* 634 (September):696–704. https://doi.org/10.1016/j.scitotenv.2018.03.350.

Yoo, Cheolhee, Daehyeon Han, Jungho Im, and Benjamin Bechtel. 2019. "Comparison between Convolutional Neural Networks and Random Forest for Local Climate Zone Classification in Mega Urban Areas Using Landsat Images." *ISPRS Journal of Photogrammetry and Remote Sensing* 157 (November):155–70. https://doi.org/10.1016/j.isprsjprs.2019.09.009.

Yuan, Fei, and Marvin E. Bauer. 2007. "Comparison of Impervious Surface Area and Normalized Difference Vegetation Index as Indicators of Surface Urban Heat Island Effects in Landsat Imagery." *Remote Sensing of Environment* 106 (3): 375–86. https://doi.org/10.1016/j.rse.2006.09.003.

Zhou, Decheng, Jingfeng Xiao, Stefania Bonafoni, Christian Berger, Kaveh Deilami, Yuyu Zhou, Steve Frolking, Rui Yao, Zhi Qiao, and José A. Sobrino. 2019. “Satellite Remote Sensing of Surface Urban Heat Islands: Progress, Challenges, and Perspectives.” *Remote Sensing*. MDPI AG. https://doi.org/10.3390/rs11010048.

Zhou, Weiqi, Ganlin Huang, and Mary L. Cadenasso. 2011. “Does Spatial Configuration Matter? Understanding the Effects of Land Cover Pattern on Land Surface Temperature in Urban Landscapes.” *Landscape and Urban Planning* 102 (1): 54–63. https://doi.org/10.1016/j.landurbplan.2011.03.009.